CO_2 Injection in Hydrate Bearing Sandstone with Excess Water

Master Thesis in Reservoir Physics

By

Christian Hågenvik

Department of Physics and Technology
University of Bergen
Norway

May 2013

Summary

It has previously been shown that methane can be produced from gas hydrates by exposing it to carbon dioxide. Since CO_2 is the preferred hydrate former below 10 °C it will spontaneously replace CH_4 as the guest molecule in the hydrate without introducing heat. This production method is beneficial because it offers long term storage of CO_2 with the added benefit of produced methane without dissociating the hydrate.

Previous experimental research on production from gas hydrates by CO_2 injection has been conducted in cores featuring relatively small amounts of free water. In nature, gas hydrates generally exist in the presence of excess water. The main objective of this thesis is to investigate how the presence of excess water will affect CO_2 injection in hydrate bearing sediments.

Ten experiments were conducted at the hydrate lab at the Department of Physics and Technology at the University of Bergen. Methane hydrate was successfully formed in Bentheim sandstone cores at various initial conditions. The experiments were conducted at gradually increasing initial water saturation in order to achieve water in excess, resulting in final water saturations up to 50 %. It was found that the residual water saturation after hydrate formation increased with initial water saturation. This might be a result of water saturating a larger fraction of the pores and thereby inhibits gas flow in certain regions, both microscopically and macroscopically. In the experiments with low initial water saturation, the hydrate formation seemed to be constrained by water availability and salinity.

After hydrate formation was completed, CO_2 injection was conducted. It was discovered that the injection of CO_2 in hydrate bearing sandstone with excess water could lead to additional hydrate formation, resulting in loss of injectivity and plugging of the core. This problem was successfully met by injecting a binary mixture of N_2 and CO_2. It was discovered that nitrogen inhibited additional hydrate formation and also increased the total methane recovery and CO_2 storage potential by dissociating a fraction of the methane hydrate. It was also found that nitrogen could be used to re-establish flow in a plugged core.

CO_2 sequestration was observed by several different methods. It was found that the injection of CO_2 in hydrate bearing sandstone could result in CO_2 sequestration either by the formation of additional hydrate with the excess water or by replacing CH_4 as a guest molecule.

The implementation of a mass flow meter improved the quantitative production calculations compared to previous experiments.

Acknowledgements

First of all I would like to thank my supervisors Professor Arne Graue and Associate Professor Geir Ersland for providing me with an interesting and educational task. Thank you for helping me with the challenges I have faced during the work with this thesis.

A special thanks to PhD candidates Lars Petter Hauge and Knut Arne Birkedal for their guidance at the hydrate laboratory and during the data analysis work. Thanks for sharing your knowledge with me and for providing answers to my numerous questions.

Thanks to all of my fellow students for your friendship and support throughout the entire study period. I have enjoyed our many amusing conversations during lunches and coffee breaks.

I would also like to thank my family for always supporting and motivating me. Thanks to my parents, Anette and Bjørn, and to my brothers, Anders and Hans Olaf.

Thanks to all my friends.

Finally I would like to thank my fiancé Natalie for her love and support during the work with this thesis. Thank you for being patient and encouraging.

Bergen, 22.05.2013

Christian Hågenvik

Table of contents

Summary ii

Acknowledgements iii

Table of contents iv

Introduction viii

Chapter 1 - Fundamentals 12

1.1 Gas hydrates 12

1.1.1 Properties of the water molecule 12

1.1.2 Water molecules in hydrates and ice 13

1.1.3 Hydrate cavities and structures 14

1.1.4 The guest molecule 15

1.1.5 Hydrate formation 17

1.1.6 Hydrate inhibitors 19

1.2 Petrophysics 20

1.2.1 Porosity 20

1.2.2 Saturation 21

1.2.3 Permeability 21

1.2.4 Gas permeability 22

1.2.5 Wettability 23

1.2.6 Relative permeability 23

1.2.7 Capillary pressure 24

1.3 Hydrates in nature 25

1.3.1 Formation and classification of hydrates in sediments 25

1.3.2 Locations of natural gas hydrates 27

1.3.3 Global estimates of gas volumes within hydrates 28

1.3.4 Hydrate growth pattern 29

1.3.5 Different conditions for gas hydrates in sediments 31
1.4 Production from gas hydrates 32
1.4.1 Gas production from hydrates by dissociation 32
1.4.2 Gas production from hydrates by exchanging the guest molecule 35
1.5 Environmental concerns related to natural gas hydrates 37
1.5.1 Geo hazards 37
1.5.2 Climate change 38
1.6 Resistivity measurements for hydrate detection 39
1.6.1 Petrophysics from resistivity measurements 39
1.6.2 Detecting hydrates by the use of resistivity measurements 40
Chapter 2 - Literature survey 42
2.1 Methane recovery from gas hydrates by CO_2 exchange 42
2.2 Effects of excess water on hydrate formation and CO_2 exchange 43
Chapter 3 - Materials and methods 45
3.1 Experimental design 45
3.1.1 Experimental set-up A: Resistivity set-up 46
3.1.2 Experimental set-up B: General Set-up 47
3.1.3 Experimental set-up C: Temperature set-up 48
3.1.4 Confinement and cooling system 48
3.2 Experimental procedures 49
3.2.1 Properties of the core samples 50
3.2.2 Preparing and saturating the core samples 51
3.2.3 Procedures for hydrate formation 52
3.2.4 Resistivity measurement procedures 52
3.2.5 Procedures for CO_2 injection 53
3.2.6 Procedures for hydrate dissociation 53

Chapter 4 - Results and discussion 55
4.1 Hydrate formation 56
4.1.1 Effect of water saturation on hydrate formation 57
4.1.1 Salinity impact on hydrate formation 60
4.1.2 Resistivity response to hydrate growth 62
4.1.3 The "memory effect" 65
4.2 CO_2 injection into hydrate bearing sandstone 66
4.2.1 Injection of CO_2 into systems with low initial water saturation 67
4.2.2 Hydrate plugs as a result of CO_2 injection 71
4.2.3 Re-establishing flow in a plugged core by injecting nitrogen 76
4.2.4 Co-injection in systems with high initial water saturation 80
4.2.5 CO_2 injection in hydrate bearing sandstones with fracture 82
4.3 Methane production by hydrate dissociation 86
4.3.1 Production by multiple steps depressurization 87
4.3.2 Production by single step depressurization 90
4.3.3 Production by thermal dissociation 93
4.4 Methane recovery 94
4.4.1 Calculating methane recovery 95
4.4.2 Comparison of methane recoveries 95
4.4.3 Methane recovery from diffusion driven CO_2 injection 98
4.5 CO_2 sequestration 99
4.6 Uncertainties 102
4.6.1 Leaks 102
4.6.2 Temperature variations 102
4.6.3 Assumptions made in the calculations 103
4.6.4 Equipment uncertainties 104

4.6.5 Calculating uncertainties 105
Chapter 5 - Conclusions and future work 107
5.1 Conclusions 107
5.2 Future work 108
References 109
APPENDIX 113
Nomenclature 114
Appendix A – Experimental Designs 115
Appendix B – In-house Database 117

Introduction

Clathrate hydrates are ice-like solids consisting of water molecules in a lattice structure stabilized by hydrophobic guest molecules. The water molecules are interconnected through hydrogen bonds in a similar way as in hexagonal ice (Ih), but features several different physical and chemical properties. Vast amounts of natural gas exist within clathrate hydrates at numerous locations worldwide. Gas hydrate deposits are generally found in two types of environments: Oceanic sediments below 300 meters of water depth and sediments in permafrost regions deeper than 100 meters (Hester and Brewer, 2009).

The world's demand for energy has increased by more than 30 % since 1990 and is expected to grow with another 35 % by 2040 (International Energy Agency, 2012, ExxonMobil, 2013). The majority of this growth will take place in developing countries (non-OECD) as a result of increase in population and standard of living. Despite the higher focus on renewable energy resources, the majority of the global energy supply in 2040 is expected to come from fossil fuel sources, i.e. oil, gas and coal. The fraction of energy supplied from coal is decreasing, while the fraction from gas is increasing, primarily in the industrial and electric power sector (U.S. Energy Information Administration, 2013a). The growing demand for natural gas has resulted in exploitation from several new natural gas sources, such as shale gas and coalbed methane. In addition, natural gas is considered to be a more environmentally friendly energy resource compared to other fossil fuels due to a lower CO_2 emission in relation to the amount of energy obtained from burning it (U.S. Energy Information Administration, 2013b).

As a result of the increased demand for natural gas, clathrate hydrates are considered to be a potential energy source for the future. Global estimates have indicated natural gas volumes within hydrates corresponding to a factor twice as large as the CH_4-equivalent of all the fossil fuel deposits worldwide (Kvenvolden, 1988). If only a fraction of this resource is produced, it may contribute to several hundred years of energy supply. In addition, gas hydrate deposits are evenly distributed worldwide compared to other fossil energy resources, making them available to a large number of countries (Makogon, 2009). The most promising production method from hydrates today is dissociation by depressurization. This method is especially effective if the hydrate deposit is in contact with a gas reservoir that can be produced by conventional pressure depletion. Other production methods include dissociation by injection of hydrate inhibitors or hot steam/water. However, the majority of hydrate deposits are located in hostile and remote environments, far from existing infrastructure, resulting in significant costs related to work and development (Moridis et al., 2009). In addition, there are several concerns related to the technical aspects of production from natural gas hydrates. Dissociation of gas hydrates within unconsolidated sediments may result in geomechanical instabilities and slope failure (Kvenvolden, 1993). There are also local risks related to drilling and production operations, e.g. casing failure or uncontrolled gas release (Yakushev and Collett, 1992). In addition, production by dissociation induces a significant production of associated water. These factors contribute to

the need for further research and new technology in order to develop production from natural gas hydrates in a safe and economical manner.

CO_2 injection in hydrate bearing sediments has been suggested as an alternative method for production from gas hydrates (Ohgaki et al., 1994) based on the assumption that CO_2 could spontaneously replace CH_4 as a guest molecule. Experimental results showed that CO_2 exchange occurred when it was exposed to methane hydrate in bulk (Ohgaki et al., 1996, Hirohama et al., 1996). This reaction was later showed to be favorable for gas hydrates in a porous media made out of silica gel (Lee et al., 2003). Graue et al. (2006c), who monitored CO_2 injection in hydrate bearing sandstone by using Magnetic Resonance Imaging (MRI), verified that when liquid CO_2 was exposed to methane hydrate at high pressure and low temperature, it would spontaneously replace methane as a guest molecule. By applying this production method, gas can be produced from hydrates without hydrate decomposition and the associated benefits of CO_2 sequestration. In addition, CO_2 hydrate is more stable than methane hydrate at most reservoir conditions, making it more resistant to global climate changes (Graue et al., 2006a).

Production from hydrates by CO_2 exposure has recently been tested at reservoir scale. The Ignik Sikumi #1 field trial was a vertical well drilled on the Alaska North Slope in 2011 in order to study the CO_2/CH_4 exchange in hydrate bearing sandstone. The project demonstrated that carbon dioxide could successfully be injected into a reservoir containing gas hydrates in order to produce methane and store CO_2, with more than 50% of the injected CO_2 remaining in the formation (Schoderbek et al., 2012).

Extensive research on different aspects of hydrate formation and the CO_2-CH_4 replacement process in porous sandstone has been reviewed by Professor Arne Graue's research group at the Department of Physics and Technology at the University of Bergen. It has been found that properties such as initial water saturation, brine salinity and water distribution have effects on both hydrate formation and CO_2 injection in hydrate bearing sandstone. However, most of the experiments have been conducted in simplified scenarios consisting of hydrate and gas. In nature, hydrates generally exist in presence of a certain amount of excess water, which is free water saturating the pores in addition to the water bound in the solid hydrate.

This thesis has investigated how the presence of excess water affects production scenarios involving CO_2 injection in hydrate bearing sandstone with respect to injectivity and methane production. Excess water was achieved in gas-water-hydrate systems by gradually increasing the initial water saturation. CO_2 was injected in different scenarios in order to investigate how excess water would respond to exposure of a preferred guest molecule. Loss of injectivity as a result of additional hydrate formation with simultaneously CO_2/CH_4 replacement was expected as result of the injections. A binary mixture of N_2 and CO_2 was injected in whole cores with final water saturations above 25 % in order to minimize injectivity problems and to investigate the effect of nitrogen on the exchange process.

Fluid saturations and recovery were obtained from mass balance calculations, while electrical resistivity measurements were used as an additional method for hydrate detection.

As part of the experimental work, significant modifications were made on the existing set-ups. The valve- and tubing configuration were adapted to include co-injection of multiple fluids, while a mass flow meter was tested and implemented in order to improve quantitative production measurements. The entire confinement system was re-built, with the implementation of a buffer, which reduced pressure fluctuations.

The work presented in this thesis is divided into five chapters. Chapter 1 presents the fundamental theory behind gas hydrates, petrophysics and resistivity measurements. Chapter 2 contains a literature survey on previous work related to CO_2 injection in hydrate bearing sediments. Chapter 3 presents the experimental design and procedures used in this thesis, while chapters 4 and 5 contain the experimental results, discussions and conclusions. All the experimental work has been conducted within the hydrate laboratory at the Department of Physics and Technology at the University of Bergen.

Chapter 1 - Fundamentals

Natural gas hydrates are ice-like solids that consist of water and gas and may form at high pressures and low temperatures. The gas molecule, often referred to as the guest molecule, is captured in cavities in a crystalline water structure. The water molecules are connected to each other through hydrogen bonds. Common guest molecules are methane, ethane, propane and carbon dioxide.

1.1 Gas hydrates

1.1.1 Properties of the water molecule

The water molecule consists of two hydrogen atoms and one oxygen atom, connected through covalent bonds. The angle between the hydrogen atoms and the oxygen atom is 104.5º. The molecule has two negative and two positive poles, as the oxygen atom is more electronegative than the hydrogen atoms, resulting in a net positive charge on each of the hydrogen atoms and a net negative charge on the oxygen atom (Stillinger, 1980).

In the presence of each other, the water molecules will orient themselves so that the positive pole in one molecule will be attracted to the negative pole of another. This is called a hydrogen bond. The water hydrogen bond is stronger than a regular van der Waals bond, but weaker than a covalent bond. It is also the reason for the abnormal properties of water, like density decrease during freezing, increase in specific heat with reduction of temperature and the high boiling point compared to molecular weight (Sloan and Koh, 2008). Water is also a good solvent for hydrophilic substances as a result of the polar properties of the molecule.

In nature, water can be found as both liquid, solid and gas, but at standard ambient pressure and temperature it will primarily be present as a liquid phase. The water molecules will then be oriented in a random network of hydrogen bonds with continuous changes in topology. As a result of the hydrogen bonding, the density of liquid water is about 9 percent higher than for hexagonal ice (Stillinger, 1980). Figure 1.1.1 shows the phase diagram for water. At high pressures and low temperatures water is present as solid ice, while at high temperatures and low pressures it is present as a vapor. Above the critical point, no distinct liquid or vapor phase exists and the water is referred to as supercritical.

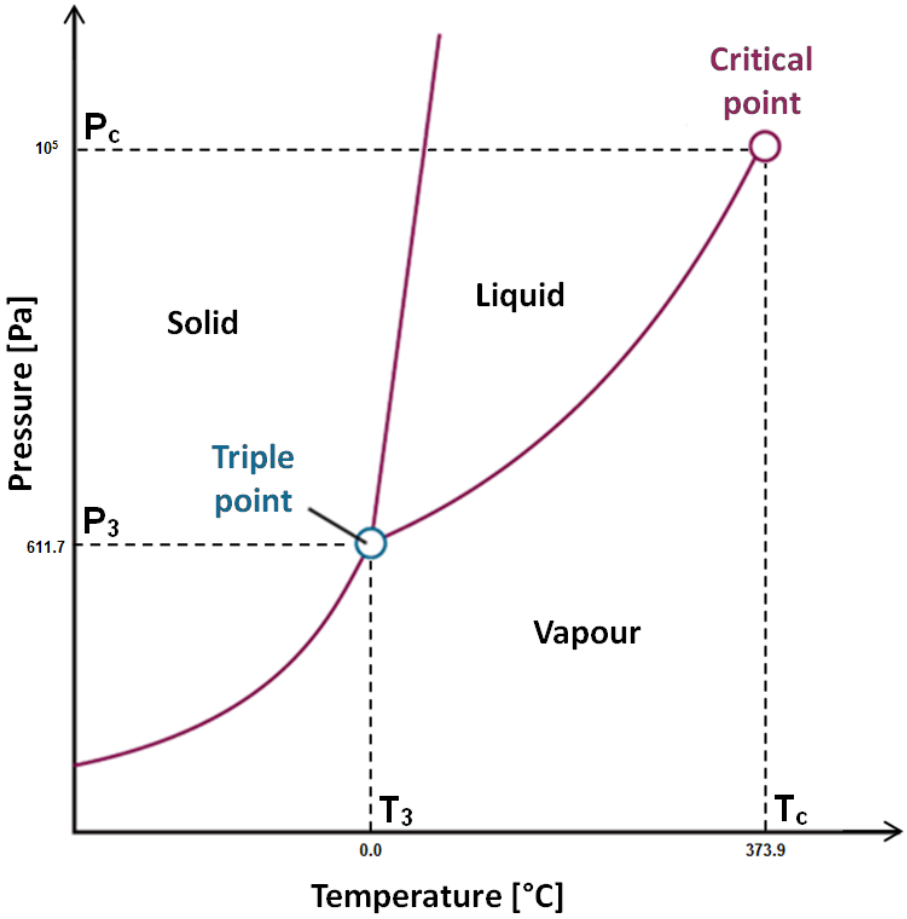

Figure 1.1.1 – Phase diagram for pure water showing solid, liquid and vapor stability zones with respect to pressure and temperature. P_3, T_3 is the triple point while P_c, T_c is the critical point. Modified from Atkins and De Paula (2006)

1.1.2 Water molecules in hydrates and ice

Ice is a solid state of water and is built up by a crystalline structure. The topology of the crystals will depend upon the conditions of the growth and the size and shape of the crystals continually undergoes changes due to recrystallization processes (Voitkovskii, 1960). Hexagonal Ice (Ih) is the most common solid form of water and consists of water molecules connected through hydrogen bonds forming a rigid hexagonal structure. Each water molecule is connected to four others with a tetrahedral angle of 109.5° between them. (Stillinger, 1980).

If hydrophobic molecules (e.g. methane or CO_2) are introduced to water molecules, *hydrophobic hydration* could occur under the circumstances of high pressures and low temperatures. The water molecules will then form hydration shells, dominated by pentagons, surrounding the hydrophobic guest molecule. The hydration shells also contain hexagons and other polygons (Stillinger, 1980).

1.1.3 Hydrate cavities and structures

Clathrate hydrates are composed of hydrogen bonded water molecules forming polyhedral cages, capable of capturing hydrophobic (guest) molecules in cavities. These cages consist mostly of pentagonal and hexagonal faces, but other faces are also known. The size and shape of the polyhedron are strongly correlated to the properties of the guest molecule. The polyhedron are labeled (n^m), where *m* is the number of faces consisting of *n* edges (Jeffrey, 1984). Clathrate gas hydrates are divided into different structures where each structure contains a certain number of different polyhedrons. The most common hydrate structures are *structure I* and *structure II. Structure I* consists of 46 water molecules per unit cell linked together by two dodecahedrons (5^{12}) and six tetrakaidecahedrons ($5^{12}6^2$). *Structure II* consists of 16 dodecahedrons and eight hexakaidecahedrons ($5^{12}6^4$) with 136 water molecules per unit cell. The cage configuration for *structure I, II* and *H* is presented in Figure 1.1.2.

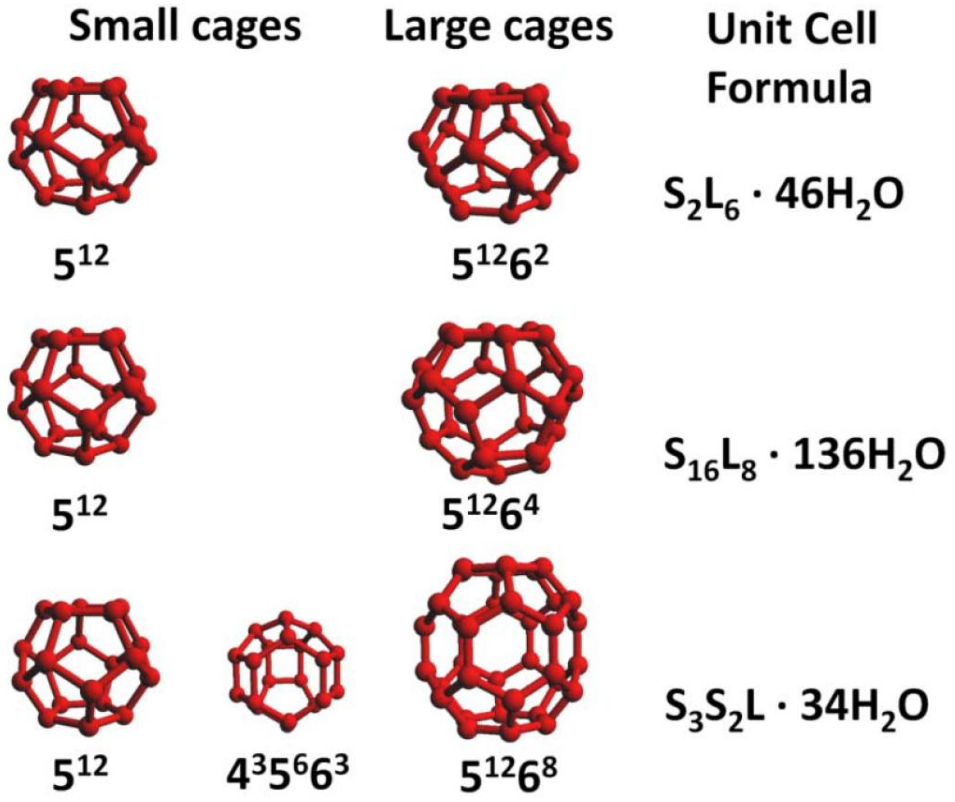

Figure 1.1.2 – Hydrate polyhedrons. The figure shows cage configuration for structure I (top), structure II (middle) and structure H (bottom), as well as the unit cell formula for each structure (Husebø, 2008).

1.1.4 The guest molecule

The guest molecules are hydrophobic compounds playing an important role in the stabilization of a hydrate structure. There are two main properties of the guest molecule determining the stabilizing effect on the hydrate cavity (Sloan and Koh, 2008); (1) the size and shape of the guest molecule and (2) the chemical nature of the guest. Hydrate structures can be stabilized by either a mixture of guest molecules or by a pure gas, referred to as simple hydrate.

If the ratio of the molecular diameter and the cavity diameter is too low, the guest molecule will not be able to stabilize the cavity. A size ratio lower bound of about 0.76 has been suggested (Sloan and Koh, 2008). On the other hand, if the guest molecule is too large, it will not be able to fit into the cavity without distorting it, which also results in destabilization. Small molecules like methane (CH_4) and hydrogen sulfide (H_2S) are able to stabilize both small and large cages in structure I hydrate. Larger molecules like propane and iso-butane can only fit into the largest cages in structure II hydrate. Therefore, structure II hydrate is usually stabilized by a gas mixture containing both large and small molecules, while structure I hydrate can be formed from a single gas, e.g. methane. Sloan and Koh (2008) also state that if a molecule stabilizes the small cavities of a structure, it will also enter the large cavities of that structure.

The chemical nature of the guest molecule will determine the intermolecular forces acting between the guest and the water molecules in the cavity. This will have a major effect on the stability of the hydrate. Molecular polarity may have positive effect on stabilizing the hydrate, but if the polarity of the guest molecule is too strong, it may break the hydrogen bonds forming the cavity (Kvamme, 2012). An example of this is methanol, which is used as a hydrate inhibitor.

Methane

Methane (CH_4) is a tetrahedral molecule consisting of a single carbon atom connected to four hydrogen atoms through covalent bonds. The bonding angle is approximately 109.5° and the molecular diameter is 4.36 Å (Sloan and Koh, 2008). It belongs to the chemical group called alkanes and is naturally occurring both as a free gas, in oil solution and as a guest molecule in Clathrate hydrates. It is the most common component in natural occurring hydrocarbon gas. As a hydrate guest molecule, methane has a beneficial molecule/cavity diameter ratio and will form structure I as simple hydrate. It is also a non-polar molecule.

Carbon Dioxide

Carbon dioxide (CO_2) is a linear molecule consisting of one carbon atom and two oxygen atoms interconnected through double covalent bonds. At standard pressure and temperature it occurs as a colorless gas, but when exposed to significant pressure it may exist in liquid or supercritical state, e.g. at most reservoir conditions. CO_2 is known to form a more stable hydrate than methane at conditions where hydrates are found in nature. The molecular diameter of carbon dioxide is 5.12 Å (Sloan and Koh, 2008), resulting in an unfavorable

molecular/cavity diameter ratio in structure I. However, the short-range forces acting between CO_2 and the water molecules are strong (Kvamme, 2012), making carbon dioxide able to stabilize both small and large cavities of structure I (Sloan and Koh, 2008). Figure 1.1.3 shows the hydrate equilibrium curves for CO_2, N_2 and CH_4 hydrate. CO_2 forms the most stable hydrate for temperatures up to 10°C.

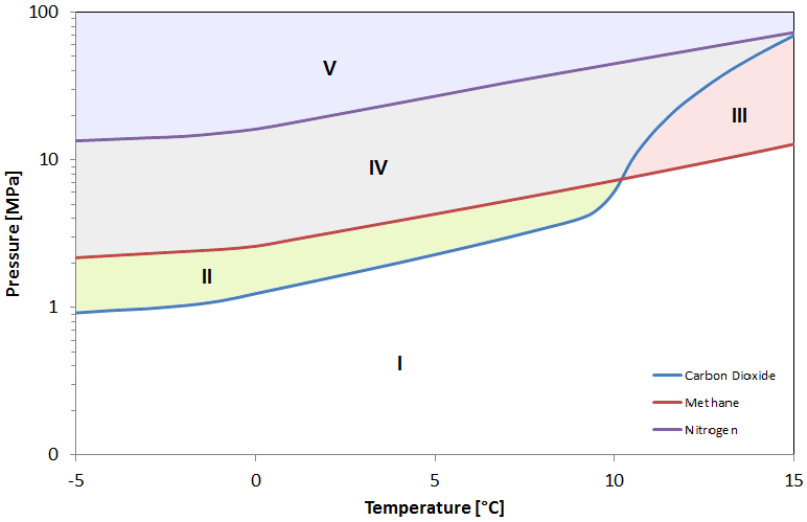

PT-Area	Hydrate phases
I	No hydrate
II	H_{CO2}
III	H_{CH4}
IV	H_{CO2}-H_{CH4}
V	H_{CO2}-H_{CH4}-H_{N2}

Figure 1.1.3 – Comparison of hydrate equilibrium curves for carbon dioxide, methane and nitrogen as simple hydrates. Generated using CSMGem with no salt present. Modified from Husebø (2008)

Nitrogen

Nitrogen is the 7th chemical element in the periodic table. At standard conditions it exists as a gas, consisting of two nitrogen atoms with a strong triple covalent bond between them (N_2). Nitrogen and water forms hydrate at relatively high pressures and low temperatures compared to other guest molecules, e.g. methane and carbon dioxide. It is a relatively small guest molecule, with a diameter of 4.1 Å (Sloan and Koh, 2008). It has therefore been assumed that it would form simple structure I hydrate. However, Davidson et al. (1986) observed by X-ray imaging that nitrogen stabilize both small and large cages of structure II hydrate, with highest occupancy ratio in the small ones. It has a molecular- to cavity size ratio of 0.62 in the large cages of structure II, which is less than the minimum value of 0.76, resulting in poor stability. Due to the small molecular size of nitrogen, it has been suggested that two N_2 molecules can occupy the large cages of structure II at the same time (Sloan and Koh, 2008).

Nitrogen has a high dissociation pressure compared to other hydrate guest molecules and can therefore be regarded as a "thermodynamic inhibitor" at conditions outside the nitrogen hydrate phase envelope, displayed in Figure 1.1.3. It has therefore been showed that it can be used to dissociate hydrate plugs or inhibit hydrate formation. Masuda et al. (2008)

observed dissociation of methane hydrate in limestone when nitrogen was injected. This happens due to the difference in chemical potential between methane within hydrate and in the gas phase. The effect of nitrogen on equilibrium pressure for different hydrates is illustrated in Figure 1.1.4. Panter et al. (2011) showed that nitrogen can dissociate hydrate plugs in natural gas pipelines, while Birkedal (2009) observed dissociation of methane hydrate in sandstone cores when N_2 was injected in relation to permeability measurements. This was also observed in recent laboratory- and full scale reservoir tests where N_2 was co-injected with CO_2 in a production scenario involving CO_2-CH_4 exchange (Schoderbek et al., 2012, Kneafsey et al., 2013). Kneafsey et al. showed that hydrate dissociation occurred due to the N_2 injection.

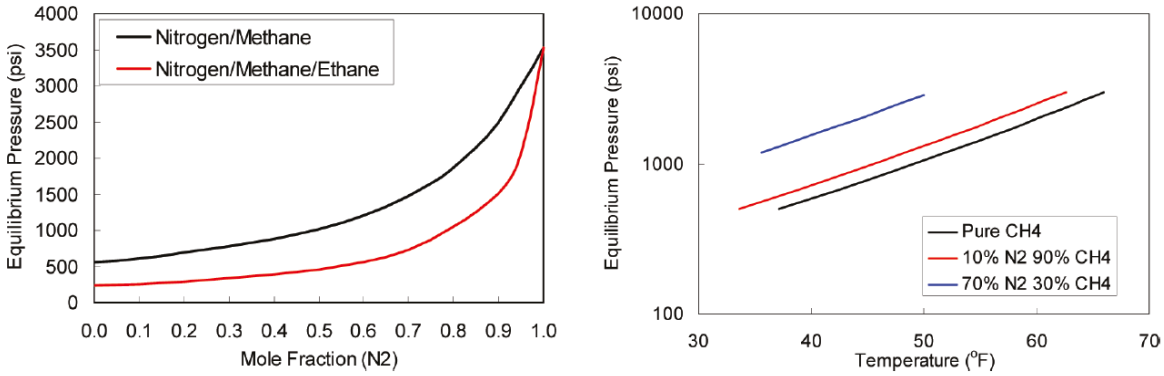

Figure 1.1.4 – Equilibrium pressure as a function of mole fraction of nitrogen (to the left) and phase diagrams for gas hydrates formed by mixtures of methane and nitrogen (to the right), computed by Panter et al. (2011) using CSMGem

1.1.5 Hydrate formation

Under suitable pressure and temperature conditions, guest molecules and water will react and form hydrate. This reaction can be described by equation (1.1) for a guest *G*, where N_H is the hydration number (Moridis et al., 2009). The hydration number is the number of water molecules per guest molecule in a hydrate unit cell and is a function of pressure, temperature and the composition of the associated components. It is directly correlated to the fill fraction, which is the occupancy ratio of the cages in a hydrate structure. For example, if all cages in structure I hydrate are occupied, the hydration number is 5.75. However, there is usually not 100 % occupancy ratio in natural occurring gas hydrates. For methane hydrate, 6.0 is considered to be a good approximation for the hydration number at pressures and temperatures where hydrates usually occur in nature (Sloan and Koh, 2008, Liu et al., 2008)

$$G + N_H H_2O = G \cdot N_H H_2O \tag{1.1}$$

The hydrate formation process can be divided in two stages: (1) The hydrate nucleation and (2) the hydrate growth. Hydrate nucleation is a microscopic process where hydrate nuclei

grow and shrink depending on size and composition. The excess Gibbs free energy of the process is described by equation (1.2) as the sum of the surface excess free energy ΔG_s and the volume excess free energy ΔG_v (Sloan and Koh, 2008)

$$\Delta G = \Delta G_s + \Delta G_v = 4\pi r^2 \sigma + \frac{4}{3}\pi r^3 \Delta g_v \tag{1.2}$$

where r is the cluster-radius, σ is the crystal-liquid interfacial tension and Δg_v is the volumetric free energy change. If ΔG reaches its maximum value, ΔG_{crit}, the volume excess free energy, ΔG_v, will dominate ΔG and the nuclei growth process becomes spontaneous as shown in Figure 1.1.5. The critical value for ΔG corresponds to the critical cluster size r_c. This implicates that when the free energy barrier becomes smaller, so does the critical cluster size needed for spontaneous growth, which could be obtained by increasing the pressure or lowering the temperature.

The nucleation process can occur either by homogeneous- (HON) or heterogeneous nucleation (HEN). Homogeneous nucleation will occur if there are no impurities present and is therefore not very common in the real world, but is useful for describing the nucleation process in theory. Mullin (2001) states that experimental investigation of true homogenous nucleation is fraught with difficulty since the production of an impurity-free system is virtually impossible.

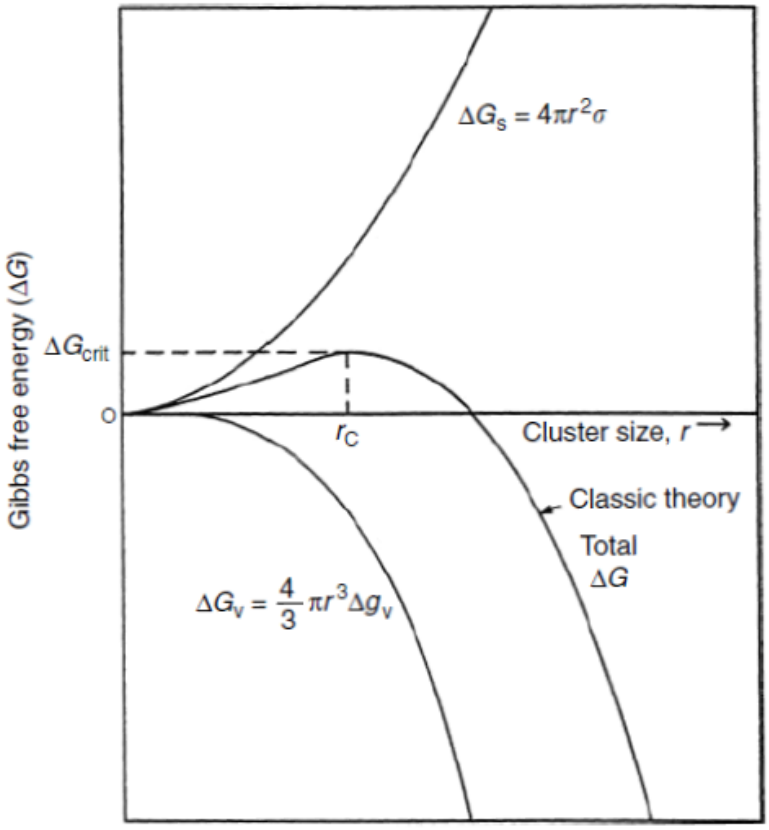

Figure 1.1.5 – Excess Gibbs free energy, Δ*G*, as a function of cluster size, *r*, (Sloan and Koh, 2008)

Figure 1.1.6 shows an example where methane hydrate is formed in an autoclave cell at constant pressure and temperature. Methane is supplied to keep the system at a constant pressure. The hydrate formation is then observed by measuring gas consumption as a function of time. The induction time (1) is defined, in practice, as the time elapsed until the consumption of a detectable amount of hydrate former gas is observed. It is most likely to be dominated by the nucleation time and the growth up to a detectable amount of hydrate (Sloan and Koh, 2008). After the induction time, massive hydrate growth will occur (2) and a significant gas consumption rate is observed. This is because the hydrate former has a higher density within the hydrate cavities than in the gas phase at most natural reservoir conditions. Eventually the gas consumption rate will decrease as the water molecules are consumed in the formation process. The total gas consumption is correlated to the amount of hydrate formed. The rate of consumption will be a function of kinetics, heat and mass transfer.

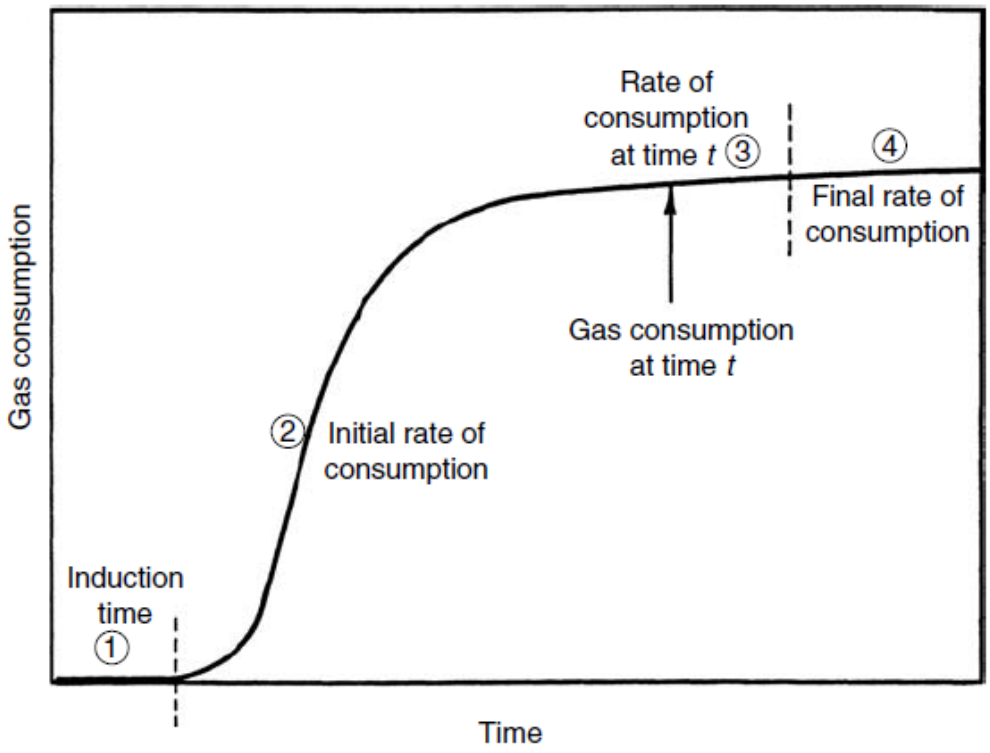

Figure 1.1.6 – Hydrate formation shown by gas consumption vs. time at constant temperature and pressure (Sloan and Koh, 2008)

1.1.6 Hydrate inhibitors

Hydrates plugging pipelines and equipment are considered a major problem in the oil and gas industry. The injection of thermodynamic inhibitors is a way to prevent hydrate formation by altering the hydrate equilibrium curve. Alcohols, glycols and salt are example of thermodynamic inhibitors. Hydrate inhibitors can also be used in production from *in situ* hydrate deposits, which are further discussed in chapter 1.4.

Alcohols will compete with apolar guest molecules when dissolved in water. This happens because the water molecules will connect with the alcohols through hydrogen bonds, instead of clustering around potential hydrate guest molecules. Methanol is the most common alcohol used as an inhibitor. Glycols inhibit hydrate formation in a similar manner, but contain an additional hydroxyl group and thereby offer more hydrogen bonding options for the water molecules. Glycols are in general less volatile then alcohols and thereby easier to recover from a hydrocarbon streams (Sloan and Koh, 2008).

Salt is known to inhibit hydrate formation by altering the thermodynamic properties of the fluid phases present (Edmonds et al., 1996). This happens due to salt ionization in water solution causing an interaction with the dipoles of the water molecules. This will result in water molecules clustering around the salt ions rather than orientating around potential hydrate guest molecules. This clustering effect will also decrease the solubility of hydrate guest molecules in water (Sloan and Koh, 2008). As a result of this, a higher pressure or a lower temperature will be required for hydrate to form, similar to the effect of methanol in Figure 1.4.2. Even though salt may affect the thermodynamics of the hydrate formation, it will not enter the hydrate structure, and will therefore not alter its properties either (Edmonds et al., 1996). This means that the salinity of the residual water will increase during hydrate formation in a confined space. For a given pressure and temperature the hydrate formation can therefore cease if a point of maximum salinity is reached. The hydrate formation kinetics will also be a function of brine salinity. Experiments on hydrate growth in sandstone demonstrate that the induction time increases with increasing salinity (Birkedal, 2009, Husebø et al., 2009) and the rate of formation increases with decreasing salinity (Husebø, 2008, Ersland, 2008).

1.2 Petrophysics

1.2.1 Porosity

Porosity is generally a static parameter describing the void spaces in a porous medium and is defined in equation (1.3) as the fraction between the medium's pore volume (V_P) and bulk volume (V_B).

$$\phi = \frac{V_P}{V_B} \tag{1.3}$$

The porosity of a reservoir rock is the reservoir's upper limit for fluid storage and will depend upon different rock parameters such as sediment type, sorting and packing. *Absolute porosity* is defined as the fraction between the total pore volume and the bulk volume, while the *effective porosity* is the ratio between the volume of interconnected pores and the bulk volume (Zolotukhin and Ursin, 2000). In laboratory measurements, it is often the *effective*

porosity that is being measured. The *residual porosity* consists of the pores that are isolated from the rest of the media.

Before a sediment deposit undergoes any significant compaction or diagenesis, it can be referred to as *unconsolidated*. When exposed to high pressure, the grains will be compacted and cemented together and the sediments become *consolidated*. In a reservoir rock the porosity will often decrease with increasing depth, due to the compaction. Gas hydrate in a porous media can be regarded as an immobile phase and will in that case reduce the effective volume where mobile fluids may flow.

1.2.2 Saturation

An oil or gas reservoir will usually contain two or more immiscible fluids. This can for example be oil, water and gas. The fluid saturation is defined in equation (1.4) as the fraction between the fluid volume and the pore volume.

$$S_i = \frac{V_i}{V_P} \tag{1.4}$$

Since the pore volumes are completely saturated with fluids, the sum of the saturations must therefore equal 1. The fluid saturation within the reservoir will vary with depth. In a gas hydrate reservoir the hydrate will be present as a solid phase, and it can be convenient to talk about the hydrate saturation. This is an important parameter affecting both the relative permeability of the other phases, as well as the total gas content of the reservoir. In this thesis, the hydrate saturation is denoted by S_H.

1.2.3 Permeability

A porous mediums ability to transmit a fluid flow is called permeability. The permeability will depend upon porosity, tortuosity, pore size, pore throat size and pore size distribution. The permeability may often vary in direction. Vertical permeability is in general lower than the horizontal permeability due to gravity induced sedimentation. Absolute permeability is the permeability when there is only a single fluid present and is described by Darcy's law for a compressible fluid, presented as equation (1.5)

$$u = -\frac{K\rho}{\mu}\nabla\psi \tag{1.5}$$

where u is the Darcy velocity, μ is the viscosity of the flowing fluid, ρ is the density, K is the absolute permeability of the porous media and ψ is the flow potential. The Darcy velocity is defined as Q/A, where Q is the volumetric flow rate and A is the cross sectional area of flow. The flow potential is defined in Equation (1.6), where p is the pressure, g is the gravity component and z is height difference between the inlet and the outlet. If the flow

is horizontal, the flow potential gradient equals the pressure gradient. The negative sign in Darcy's law is because the fluid flows in the direction of decreasing pressure.

$$\psi = gz + \int_{p_0}^{p} \frac{dp}{\rho(p)} \tag{1.6}$$

The *SI* unit for permeability is m^2, but the unit Darcy [*D*] is also commonly used. In order to use Darcy's law, some basic conditions have to be fulfilled: The porous medium has to be 100 % saturated with the fluid, while the flow has to be laminar on a constant transverse cross-section. It is also required that there is no ion exchange or chemical reaction between the fluid and the solid surface.

In practical cases, such as water- or gas injection wells, it may be convenient to introduce injectivity. Injectivity is a function of permeability and is defined as a formations capacity to accommodate injected fluids. When natural gas hydrate is present in a porous media, it can be considered as an inert immobile phase and will increase the resistance to flow through the media. The permeability and injectivity may therefore decrease with increasing hydrate saturation. The role of growth habit for hydrate in sediments is further discussed in chapter 1.3.4.

1.2.4 Gas permeability

Gas flowing through a porous medium is somehow different from a liquid flow. Compared to liquids, gases are highly compressible fluids, which mean the density will be strongly affected by the pressure. When measuring gas permeability it is therefore necessary to implement a suitable equation of state in Darcy's law to describe how the density changes with the pressure. Another important difference is that when a liquid is flowing through a porous medium, the velocity along the solid surface will be zero because of capillary forces between the liquid and the solid. In the case of a gas flow, the absence of adhesive forces between the gas and the solid surface will result in a *slippage* effect. This leads to a higher mean velocity, as well as higher permeability values in measurements conducted with gas. This effect is known as the *Klinkenberg Effect* and can be corrected for when measuring gas permeability. An increase in flow velocity will move the flow towards the *Forchheimer* flow regime, which is a laminar flow with inertia effects. These effects occur due to compression and expansion as a result of change in hydraulic diameter when flowing between pore throats and pore bodies. A gas flow in the *Forchheimer* flow regime will reduce the apparent permeability and must therefore be taken into account. If the flow velocity is further increased, the flow could become turbulent. Since laminar flow is one of the conditions for using Darcy's law, this could affect permeability measurements. As the flow becomes more turbulent, the measured permeability will appear to be lower than the actual permeability of the porous media (Zolotukhin and Ursin, 2000). This effect will be more comprehensive for the high velocity flow regime and should also be taken into account. The Reynolds number is defined by equation (1.7) as the ratio of inertial forces to

viscous forces and is used to determine whether a flow is turbulent or not. ρ is the density of the fluid, v is the average velocity, D_H is the hydraulic diameter of the flow and μ is the viscosity of the fluid. Experimental observations show that laminar flow occurs for a Reynolds number below 2300, while turbulent flow occurs for values above 4000. The interval between these values is characterized as the transition zone, where other factors will be determinant (McCabe et al., 2004).

$$R_e = \frac{\rho v D_H}{\mu} \tag{1.7}$$

1.2.5 Wettability

When multiple immiscible fluids coexist near a solid surface, there will be forces acting between the fluids and the surface. If one of the fluids has a stronger attractiveness to the surface, it will be considered as the *wetting fluid* and will tend to spread out on the surface. Wettability is the result of intermolecular forces and will depend on the molecular properties of the solid and the fluids present. A porous medium containing water and gas could for example be water-wet. The gas would then be localized in the center of the pores, while the water would coat the pore surfaces. The contact angle is defined as the angle between two fluids in their intersection point with a solid surface and is used to measure the degree of wettability. The contact angle is usually measured through the wetting fluid.

When hydrate is present in a porous media, it has been showed that hydrate may form in the pore centers, leaving a thin layer of water wetting the pore surface (Tohidi et al., 2001). However, the hydrate growth habit in the presence of a mineral surface will depend on the properties of the mineral and whether the hydrate forms from guest molecules in solution or in a gas phase (Jung and Santamarina, 2012).

1.2.6 Relative permeability

The absolute permeability of a porous medium is described by Darcy's law, assuming that the porous medium is 100 % saturated with a single fluid. When multiple immiscible fluids are present, the flow properties of each fluid will be strongly affected by their saturations. The *effective permeability* (K_i) is the permeability of a single fluid phase when multiple immiscible fluids are present. In practical applications, it may be more convenient to use the relative permeability, which is the ratio between the effective permeability of a fluid to the absolute permeability of the porous medium, defined in equation (1.8).

$$K_{ri} = \frac{K_i}{K} \tag{1.8}$$

where K_i is the effective permeability of a fluid phase *i* and K_{ri} is the relative permeability. The relative permeability will depend upon wettability, fluid saturation- and distribution. Note that in the case of a gas, due to gas solubility in the liquid phase, the gas relative permeability will be zero until the critical gas saturation is reached. This is the saturation where the gas phase becomes continuous and is able to flow as a single phase.

1.2.7 Capillary pressure

The pressure difference across the interface between two immiscible fluids is defined as the capillary pressure. The capillary pressure is a result of the internal and external electrostatic forces acting between the molecules of the two fluids. Equation (1.9) defines the capillary pressure

$$P_c = P_{nw} - P_w \tag{1.9}$$

where P_{nw} is the pressure in the non-wetting phase, while P_w is the pressure in the wetting phase. In a case with water and gas, water will usually be the wetting phase.

The Young-Laplace equation states that the capillary pressure is a function of the interfacial tension between the faces, the wetting angel and the curvature of the meniscus between the faces. In the case of a tube or a pipe, the capillary pressure can then be given by equation (1.10), where σ is the interfacial tension between the faces, θ is the wetting angle and r is the radius of the pipe.

$$P_c = \frac{2\sigma \cdot \cos\theta}{r} \tag{1.10}$$

In a porous media, the capillary pressure will be a function of the pore sizes, the permeability and the fluid saturations. It is therefore useful to plot the capillary pressure as a function of saturation. Figure 1.2.1 shows an example of a capillary pressure curve for a primary drainage, an imbibition and a secondary drainage process. Drainage is the process where the non-wetting phase displaces the wetting phase, while an imbibition is the process where the wetting phase displaces the non-wetting phase. The difference between the drainage curves and the imbibition curves is called capillary hysteresis and is a result of the negative capillary pressure developed around the saturation point S_{nc}.

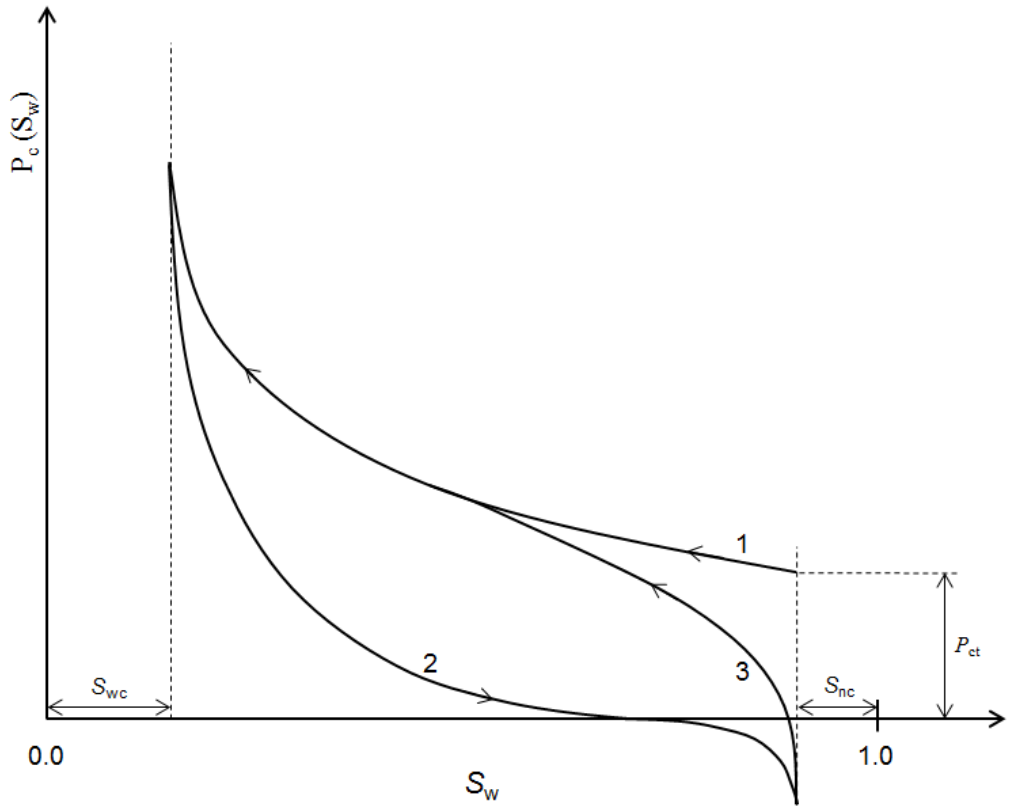

Figure 1.2.1 – Capillary pressure curves showed for a (1) drainage, (2) an imbibition and a (3) secondary drainage in a water-wet rock. The capillary pressure is presented as a function of the wetting phase saturation. P_{ct} is the threshold capillary pressure and S_{wc} and S_{nc} is the connate saturations for the wetting and the non-wetting phase

1.3 Hydrates in nature

Natural occurring gas hydrate deposits are found in two types of environments: (1) Oceanic sediments below 300 meters of water depth and (2) sediments in permafrost regions deeper than 100 meters (Hester and Brewer, 2009). Gas hydrates in nature were first discovered when drilling the Markhinskaya well in the permafrost region of Yakutia in 1963 (Makogon, 1981). Oceanic deposits, however, were discovered some decades later. From the discovery of hydrates in nature, until today, extensive research has been conducted in order to estimate the amount of natural gas that exists as hydrates. There are large variations in the predictions, but even the most conservative estimates, indicate vast amounts of gas trapped within hydrates. This makes natural gas hydrates a potential energy resource for the future (Moridis et al., 2009).

1.3.1 Formation and classification of hydrates in sediments

Natural gas hydrates are formed under the conditions of high pressure and low temperature. In nature these conditions will occur within a small depth span, known as the hydrate

formation zone (HFZ), or the hydrate stability zone. The thickness of the hydrate formation zone will depend on the properties of the hydrate forming gas, the reservoir rock and the salinity of the formation water. (Makogon, 2009). Gas hydrates occurring in nature are usually formed by a gas mixture of methane and a small amount of heavier hydrocarbon components, together with water. The origin of the source gas affects the properties of the hydrate accumulations. The gas can be supplied either by migration of gas from a source rock or from *in situ* gas production within the sediments (Hester and Brewer, 2009). In hydrate accumulations created from gas migrating into the hydrate stability zone, referred to as High Gas Flux systems, the gas source can be both biogenic and/or thermogenic. Biogenic gas is created directly from bacterial activity, while thermogenic gas is produced from kerogens exposed to high pressure and temperature. In these deposits, hydrates often exist throughout the formation zone and are often found as massive shallow marine accumulations. Another feature of the High Gas Flux systems is the presence of free gas within the hydrate stability zone. In accumulations where the hydrate origins from *in situ* gas production, free gas exists only below the lower boundary of the stability zone. These accumulations are referred to as Low Gas Flux systems, where the gas is mainly from microbial origins. The composition of hydrates may change over time due to changes in pressure and temperature as well as migration of water and gas. This may also alter the hydrate formation zone and bring the existing hydrate out of stability. An example of this is the Messoyakha field, where the temperature has increased to a level where hydrate decomposition is occurring (Makogon, 2009). Figure 1.3.1 shows the hydrate formation zone in a cross-section of the Messoyakha field in the north-western part of East Siberia.

There are basically two types of environments where gas hydrates can be found. Based on these, the hydrate deposits are divided into primary- and secondary deposits. Primary deposits are usually located in deep sea environments, below water depths of about 300 m. The temperature in these areas remains fairly stable over time, so the hydrates do not dissociate after formation. The thickness of the hydrate formation zone is limited by the rapid increase in the geothermal gradient below the seafloor. High porosity and low rock strength are characteristic for primary hydrate deposits and the hydrates will therefore contribute to the stabilization of the sediments. Because these deposits are formed from gases dissolved in the reservoir water, a reservoir seal or barrier may not always be required (Makogon, 2009).

Secondary gas hydrate deposits are generally found in Arctic onshore environments. They are usually formed from natural gas reservoirs where the temperature is lowered over time during geologic time cycles. The underlying layers are therefore often saturated with gas. The Messoyakha field is an example of a secondary hydrate deposit (Makogon, 2009). Several secondary hydrate deposits are considered to be promising production targets because they are located onshore and are often connected to an underlying mobile phase that could be produced through depressurization. This topic is dealt with in chapter 1.4.

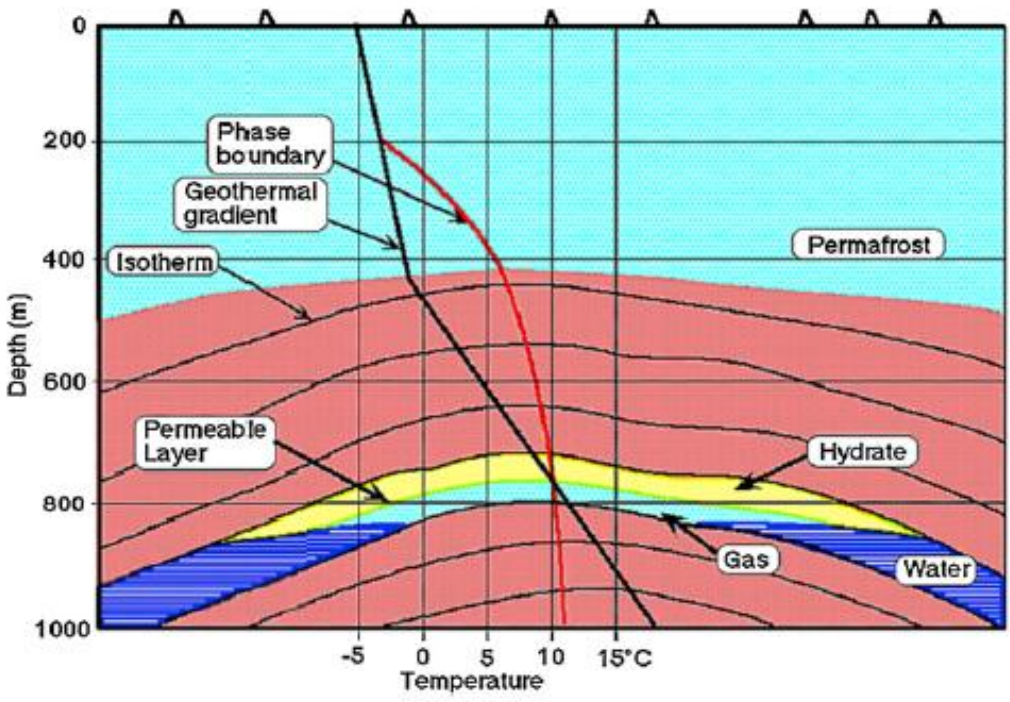

Figure 1.3.1 – Cross-section of the Messoyakha field in East Siberia (Makogon, 2009)

1.3.2 Locations of natural gas hydrates

Natural gas hydrate deposits are normally found in deep sea environments at sea levels exceeding 300 m and in Arctic onshore permafrost areas. 99% of all the hydrate deposits are within the oceanic deposits, while only 1 % is located in the permafrost regions (Sloan and Koh, 2008). Figure 1.3.2 shows a global map of more than 90 discovered gas hydrate locations. "Inferred hydrate deposits" are deposits that are discovered mainly by the use of seismic reflectors while "known hydrate deposits" are from areas where hydrate saturated core samples have been collected.

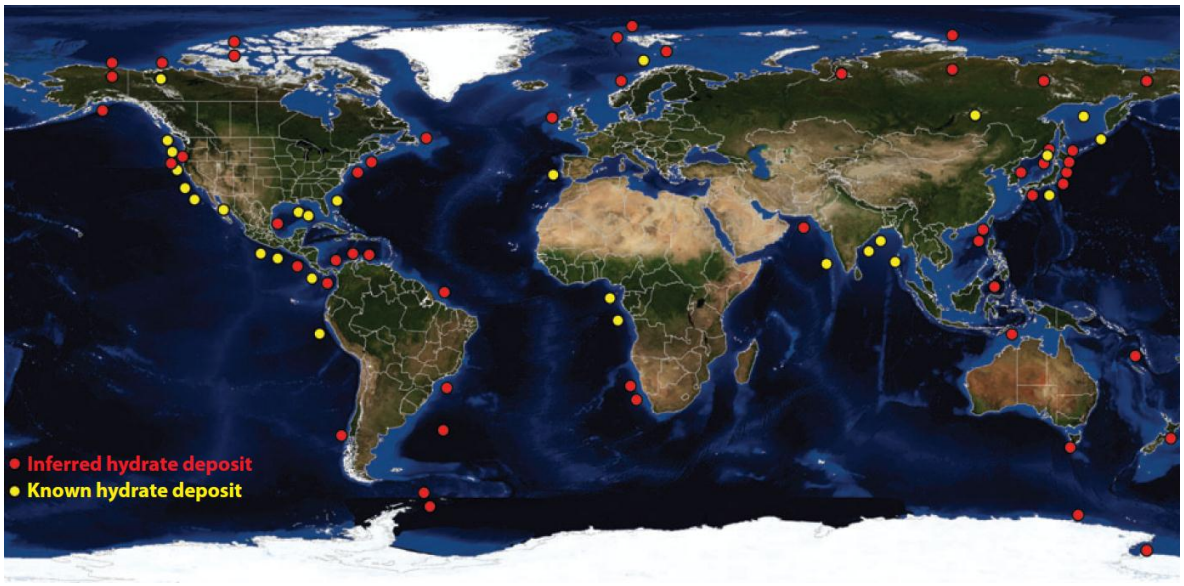

Figure 1.3.2 – Global distribution of more than 90 discovered gas hydrate occurrences. Known hydrate deposits have been identified through drilling samples, while inferred hydrate deposits are mainly from seismic reflectors (Hester and Brewer, 2009)

1.3.3 Global estimates of gas volumes within hydrates

Data on *in situ* occurrences of gas hydrates are based on either seismic refraction or core samples. The major part of the seismic data is from low quality 2D-seismic (Moridis et al., 2009). The large uncertainty related to the collection of data has also given a huge span in the volumetric estimates of natural gas trapped within hydrates. A maximum estimate of 3.1×10^{18} m^3 STP CH_4 has been made based on the assumption that gas hydrates will occur in all locations where pressure and temperature are adequate for hydrate formation (Trofimuk et al., 1973). On the other hand, a minimum estimate of 2.0×10^{14} m^3 STP CH_4 has been made by taking limiting factors, such as methane availability, into account (Soloviev, 2002). Kvenvolden (1988) has estimated an amount of 1.8×10^{16} m^3 STP CH_4 in hydrates, corresponding to a factor twice as large as the CH_4 equivalent of all the fossil fuel deposits worldwide.

Even though the most conservative hydrates estimates indicates vast amounts of methane hydrate in nature, it is only a fraction of these that provide as potential production targets. The gas hydrate resource pyramid (Boswell and Collett, 2006), showed in Figure 1.3.3, is used to display the relative size and producibility of the different categories within the world's natural gas hydrate resources. The peak of the pyramid represents deposits within Arctic sandstones that are characterized by quality reservoir rock, i.e. high permeability and porosity. The deposits also exist at high hydrate saturations (S_H) and nearby existing infrastructure. The second tier of resources is of similar quality to the first ones, but away from existing infrastructure. Then there is the deep-water oceanic deposits featuring good quality reservoirs and high S_H. At the bottom of the pyramid are the oceanic deposits in which the accumulations are disseminated in poor quality reservoirs with low S_H. These

accumulations represent the major part of the world's gas hydrate resources and provide very poor recovery possibilities with current technologies (Moridis and Sloan, 2007). The gas resource pyramid for all non-gas hydrate resources is also presented in Figure 1.3.3 for comparison.

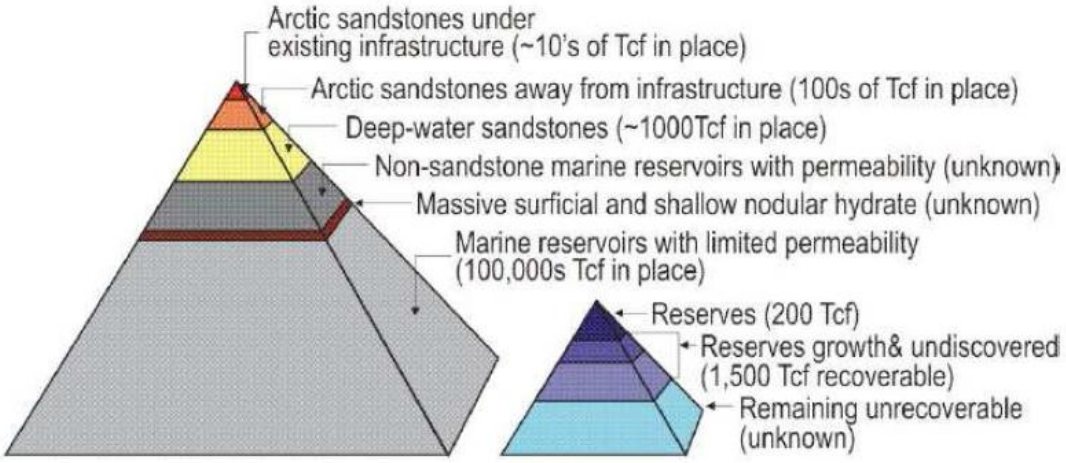

Figure 1.3.3 – The Gas hydrate resource pyramid to the left and the gas resource pyramid for all non-gas hydrate resources to the right (Boswell and Collett, 2006)

1.3.4 Hydrate growth pattern

There are different theories addressing the phenomena of hydrate growth in a porous media. The different theories are based on the interactions between hydrate and an unconsolidated packing of mineral grains, whether the hydrate forms at the grain contacts and act as cement or if it forms in the center of the pores, partially supporting the structure (Helgerud, 2001). Experiments using synthetic porous media by means of glass micromodels have indicated that hydrate are likely to grow in the center of pores, rather than on grain surfaces, if the surface is water-wet (Tohidi et al., 2001). NMR measurements of hydrate growth in deep sea environments have given similar results, that the growth of methane hydrate is primarily pore-filling, not grain-cementing. These measurements have also showed that hydrate grows preferentially in the coarsest sediments available (Kleinberg et al., 2003).

The hydrate growth process is also strongly correlated to pore size and it is generally accepted that hydrate growth is inhibited in very small pores (Clennell et al., 1999). This is based on arguments in which gas cannot enter the smallest water-saturated pores due to capillary pressure. In addition, the pore surfaces consisting of silica, tends to be water-wet in the presence of hydrate (Kleinberg et al., 2003) and thereby inhibit hydrate formation close to the mineral grains. It has been documented that when ice is present in a porous media, most grains are coated with a thin film of water 5-50 nm thick that remains unfrozen (Churaev et al., 1993).

When hydrate is partially saturating a porous media, it can be considered as an addition to the solid grain structure, resulting in a reduction in effective porosity and relative permeability of the fluids present. It may also act as cement between the grains, supporting the framework of the sediments. However, experimental results indicate that hydrate saturations above 30 % are required to affect the stiffness of the formation (Kingston et al., 2008). Figure 1.3.4 shows an illustration of how hydrate can be present in a porous media, together with water and gas. In this figure, the hydrate is presented to grow on the interface between water and gas. The porous media is water-wet, so that the mineral grains are coated by water, while the gas is located in the center of the pores. In addition, two types of pore water are introduced: (a) Equilibrium pore water and (b) Metastable pore water. Equilibrium pore water is the part of the water that cannot transform into hydrate under the given thermodynamic and geochemical conditions, e.g. high salinity. Metastable pore water on the other hand, can form hydrate, but will not, due to kinetic limitations (Chuvilin et al., 2011). This is further discussed in chapter 1.3.5.

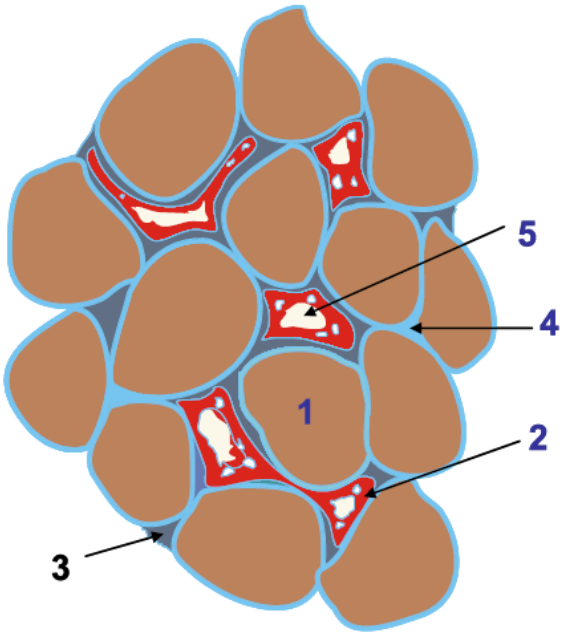

Figure 1.3.4 – Illustration of gas hydrate, water and gas within water-wet sediments. (1) Mineral grain, (2) Gas hydrate, (3) Metastable pore water, (4) Equilibrium pore water, (5) Gas (Chuvilin et al., 2011)

Another important characteristic of the hydrate growth pattern is the hydrate distribution within the porous media. The hydrate distribution will affect the phase connectivity which may have an impact on properties such as electric- and thermal conductivity, response to pressure changes, relative permeability and seismic velocity. X-ray CT observations have showed that hydrate initially forms in dendritic structures and recrystallizes over time, resulting in density redistributions for periods up to 60 days (Rees et al., 2011). Hydrate

redistribution was also observed by Tohidi et al. (2001) in glass micromodels containing methane hydrate. Figure 1.3.5 shows micromodel pictures of hydrate redistribution over a two days period of time.

Hydrate distribution is a function of initial water distribution in a porous media. Magnetic Resonance Imaging (MRI) of hydrate formation- and dissociation in sandstone cores has showed that hydrate distributed more evenly after a second hydrate formation due to improved water distribution after dissociation (Ersland, 2013).

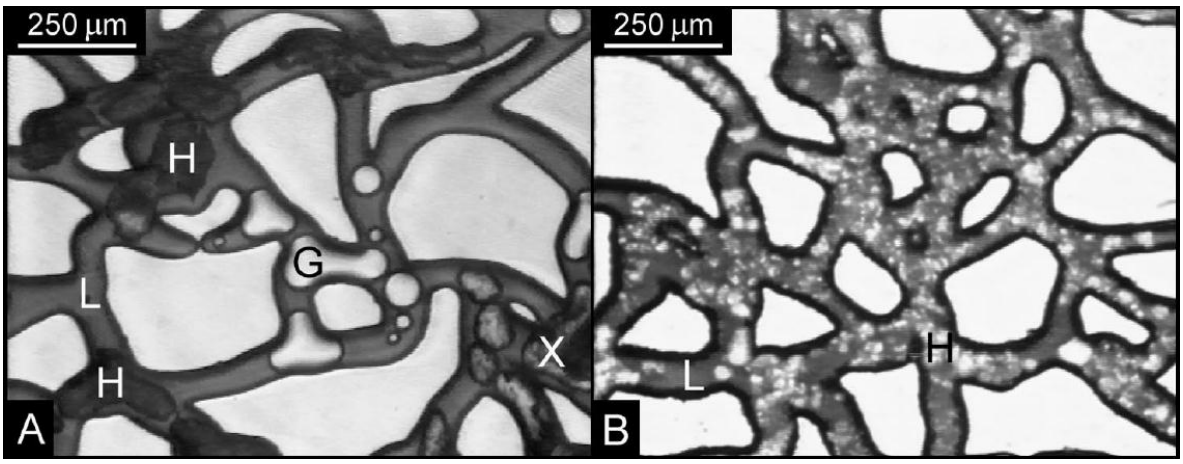

Figure 1.3.5 – Micromodel pictures of methane hydrate formation. Picture A: Methane bubbles (G), liquid (L), newly formed hydrate (H) and hydrate that is forming (X). Picture B: Redistribution of hydrate after 2 days. The grains are represented as the massive white areas. Modified from Tohidi et al. (2001)

1.3.5 Different conditions for gas hydrates in sediments

Gas hydrate in a porous media can exist within two scenarios: (1) excess water systems and (2) excess gas systems. The two are also referred to as *wet conditions* and *dry conditions*. An excess water system is a system where the hydrate formation is constrained by the gas availability. Free gas should not be present within the hydrate stability zone and residual water will form additional hydrate if exposed to gas (Handa, 1990). The porous rock is initially saturated with brine and hydrate forms as gas migrates into the hydrate stability zone. The residual water that does not form hydrate is referred to as nonclathrated water. There are two types of nonclathrated water, water that cannot form hydrate under given thermodynamic conditions and water that can form hydrate, but does not due to the absence of gas (Chuvilin et al., 2011).

An excess gas system is a system where the hydrate formation is controlled by water availability. This is the general case in natural gas pipelines in the process industry. It is also common in laboratory experiments because it is easier to form hydrate in a porous media with excess gas. In a porous media containing hydrate and excess gas there is also

excess water present, but this water is unavailable for hydrate formation. There are several reasons for this. First, if the grain surface is water-wet, which is the general case, hydrate formation is inhibited near the grain surface, leaving a thin layer of water coating the grains. Second, the initial water will usually contain some amount of salt in solution. During hydrate formation the salinity of the residual water will increase because salt cannot enter the hydrate structure (Handa, 1990). This water will eventually reach a salinity in which hydrate will no longer form. I.e. the water is no longer reactive with the hydrate former. Water that cannot form hydrate under given thermodynamic and geochemical conditions is referred to as *equilibrium water* (Chuvilin et al., 2011).

The only way reactive water may be present in an excess gas system is when it is not in contact with the gas. This could be the case for very small pores where gas cannot enter due to capillary forces (Clennell et al., 1999) or in areas where gas are not present. This water is referred to as *metastable water*. These arguments imply that the initial water distribution has a major effect on the rate of hydrate formation as well as the final hydrate saturation. A heterogeneous water distribution could result in a smaller surface area between water and gas compared to a homogeneous case. The rate of hydrate formation would therefore be lower, while the excess water volume after hydrate formation would be higher.

In nature, gas hydrates will in general exist in the presence of water, either as a pure excess water system without gas, or in an excess gas system with equilibrium water and/or metastable water.

1.4 Production from gas hydrates

1.4.1 Gas production from hydrates by dissociation

The most promising production method from natural gas hydrates is by dissociation. Hydrate dissociation can be divided into three main methods: Depressurization, where the pressure is lowered to a point below the hydrate equilibrium pressure, (2) Thermal injection, where the temperature is increased to a point above the hydrate equilibrium temperature, and (3) inhibitor injection, where the hydrate P/T equilibrium curve is shifted upwards as showed in Figure 1.4.2. This shifting will occur because the hydrate inhibitors, such as alcohols and salts, will compete for the guest- and host molecules during the hydration. However, a long term production strategy will often include a combination of the three methods mentioned above (Moridis et al., 2009). An illustration of the different dissociation methods are presented in Figure 1.4.1.

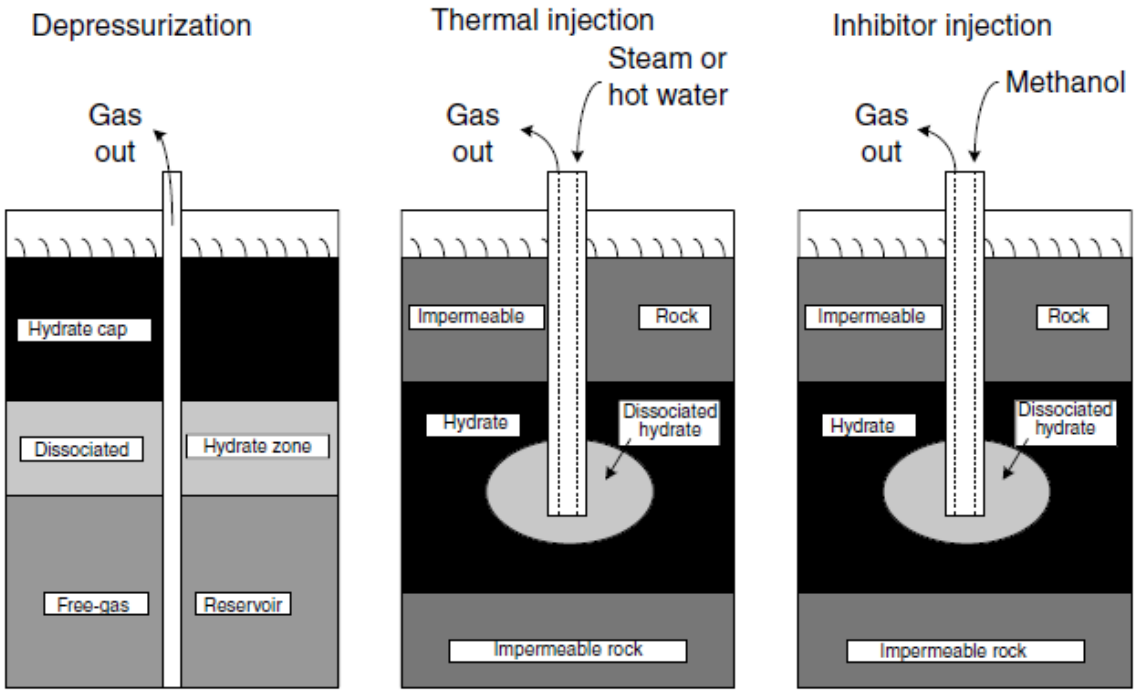

Figure 1.4.1 – The three production methods from gas hydrates by dissociation: (1) Depressurization, (2) Thermal injection and (3) Inhibitor injection. Modified from Makogon (1997)

The selection of production method will depend upon the properties of the gas hydrate deposit evaluated. Based on reservoir and geological properties, hydrate accumulations are divided into three main classes. Class 1 is characterized by a hydrate bearing layer on top of a two-phase fluid zone of mobile gas and water. In Class 2 there is only a mobile water zone below the hydrate bearing layer, while Class 3 consist only of a single zone, the hydrate bearing layer.

Class 1 hydrate deposits have been referred to as "hydrate-capped gas reservoirs" (Gerami and Pooladi-Darvish, 2006) and is considered the most desirable deposit to produce from because of the underlying gas cap. Depressurization appears to be the best suited production method for this class and involves drilling through the hydrate bearing layer and producing from the free gas zone beneath it. This will result in a pressure reduction in the gas cap, which again will lead to dissociation of the overlying hydrate (Pooladi-Darvish, 2004).

Depressurization-induced dissociation also appears to be the optimal production method for class 2 deposits. In the case of class 3 deposits, the situation is more complex, due to the absence of an underlying mobile phase. In this case the production has to take place in the hydrate bearing layer where the permeability may be very low due to hydrate saturating the pore space and blocking the flow paths (Moridis et al., 2009).

The Messoyakha hydrate accumulation in Siberia is an example of a class 1 hydrate deposit undergoing production. It was discovered in 1967 and is located in the permafrost region on

the eastern border of West Siberia. The production started in December 1969, without considering the presence of hydrates in the reservoir. The production mechanism was by depressurization in the lower free-gas region from 57 drilled wells. After analyzing the production data it was discovered that the production data started to deviate from the predicted decline relations, indicating hydrate dissociation taking place (Makogon and Omelchenko, 2013).

Production from gas hydrates by dissociation is the only commercially applied production mechanism today, often as a combination of the three methods listed above (Moridis et al., 2009). However, there are several disadvantages related to these production methods. First of all, hydrate dissociation is an endothermic process, resulting in temperature decrease as hydrate dissociates. A large amount of energy is therefore required to be able to produce the gas. Along with the gas, there is also associated water produced, putting requirements on the process separation equipment (Graue et al., 2006a). Another disadvantage by dissociation induced production from hydrates is related to the geological stabilizing effect of gas hydrate and is discussed in chapter 1.5.1.

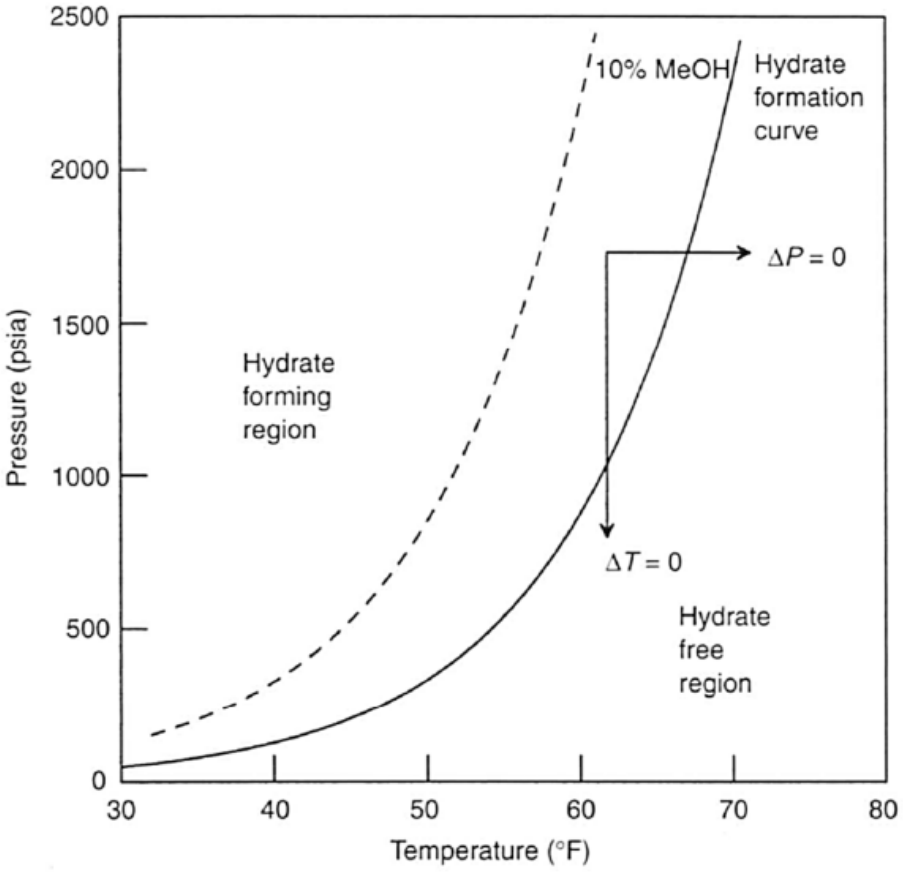

Figure 1.4.2 – A pressure versus temperature plot showing the hydrate stability zone. The three hydrate dissociation methods are showed by (1) decreasing pressure (2) increasing temperature or (3) shifting the hydrate equilibrium curve upwards by the use of an inhibitor (Sloan and Koh, 2008)

1.4.2 Gas production from hydrates by exchanging the guest molecule

Methane and CO_2 are both potential guest molecules in simple structure I gas hydrate. In natural occurring hydrate deposits, methane is by far the most common guest molecule. However, it is known that CO_2 forms a more stable hydrate than methane at relevant pressures and temperatures (see Figure 1.1.3). It has therefore been suggested that methane can be produced from hydrates by replacing the guest molecule (methane) with CO_2. In the small cages of structure I hydrate, CO_2 is a rather poor guest molecule compared to methane due to the ratio of molecular size to cavity diameter. For the large cages however, NMR measurements have showed that CO_2 is better suited as a guest molecule. For pure methane hydrate, the methane occupancy ratio between small and large cages ($\theta_{L,CH4}/\theta_{S,CH4}$) was ~1.26. The ratio was observed to decline steadily with increasing CO_2 content in the gas mixture, indicating CO_2 exchange in the large cages. Since the large cages outnumber the small ones by a factor of three, the exchange between CO_2 and methane hydrate is therefore favorable (Lee et al., 2003). However, the reaction appears to be a slow process restricted by both reaction kinetics and mass transport. Figure 1.4.3 is illustrating the replacement of CO_2 with methane in structure I hydrate. Both the small and large cages break up. However, CO_2 only replaces methane in the large ones (Ota et al., 2005).

Whether the methane production is a result of direct exchange alone could also be discussed. When CO_2 is injected into a reservoir with intermediate hydrate saturation, it could react with residual water in the pores and form CO_2 hydrate. This is an exothermic reaction that will generate heat that may lead to melting of methane hydrate. The water generated from this melting will then form additional CO_2 hydrate (Kvamme, 2012). This may happen because the generated heat from CO_2 hydrate formation (-57.98 kJ/mole) is greater than the heat required to dissociate CH_4 hydrate (54.49 kJ/mole) (Nago and Nieto, 2011). This implies that the exchange process could be a result of microscopic dissociation and reformation in addition to the direct exchange.

Production of methane from gas hydrates by CO_2 exchange is beneficial because it offers long term storage of CO_2 while producing the methane hydrate without adding any heat and no associated water produced. Another advantage with this production method is that the CO_2 hydrate is more stable than methane hydrate, making it more resistant to global climate changes (Graue et al., 2006a).

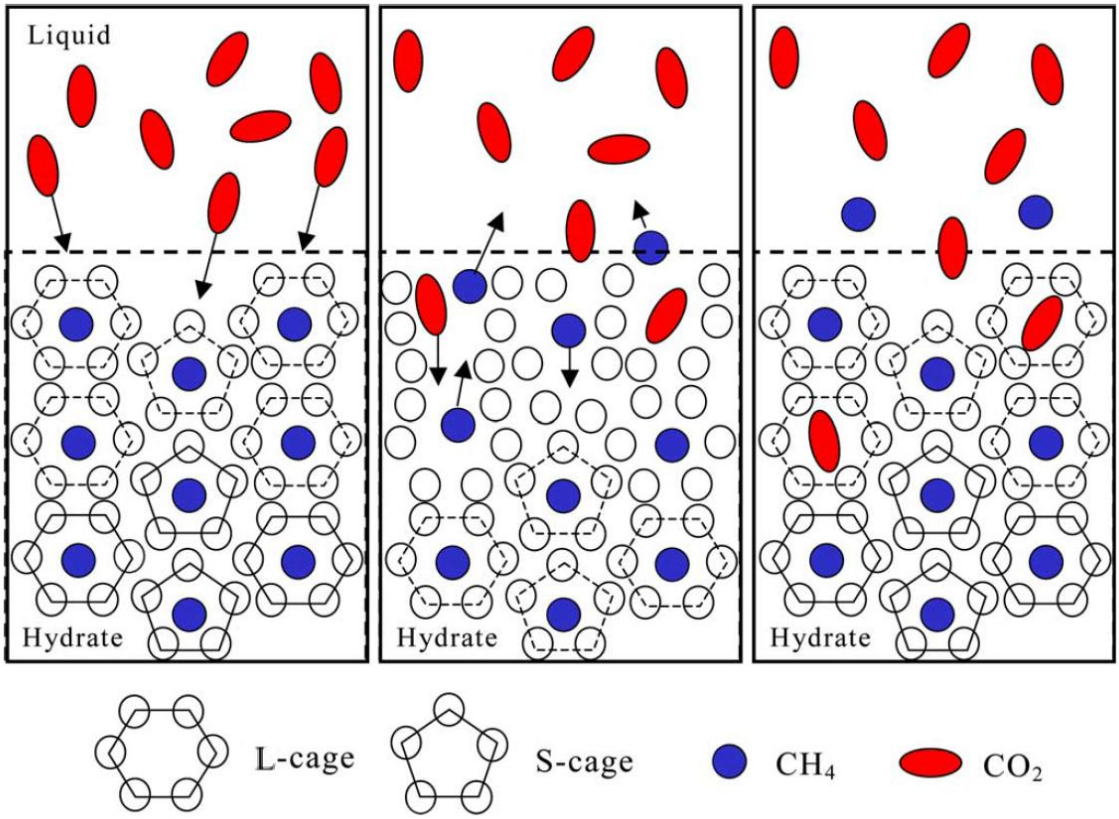

Figure 1.4.3 – Illustration of CO_2 replacing methane as guest molecule in structure I bulk hydrate. CO_2 is only replacing methane in the large cages. Modified from Ota et al. (2005)

Gas production from hydrates by replacing guest molecules has recently been applied in a full scale reservoir field test on the Alaska North Slope. The Ignik Sikumi #1 field trial was a vertical well drilled in 2011 in order to study the CO_2/CH_4 exchange in hydrate bearing sediments. The well was drilled to a depth of 790 m and encountered four hydrate bearing sandstone layers beneath the permafrost. The field trial faced two major challenges based on the reservoir characteristics: (1) Injection problems as a result of the pressure exerted by the CO_2 column and (2) Injectivity loss as a result of CO_2 hydrate formation with the excess water in the near wellbore region. In order to reduce injectivity problems, N_2 was injected along with the liquid CO_2. An optimized CO_2/N_2 rate was determined as part of the field trial. This project confirmed laboratory results and successfully demonstrated that liquid CO_2 can be injected into natural gas hydrate reservoirs for methane production and carbon sequestration (Schoderbek and Boswell, 2011, Schoderbek et al., 2012). More than half of the injected CO_2 remained in the formation after production had ceased. The production data from the Ignik Sikumi field trial is presented in Figure 1.4.4.

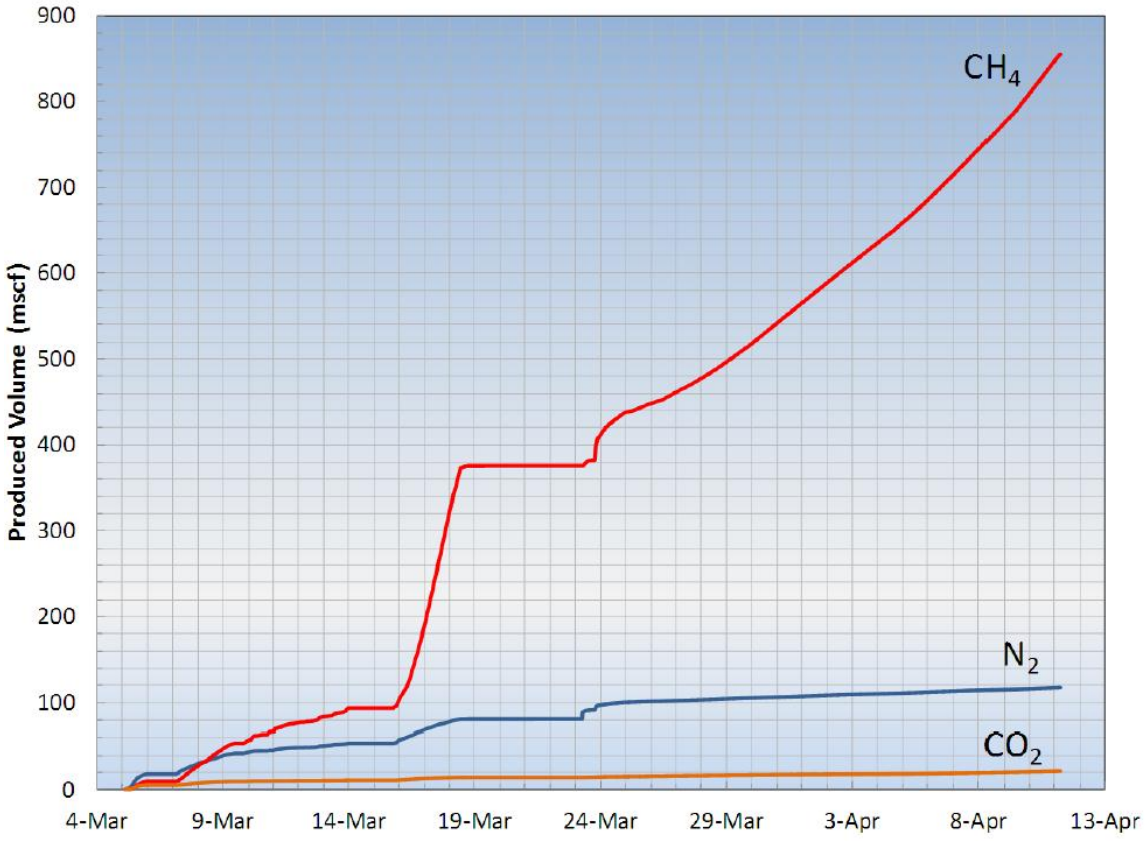

Figure 1.4.4 – Produced volumes of CH_4, CO_2 and N_2 in the Ignik Sikumi field trial (Schoderbek et al., 2012)

1.5 Environmental concerns related to natural gas hydrates

1.5.1 Geo hazards

Estimates of global hydrate occurrences dictates that 99 % of the world's gas hydrate reserves are located within unconsolidated marine sediments (Sloan and Koh, 2008). The presence of hydrate is supporting the framework of these sediments, working as cement. This strengthens the formation, but also inhibits further diagenesis. Dissociation of hydrates located in unconsolidated sediments, either by production or due to natural processes, is therefore of major concern. If the cementing hydrate is dissociated, a zone of weakness could be generated, which may lead to submarine slope failure (Kvenvolden, 1993). Another result of the dissociation would be the release of a significant amount of gas, creating a local overpressure that could either amplify the geological instabilities or migrate up to the surface (Schmuck and Paull, 1993). Apart from the global geological hazards associated with hydrate dissociation, there is also local risk related to drilling and production operations, e.g. casing failure or uncontrolled gas release (Yakushev and Collett, 1992). In addition, dissociation of hydrates within unconsolidated sediments can result in the production of large volumes of sand (Moridis et al., 2009).

1.5.2 Climate change

There is a growing concern about the release of *greenhouse gases* into the atmosphere and how it will affect the global climate. The majority of these concerns are related to CO_2 emission. However, methane is a greenhouse gas with a global warming potential 20 times larger than the equivalent amount of CO_2. Measurements on Antarctic ice cores have shown that the methane concentration in the atmosphere has more than doubled over the past few centuries, starting to increase at the time of the industrial revolution (Etheridge et al., 1998). Even though actions are made in order to reduce the emission of greenhouse gases into the atmosphere, the contribution from natural sources, such as geologically stored methane, may be relevant (MacDonald, 1990).

The thickness of the hydrate stability zone is correlated to the surface temperature and the geothermal gradient, making natural gas hydrates sensitive to surface disturbances (Hester and Brewer, 2009). Global changes in surface temperature could therefore lead to a significant release of methane from gas hydrates that could have a further impact on the global climate. However, the majority of the hydrate accumulations on Earth features low hydrate saturation and occur at depths that require a significant temperature change to dissociate the hydrate. A climate change due to hydrate dissociation at those depths is therefore not expected for at least 10^3 years with today's temperature increase (Ruppel, 2011). In addition, a change in surface temperature would have a different effect on oceanic hydrate deposits than for continental deposits according to Kvenvolden (1993). Figure 1.5.1 is illustrating the effect of hydrate decomposition on the glacial cycles for oceanic and continental deposits. The figure shows that global warming will result in an increase in surface temperature which will lead to destabilization of continental hydrate deposits. The temperature increase will also initiate deglaciation that leads to an increase in sea level. A direct result from this is an increase in hydrostatic pressure and stabilization of oceanic hydrate deposits. Global cooling however will induce glaciation, which will decrease the sea level and hydrostatic pressure and thereby destabilize the oceanic gas hydrates. The temperature decrease will also stabilize the continental hydrate deposits. According to Kvenvolden (1993), changes in surface temperature will therefore have opposite effect on oceanic and continental deposits.

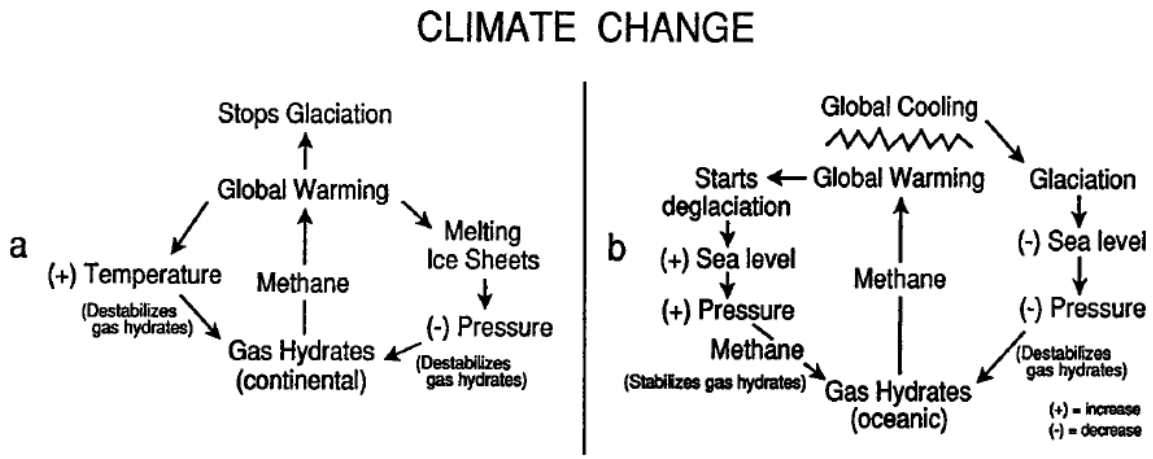

Figure 1.5.1 – Illustration on how gas hydrate dissociation could affect the glacial cycles: (a) Continental deposits and (b) oceanic deposits. Modified from Kvenvolden (1993)

1.6 Resistivity measurements for hydrate detection

Electric resistivity is a materials capacity to resist a flow of electric current. A good conductor has a low resistivity. The SI unit of electrical resistivity is ohm-meter (Ω·m). The difference between electrical resistance and resistivity is that the resistivity is a material property, while electrical resistance is also a function of geometry, i.e. length and cross-section. The inverse of resistivity is defined as conductivity.

1.6.1 Petrophysics from resistivity measurements

Porous rocks are built up by a network of mineral grains interconnected with void spaces in between. The solid matrix of the rock will usually not conduct electric current, with the exception of some clay minerals. The electric properties of a porous rock will therefore depend on the fluids saturating it, as well as the electric currents flow path through the media, i.e. the tortuosity. Resistivity measurements can therefore be used to determine petrophysical properties like porosity and saturation both in laboratory measurements and in well logs (Lien, 2004). Two reservoir parameters are used to describe how these properties affect the resistivity: (1) the formation factor and (2) the resistivity index. The formation factor (F) is defined in equation (1.11) as the ratio between the resistivity for a porous rock when it is 100 % saturated with brine (R_0) and the resistivity of the brine itself (R_w). The formation factor depends on rock properties such as effective porosity and tortuosity.

$$F = \frac{R_0}{R_w} \tag{1.11}$$

The resistivity index (I) is used to determine fluid saturation. It is defined in equation (1.12) as the ratio between the rocks resistivity at a specific fluid saturation (R_t) and the resistivity of the rock when it is 100% saturated with brine (R_0). The resistivity index is a function of the same rock properties as the formation factor, but the saturation distribution and rock wettability could also have an effect on it. In order to distinguish between fluids in resistivity measurements, the fluids need to have different electric conductive properties, e.g. oil and water.

$$I = \frac{R_t}{R_0} \tag{1.12}$$

Archie's laws (Archie, 1942) are empirical expressions relating formation factor and resistivity index to porosity and fluid saturation. Archie's first law is given by equation (1.13) where ϕ is the porosity and a is a function of tortuosity and pore size distribution. m is related to the grain cementation and has been found to lie between 1.8 and 2.0 for consolidated sandstones (Archie, 1942).

$$F = a\phi^{-m} \tag{1.13}$$

Equation (1.14) displays Archie's second law where b is a function of tortuosity, S_w is the brine saturation and n is known as the *saturation index*. This index appears to be ~2 for both consolidated and clean unconsolidated sands. A decrease in water saturation will therefore lead to an increase in resistivity index, which means that the resistivity of the rock will be higher. In order for this to be true, the other phases, besides water, need to be electric isolators.

$$I = bS_w^{-n} \tag{1.14}$$

In practical applications, it is sometimes easier to measure the resistance of the conductor instead of the resistivity. Equation (1.15) can be used to calculate resistivity (R_t) from the resistance (R), where A is the cross sectional area, L is inductance and φ is the phase angle.

$$R_t = R \cdot \frac{A}{L} \cdot \cos\varphi \tag{1.15}$$

1.6.2 Detecting hydrates by the use of resistivity measurements

Resistivity measurement is a commonly applied method to determine petrophysical properties such as porosity and saturation both in laboratory measurements and in well logs. Another application of the resistivity log is the detection of gas hydrates in porous rocks.

Brine with sufficient salinity is able to conduct electricity due to ions in solution. Hydrate, on the other hand, is a solid with no ions present, and can be considered an electric isolator

(Gabitto and Tsouris, 2010). Hydrate growth in a porous rock will therefore block the flow path of the electric current, resulting in a poor connectivity and an increase in the overall resistivity of the rock (Li et al., 2010). Experiments have showed that the resistivity measurements are most sensitive at higher hydrate saturations (Hauge, 2011, Birkedal et al., 2013b). The explanation for this could be that the connectivity of the brine remains intact at low hydrate saturations.

The salinity of the brine is strongly correlated to its ability to transmit a flow of electric current. Changes in salinity will therefore have an impact on the measured resistivity. The salt is present as ions in water solution and cannot participate in the hydrate structure. As hydrate forms, the salinity of the remaining water increases (Li et al., 2010). This effects the resistivity measurements and must be taken into account when calculating hydrate saturation from resistivity. Figure 1.6.1 shows how the brine connectivity changes as hydrate forms.

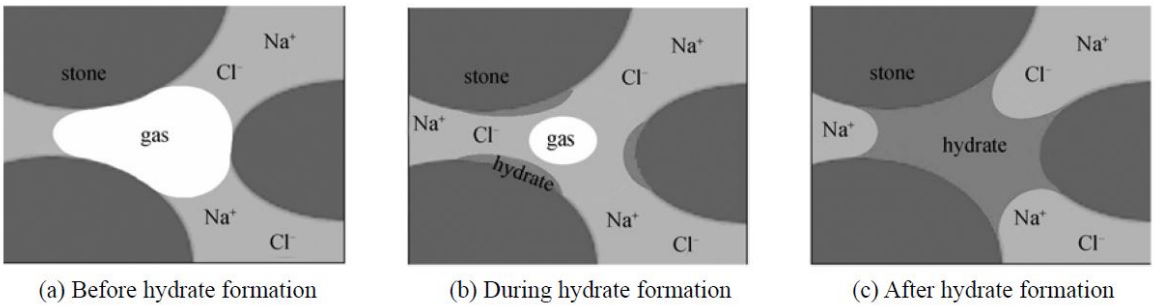

Figure 1.6.1 – Brine connectivity and resistivity change during hydrate formation in porous rocks (Li et al., 2010)

Chapter 2 - Literature survey

In this chapter several experimental and theoretical studies will be reviewed with emphasis on methane recovery from gas hydrates by CO_2 exchange and the effect of excess water on hydrate formation, CO_2 exchange and dissociation.

2.1 Methane recovery from gas hydrates by CO_2 exchange

It has long been known that CO_2 provide a more stable gas hydrate than CH_4 at temperatures below approximately 10°C (Figure 1.1.3). This fact resulted in the hypothesis on whether CO_2 could spontaneously replace CH_4 as a guest molecule in gas hydrate (Ohgaki et al., 1994). The hypothesis was investigated through several experiments on bulk methane hydrate in contact with CO_2 in both liquid and gaseous phase (Hirohama et al., 1996, Ohgaki et al., 1996). Through these experiments they found out that the exchange process had significant kinetic limitations, possibly due to the interaction surface available at bulk hydrate. CO_2-CH_4 exchange experiments on methane hydrate in high pressure cells showed that the exchange rate was high during the first 200 minutes followed by a decrease in rate to a relative low level (Yoon et al., 2004).

Lee et al. (2003) investigated the possibility of favorable CO_2-CH_4 exchange in a porous media made out of silica gel using both pure and mixed-phase hydrate. They showed that the exchange reaction in a laboratory setting is favorable with respect to both equilibrium thermodynamics and kinetics.

Graue et al. (2006c) used Magnetic Resonance Imaging (MRI) to monitor formation and CO_2 exchange on methane hydrate in porous sandstone. They verified that when liquid CO_2 is exposed to methane hydrate at high pressure and low temperature, it will spontaneously replace methane as the guest molecule. These results states that by using this method, methane can be produced from hydrate bearing sediments without any heating and with no associated water production. Similar experiments have been conducted, investigating different impacts on the exchange process, showing repeatable results (Birkedal, 2009, Ersland et al., 2010, Hauge, 2011, Bringedal, 2011).

McGrail et al. (2007) injected a micro emulsion of liquid CO_2 and water into a methane hydrate bearing porous media. The temperature of the micro emulsion was higher than the stability point of CH_4 hydrate, resulting in thermal dissociation. The CO_2 reacted with the excess water and formed hydrate. This generated heat that was used to further dissociation of CH_4 hydrate. These results indicate that the CO_2/CH_4 replacement process could be a result of microscopic dissociation and reformation in addition to the direct exchange of guest molecule.

The CO_2/CH_4 exchange process has also been described through thermodynamic and kinetic modeling (Kvamme et al., 2011). They have derived a complete thermodynamic model consisting of aqueous, fluid and hydrate phases. Analysis of the exchange process showed that it is highly dependent on entropy changes.

It has been suggested that CO_2 cannot replace more than 2/3 of the CH_4 molecules in structure I (sI) methane hydrate due to an unfavorable molecule- to cage size ratio in the small sI cages (Lee et al., 2003). However, Park et al. (2008) achieved ~85 % methane recovery in sI hydrate by using a flue gas mixture of CO_2 and N_2 in the replacement process. They found out that for the small sI cages, N_2 would compete with CH_4 for occupancy, while the large cages were preferentially occupied by CO_2. The results were obtained by the use of spectrometry. However, whether nitrogen could be used to increase the methane recovery from hydrates will depend on the thermodynamic conditions of the system. Masuda et al. (2008) showed that nitrogen can be used to dissociate methane hydrate in a porous media. Similar results were obtained by Kneafsey et al. (2013) who co-injected N_2 along with CO_2 into hydrate bearing sediments featuring hydrate saturations around 20-40 %.

Several studies have been done to investigate how the CO_2-CH_4 exchange is affected by salinity, initial water saturation and temperature. The impact of initial brine salinity on CO_2-CH_4 exchange rate was studied by Husebø (2008). The experiments showed that systems of lower salinities (>3.0 wt% NaCl) had a lower initial production rate than the systems of higher salinities (5.0 wt% NaCl). The total methane produced however, were similar for all systems. As was the time of maximum total production. The CO_2-CH_4 exchange rate was also studied by Ersland (2008) who found out that high residual water saturations increased the exchange rate, indicating that the water may provide as a transport option for CO_2 and CH_4. However, the residual water saturation did not seem to affect the total recovery. Bringedal (2011) investigated the effect of temperature on the exchange process and acquired results that indicated a more favorable replacement ratio at 10 °C than for 4 °C and 0.5 °C.

Gas production from hydrates by replacing guest molecules has also been tested at reservoir scale. The Ignik Sikumi #1 field trial was a vertical well on the Alaska North Slope drilled in 2011 in order to study the CO_2/CH_4 exchange in hydrate bearing sandstone. The project demonstrated that carbon dioxide could successfully be injected into a reservoir containing gas hydrates in order to produce methane and store CO_2, with more than 50% of the injected CO_2 remaining in the formation (Schoderbek et al., 2012).

2.2 Effects of excess water on hydrate formation and CO_2 exchange

In nature, hydrates will generally exist in the presence of excess water or ice. Handa (1990) emphasizes that free gas should not exist within the hydrate stability zone as long as there is water or ice in excess. This includes gas dissolved in the water phase, because it has a preference to be in a hydrate structure over being in an aqueous solution. The introduction of hydrate forming gases in an excess water system would therefore lead to additional formation. This effect was studied by Kleinberg et al. (2003) who performed NMR

measurements on hydrate bearing sediments in deep sea environments using an ROV. They observed a significant reduction in hydraulic permeability as hydrate formed.

In laboratory settings there are three ways to form natural gas hydrates in sediments: (1) The sediments are saturated with water and then pressurized with gas, (2) the sediments are saturated with gas and pressurized using water and (3) the hydrate is formed out of a water phase containing dissolved gas (Kingston et al., 2008). The first method results in an excess gas system, while the two others give pure excess water systems.

Jung and Santamarina (2010) monitored bulk CH_4 hydrate formation, CH_4/CO_2 replacement and hydrate dissociation on a thin cylindrical water layer by measuring resistivity and relative stiffness. They found out that in the absence of fluid flow, reactive excess water could exist in an excess gas system for a relatively long time, because the hydrate formation was controlled by gas diffusion.

Deusner et al. (2012) studied production from methane hydrates by the injection of hot, supercritical CO_2. They found that cooling of the CO_2 could result in hydrate formation with the excess water and thereby reduction in permeability.

As discussed in chapter 1.3.5, excess gas systems will in general contain water that will not form hydrate, limited by either mass transport or inhibited by thermodynamics, e.g. high salinity. However, if a gas that provide as a more suitable guest molecule is introduced, a higher salinity is then required to inhibit hydration, and additional formation could therefore occur. Birkedal (2009) showed that when CO_2 was injected into a porous sandstone containing methane hydrate and free water, it formed additional hydrate with the excess water, clogging the formation. The same phenomena was observed by Hauge (2011) and Bringedal (2011). Kang et al. (2005) used numerical simulation to study the exchange process and found that injected CO_2 formed hydrate with the excess water at low velocities, clogging the formation. This inhibited further CO_2/CH_4 exchange. The reduction in hydraulic permeability with increasing hydrate saturation has been confirmed by Kleinberg et al. (2003) from NMR measurements. The same phenomena was observed by Ersland et al. (2008) who used MRI when measuring gas permeability in 1.1 Darcy sandstone cores.

The Ignik Sikumi #1 field trial, presented in chapter 1.4.2, was conducted in sandstone containing primarily methane hydrate and excess water. One of the major issues of the project was therefore the potential permeability reduction near the well, due to CO_2-hydrate formation with the excess water in the pore space. To address this issue, they injected a binary mixture of CO_2 and N_2. One of the results from the project was the identification of an optimized N_2/CO_2 mixture that would keep the injectivity problems at a minimum (Schoderbek et al., 2012). This was further investigated in laboratory tests where it was found that hydrate dissociation occurred as a result of the injected nitrogen (Kneafsey et al., 2013).

Chapter 3 - Materials and methods

In this study, a series of experiments have been conducted to investigate the effect of excess water on hydrate formation and CO_2/CH_4 exchange for production and carbon sequestration. The principles of excess water are discussed in chapter 1.3.5. The experiments were conducted at initial water saturations in the range of 40-81% and with salinities ranging from 0.1 - 3.5 wt% NaCl. In the experiments with high initial water saturation, the injection was performed with a mixture of CO_2 and N_2 to avoid plugging of the core and tubing. All experiments were conducted at 8.3 MPa and approximately 4 °C in Bentheim sandstone cores, with the exception of CO2-20, where the CO_2 injection was conducted at 9.4 °C. Both whole- and fractured cores were used. The fractured cores were cut into two core halves with a spacer in between them and were used in the two experiments with the highest initial water saturations. The laboratory work took place at the Hydrate lab at the Department of Physics and Technology at the University of Bergen in cooperation with co-student Hans Berge.

3.1 Experimental design

Three experimental set-ups have been used to carry out the experiments. Existing experimental set-ups were available from previous gas hydrate research conducted at the University of Bergen (Ersland, 2008, Husebø, 2008, Hauge, 2011, Birkedal, 2009). However, some modifications have been made in order to make the set-ups more efficient and reduce the experimental uncertainties. All three set-ups were connected to a gas chromatograph (GC), while one of the set-ups contained resistivity measurements for hydrate detection. A mass flow meter (MFM) was implemented and tested as part of the work with this thesis. Figure 3.1.1 shows a general set-up used in this thesis, representative for all three set-ups. Appendix A contains a picture of experimental set-up B (Figure I) and a 3D-model of the core holders used in set-up B and C (Figure II).

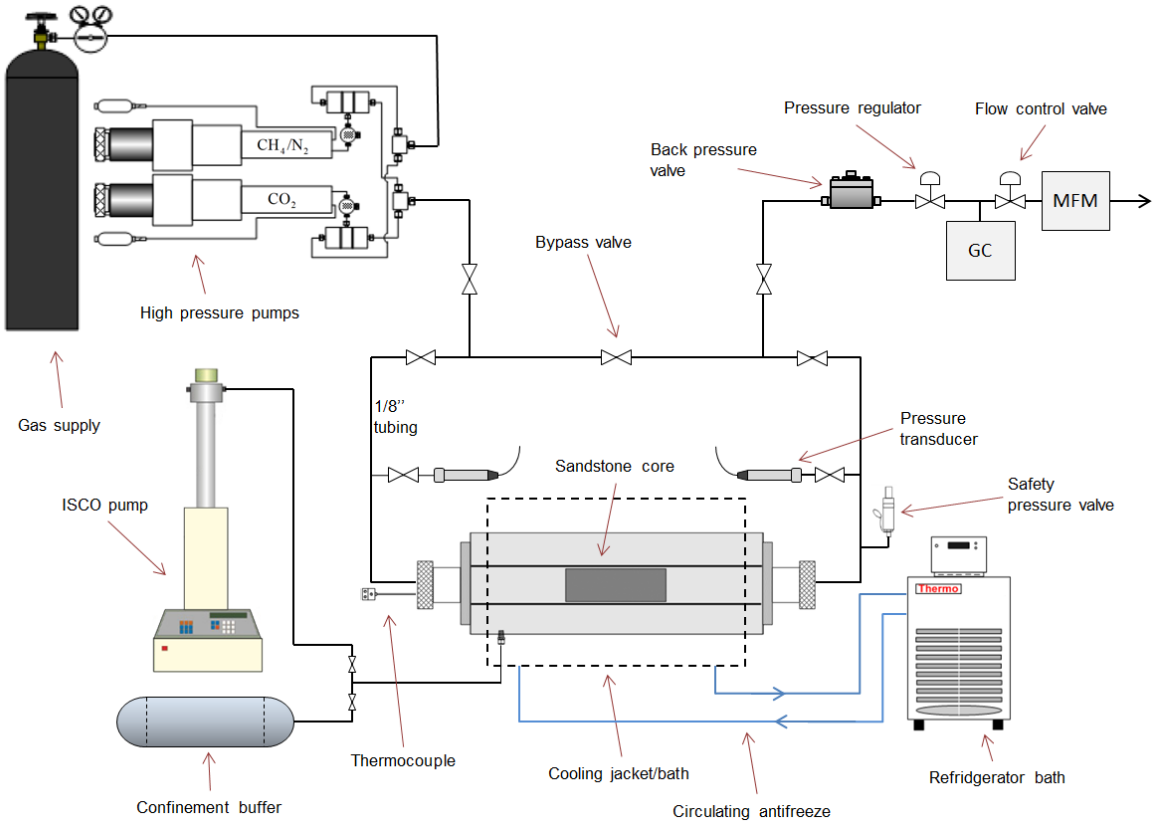

Figure 3.1.1 – General hydrate set-up, representing set-up A, B and C. Confinement system consisting of an ISCO pump and a buffer. The refrigerator bath circulated antifreeze to control system temperature. The system inlet was connected to two high pressure pumps used for hydrate formation and CO_2/N_2 injection

3.1.1 Experimental set-up A: Resistivity set-up

The resistivity set-up consisted of a core holder coated in a cooling jacked, placed in a rack. Two end pieces were used to distribute the injected fluids at the core ends and to conduct electric current through the sample when measuring resistivity. They were connected to the inlet and the outlet of the system. At the inlet there were two high pressure pumps supplying gas to the system: (1) Stigma 500 (one cylinder), Sanchez Technologies and (2) Quizix Q5200 (two cylinders). All valves, tubings and fittings were replaced as part of the work within this thesis. In addition, the tubing configuration was modified so that so that the pumps were connected to set-up B and C as well. Both pumps could then be used at each of the systems. The system outlet was connected to a Back Pressure Valve (BPV) and a pressure regulator, which were used to reduce the pressure. The BPV was pressurized using a buffer connected to a nitrogen tank. A Gas Chromatograph (GC) was located downstream from the pressure regulator and was used to analyze the composition of the effluent. This was followed by a flow control valve and a CORI-FLOW Mass Flow Meter (MFM) that monitored the effluent mass flow. The purpose of the flow control valve was to maintain a steady flow through the GC and the mass flow meter. However, the mass flow

meter was implemented during the work with this thesis and was therefore not included in all the experiments. The differential pressure across the core was measured by pressure transducers connected to both inlet and outlet, separated by a two-way bypass valve. Set-up A used a floating end piece on one side of the core and it was therefore required to remove the sleeve from the system in order to insert the core. To do so, the system had to be drained of confinement oil for every experiment. Figure 3.1.2 shows a cross section of the core holder. A temperature gauge was located at the outlet end piece in order to monitor the temperature, while the electric resistance was measured across the core with the end pieces connected to a Hewlett Packard LCR-meter. The resistivity was then calculated from the resistance. It was not possible to log the resistivity directly, because when the LCR-meter was connected to a computer which affected the measurements. A camera pointing at the display of the LCR-meter was therefore used to log the resistivity data.

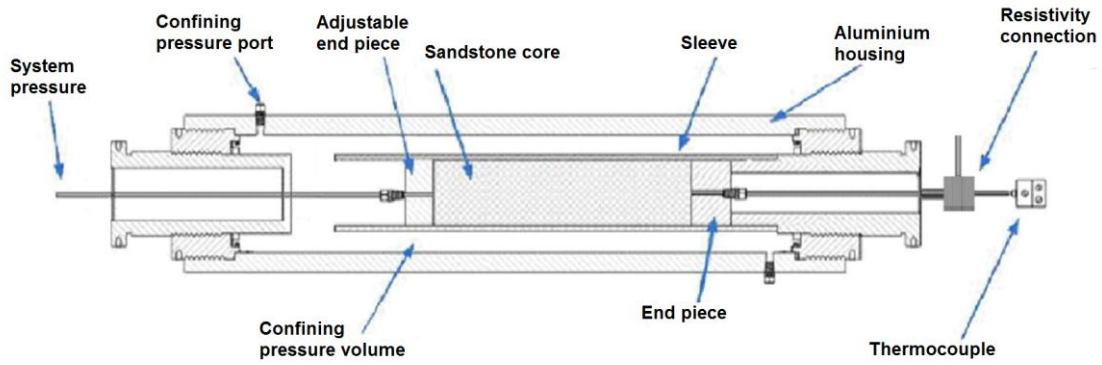

Figure 3.1.2 – Cross section of the core holder in set-up A, including confinement volume, adjustable end piece and a 2-pin resistivity connection. Modified from Birkedal et al. (2011)

3.1.2 Experimental set-up B: General Set-up

In set-up B, the hydrate formation was measured only from gas consumption logs, temperature and pressure. The set-up consisted of a standard Hassler core holder coated by a cooling jacket and mounted in a rack. In this set-up the sleeve was fixed within the core holder, allowing the confinement oil to remain in the system when the core was removed. Figure 3.1.3 shows a cross section of the core holder. The valve and tubing system was renewed and constructed in the same way as in set-up A. The system inlet was connected to the same two high pressure pumps as set-up A and the outlet was also connected to the GC and MFM. Another modification made on this set-up was the implementation of temperature gauges at the system inlet and outlet, as well as in the confinement oil. This was done because the temperature measurements were required in numerical hydrate simulations.

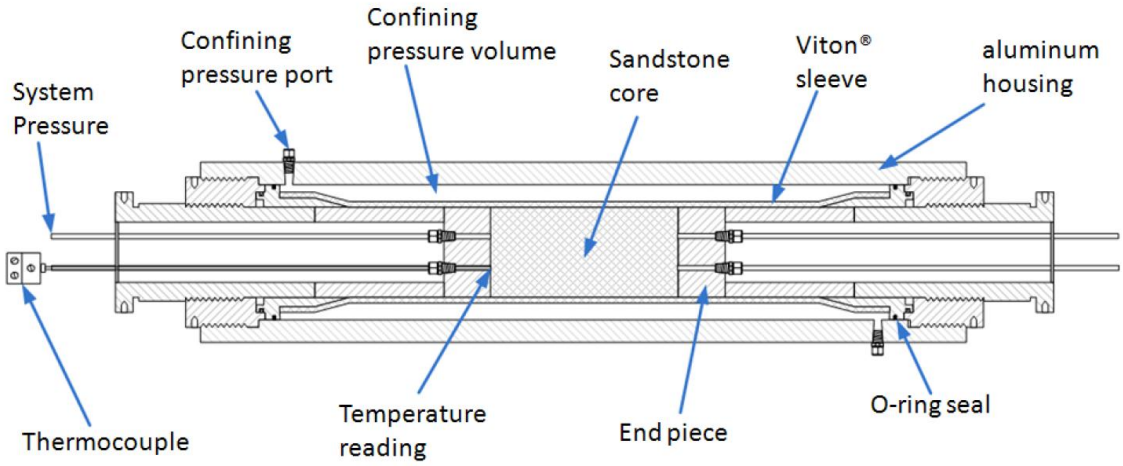

Figure 3.1.3 – Cross section of the core holder used in set-up B and C, including confinement volume and temperature gauge (Husebø, 2008)

3.1.3 Experimental set-up C: Temperature set-up

Set-up C was used in one of the experiments and comprised the same valve and tubing configuration as set-up A and B. It consisted of a standard Hassler core holder with a fixed sleeve within it. However, the core holder was originally placed in an open cooling bath instead of cooling jacket. This had the advantage of cooling a larger part of the tubing than the cooling jacket, but the core holder had to be removed from the cooling bath in order to replace the core and start a new experiment. The cooling bath was therefore replaced with a cooling jacket so that the system became identical to set-up B. This set-up was primarily used in experiments where the CO_2 injection was conducted at temperatures above 4 °C.

3.1.4 Confinement and cooling system

In order to pressurize the core samples, a confinement pressure larger than the pore pressure was required. In the first couple of experiments performed in this study, the confinement oil was pressurized using Haskell pumps. During the experimental work in this thesis, the entire confinement system was modified. The new confinement system was supporting all set-ups and included an Isco D-series pump and a buffer. The Isco pump was used to increase confinement pressure, while the buffer maintained the pressure once pressurized. N_2 was used to keep the pressure in the buffer. A three way valve was implemented in the set-ups to switch between the pump and the buffer. The new confinement system was able to keep the confinement pressure within a few bars from the set point compared to the Haskell pump, which caused pressure fluctuations in the range of 10 bars. It was also quicker to refill confinement oil in set-up A when a new experiment was initiated. The buffer could easily be repressurized either by using the Isco pump or with the nitrogen tank.

In set-up A and B the core holder was coated by a cooling jacket. The cooling jackets were connected to a shared refrigerated bath, called Thermo Neslab RTE-17, which circulated antifreeze through the systems to maintain the desired temperature of 4.0 ± 0.6 °C. The cooling system could supply antifreeze to either one of the set-ups or both of them. In all experiments hydrate formation was initiated by reducing the temperature in the refrigerated bath. The refrigerator bath is presented in the general system set-up in Figure 3.1.1. In set-up C, the core holder was originally situated in an open cooling bath and connected to its own refrigerated bath, as described in chapter 3.1.3.

3.2 Experimental procedures

Most of the experiments performed in this study comprised of hydrate formation, CO_2/CH_4 exchange and hydrate dissociation within Bentheim sandstone, with the exception of some experiments involving depressurization of pure methane hydrate in a porous media. The experiments were conducted to mimic production scenarios from natural hydrate reservoirs. Figure 3.2.1 shows a simple illustration of the three stages in a general experiment performed in this thesis. Methane (CH_4) and brine was used to form hydrate within the core samples, while liquid carbon dioxide (CO_2) was used in the injections. In some of the experiments, nitrogen (N_2) was used to dissociate hydrate plugs and to prevent further hydrate formation. According to The National Institute of Standards and Technology (2013), methane and nitrogen exist within supercritical state at the current experimental conditions (8.3 MPa and 4° C). However, for convenience they are referred to as gases, because there are no significant changes in density or viscosity as they go from gaseous to supercritical state.

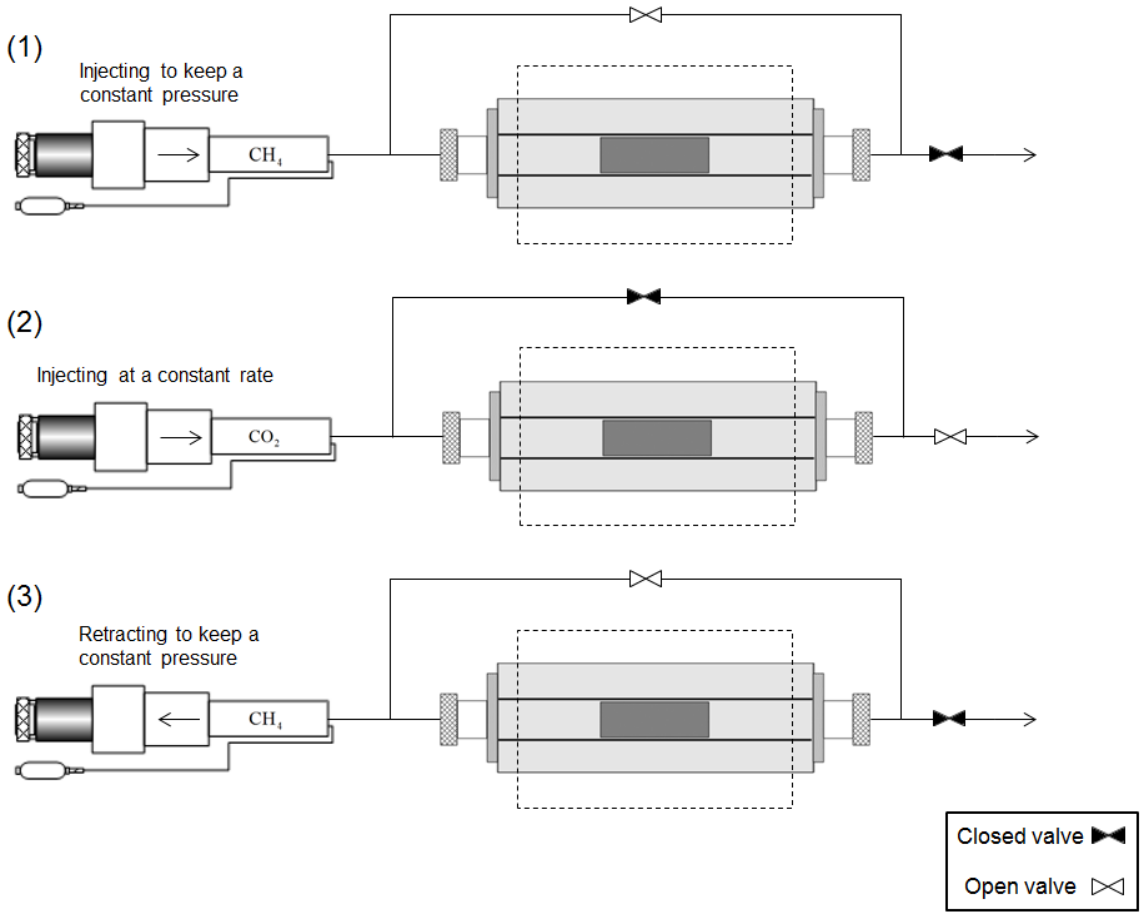

Figure 3.2.1 – A simplified illustration of the three different stages in a general hydrate experiment. (1) Hydrate formation: The pump injects methane to keep the pressure constant as hydrates form, (2) CO_2 injection: CO2 is injected at a constant rate with the bypass closed, and (3) Dissociation: The pump is retracting to receive the produced gas from the dissociation. In the single steps depressurization, the bypass was closed

3.2.1 Properties of the core samples

Due to the cost of natural reservoir cores, outcrop cores are usually used in laboratory experiments. In this study, the experiments have been conducted using Bentheim sandstone, which is an outcrop rock from Germany. Bentheim sandstone is considered a relatively homogeneous rock consisting mainly of quartz (99 %). It has a grain density of 2.65 g/cm^3, porosity around 20-25 % and a permeability of approximately 1.1 Darcy (Graue et al., 2006b). The core samples used in this study were cut into approximately 5 cm diameter and 14 cm length. Figure 3.2.2 shows an example of a Bentheim sandstone core used in the experiments.

Figure 3.2.2 – Whole Bentheim sandstone core, cut into approximately 5 cm diameter and 14 cm length

3.2.2 Preparing and saturating the core samples

The Bentheim sandstone cores were placed in a heating cabinet for one day to remove any water present. Then it was cooled down to room temperature and the dry weight was registered before it was saturated. This was conducted to minimize water evaporation after the core had been saturated. The brine was prepared using distilled water with added salt (NaCl). Brine salinities of 0.1 wt% NaCl and 3.5 wt% NaCl were used. Two different methods were applied to saturate the core samples in this study, depending on the saturation goal of the experiment. In the experiments featuring initial water saturations above 70 %, the cores were evacuated, using a vacuum pump, before exposed to the brine. This resulted in water saturations close to 100 %. The cores were then wrapped in paper and evacuated until the saturation goal was reached. The saturation was calculated by measuring the final weight of the saturated core. In the experiments with initial water saturations below 65 %, the cores were submerged in brine allowing the capillary forces to imbibe water into the pores. Then the cores were wrapped in paper and evacuated in the same manner as the first method. The evacuation resulted in evenly distributed brine throughout the core, which improved the hydrate distribution as well. To protect the sleeves from CO_2, the cores were wrapped in a layer of plastic foil and a layer of aluminum foil before they were placed in the core holders. In the experiments including a spacer, the core was cut in half and saturated in the same way as explained above. A POM spacer was placed between the core halves before they were wrapped in plastic and aluminum as shown in Figure 3.2.3.

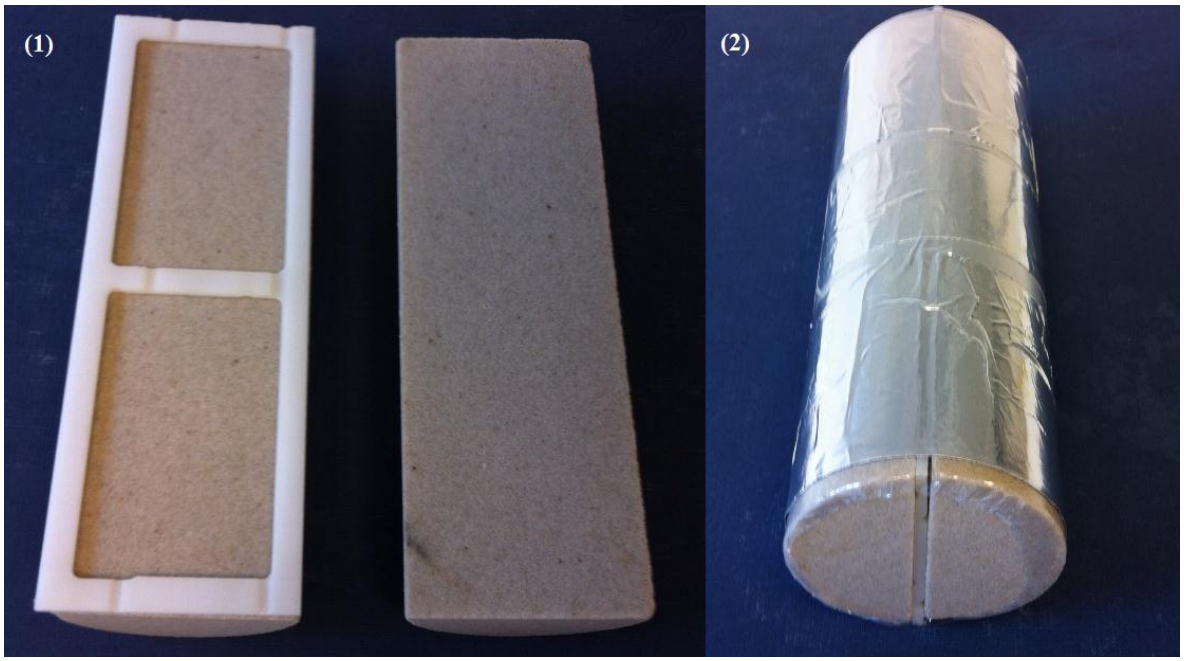

Figure 3.2.3 – Preparing core with fracture, held open by a spacer. (1) The two saturated core halves and the spacer. (2) The core halves, wrapped in plastic and aluminum foil, with the spacer in between

3.2.3 Procedures for hydrate formation

After the core had been saturated, prepared and placed in the core holder, it was pressurized to 8.3 MPa using methane. The core was pressurized from both sides by keeping the bypass valve open. The confinement pressure was kept approximately 3.4 MPa above the pore pressure at all times. Then a leakage test was performed for one day, giving estimates of the leakage rate. If the leakage was sufficiently low, hydrate formation could be initiated. This was done by reducing the system temperature to approximately 4 °C. The high pressure pump was used to maintain a constant pressure of 8.3 MPa, so as hydrate formed, the pump compensated for the methane consumption. The methane consumption was measured in order to calculate phase saturations.

3.2.4 Resistivity measurement procedures

In set-up A, resistivity measurements was used as an additional method for hydrate detection. The resistance was measured through the entire core by using an LCR-meter, connected to the end-pieces. The data logging was conducted using a camera pointing at the LCR-meter display in order to avoid electrical disturbances which occurred when the LCR-meter was directly connected to a computer. The resistance (R) was used to calculate the resistivity (R_t) by using equation (1.15). The water saturation could then be calculated from Archie's second law, presented in equation (1.14). As hydrate formed, the salinity of the residual water increased, affecting the measured resistance. This was taken into account in

the calculations by using a relationship between resistance and salinity obtained from R_0 measurements conducted by Hauge (2011) and Birkedal (2011).

3.2.5 Procedures for CO_2 injection

The primary goal of these experiments was to investigate the production scenario involving CO_2/CH_4 exchange and how the presence of excess water would affect the process. The CO_2 injections were conducted using two different methods: (1) Continuous injection and (2) Diffusion driven injection. The first method was performed by closing the bypass valve and injecting CO_2 at a constant rate of 1.2 ml/h using a high pressure pump, while the system outlet was kept at a constant pressure with a back pressure valve set to approximately 8.5 MPa. The Gas Chromatograph (GC) took fluid samples out of the produced fluid flow and analyzed its composition, while the Mass Flow Meter (MFM) measured the effluent mass flow. In the experiments with high initial water saturations ($S_{wi} > 0.6$), a mixture of CO_2 and N_2 was used in order to prevent additional hydrate formation and loss of injectivity. The injection kept going for approximately five days.

The second method, called diffusion driven injection, was performed by injecting CO_2 at higher rates in order to quickly displace the free methane present in the core. The injection was conducted as subsequent flushes instead of a continuous injection. The GC was used to monitor the composition of the produced fluids, while the Mass Flow Meter measured the mass flow. Approximately one pore volume of CO_2 was injected during a flush. Then the core inlet and outlet was closed and the core was left without any pressure support for approximately one week in order for the exchange process to take place. After this, a second CO_2 flush was conducted. This was performed in order to recover the produced methane from the exchange process and to supply the system with additional CO_2 to keep the exchange going.

3.2.6 Procedures for hydrate dissociation

After the CO_2 exchange was completed, the core was flooded with methane and the hydrate was dissociated. This was done by using one of three different methods: (i) Multiple steps depressurization, (ii) Single step depressurization and (iii) Thermal dissociation. The multiple steps depressurization method was applied in order to decide the dissociation pressure of the mixed CO_2/CH_4 hydrate, and thereby estimate its composition. It was performed by reducing the pressure stepwise from both sides of the core and measuring the amount of gas produced. Gas production indicated hydrate dissociation and was correlated to the composition of the hydrate by using CSMGem (Sloan and Koh, 2008). Dissociation was expected at several pressure steps, because the hydrate contained a mixture of CO_2 and CH_4. The second method, single step depressurization, was used on both mixed and pure CH_4 hydrate. The method was based on depressurization from one side of the core and was primarily used in order to obtain data for numerical simulations. After the core had been

flushed with methane, the pressure was slowly reduced to a pressure above the dissociation pressure of pure methane hydrate in order to minimize the impact of temperature change during pressure reduction. When the pressure and temperature had stabilized, the pressure was further reduced to an adequate pressure below the dissociation pressure of pure methane hydrate, with the bypass valve closed. The pump was set to maintain a constant pressure while monitoring gas production, differential pressure and temperature. A third method, referred to as thermal dissociation, was applied in one of the experiments. This method involved thermal dissociation by increasing the temperature of the refrigerator bath to 20 °C while the pump was set to keep a constant pressure. As a result of this, the core was radially heated by the circulating antifreeze and the hydrate was dissociated. Gas production, temperature and pressure were measured during the process. The reason for using several methods of dissociation was related to time consumption and the data quality of the different methods. The multiple steps depressurization method had the advantage of obtaining a dissociation pressure of the mixed hydrate, and thereby its composition. However, the method was time consuming and resulted in a large span of dissociation pressures due to the heterogeneous mixture of CO_2 and CH_4 hydrate. Single step depressurization and thermal dissociation was quick and easy to perform compared to the multiple steps depressurization. The two methods resulted in hydrate dissociation curves that could be used to compare the rate of hydrate dissociation as well as the total gas volume produced during dissociation.

Chapter 4 - Results and discussion

The majority of the previous experimental research on CO_2 injection in hydrate bearing sediments has been conducted in simplified systems containing hydrate and gas. In nature, gas hydrates will in general exist in the presence of excess water. The injection of CO_2 will risk additional hydrate formation and severe loss of injectivity. As part of the work with this thesis, a series of experiments were conducted in order to investigate how the presence of excess water would affect formation and CO_2 injection in hydrate bearing sandstone. The first couple of experiments were performed as baseline cases, featuring low initial water saturations (S_{wi} ~ 0.4). These were followed by three experiments where the initial water saturation was increased (S_{wi} ~ 0.65) in order to achieve water in excess. After multiple successful CO_2 injections, the initial water saturation was further increased (S_{wi} > 0.7) in the following experiments. However, these experiments were conducted in fractured cores, held open by a spacer. This was done to minimize injection problems expected at such high water saturations. In addition, a single experiment (DEP5) was performed to investigate multiple hydrate formations and dissociations in a whole core and to obtain data for numerical simulations. In this chapter, the experimental results are presented and discussed in the same order in which most of the experiments have been conducted: Hydrate formation, CO_2 injection and depressurization. CH_4 recovery and CO_2 sequestration are presented and discussed in individual chapters. Table 4.1 shows an overview of the experiments performed in this study. All experiments except CO2-20 were performed at 8.3 MPa and 4 ± 0.6 °C in Sandstone cores. In CO2-20, the hydrate formation was performed at 4 ± 0.6 °C, while the CO_2 exchange took place at 9.4 ± 0.6 °C. The table features the initial water saturation and salinity, as well as final water and hydrate saturations. Methane recovery is also included in the experiments where it was possible to calculate it.

Table 4.1

Overview of the experiments performed in this study including initial and final properties of the core samples

Name	Core	Injection	Salinity [wt %]	S_{wi} [frac]	S_h [frac]	S_{wf} [frac]	Temp [°C]	R_{CH4} [%]	Comments
CO2-20	Whole	CO2	0.1	0.42	0.53	0.04	9.4	-	Melted
CO2-25	Whole	CO2	0.1	0.41	0.51	0.05	4.3	45.2	
HR47	Whole	CO2	3.5	0.42	0.38	0.12	4.0	-	Plugged
HR48	Whole	CO2	3.5	0.40	0.42	0.08	4.0	22.8*	
HR49	Whole	CO2 + N2	3.5	0.64	0.46	0.29	4.0	26.1*	
HR50	Whole	-	3.5	0.65	0.47	0.28	4.0		Leakage
HR51	Whole	CO2 + N2	3.5	0.67	0.51	0.27	4.0	61.5	
HR52	Spacer	CO2	3.5	0.74	0.35	0.47	4.0	29.5	Plugged
HR53	Spacer	-	3.5	0.81	0.41	0.50	3.6	-	Plugged
DEP5	Whole	CO2	0.1	0.43	0.46	0.06	4.0	-	Plugged

* Recovery calculated without mass flow meter

4.1 Hydrate formation

The core preparation and hydrate formation was performed according to the procedures described in chapter 3.2. The gas consumption as a function of time was the major parameter used to describe the formation process and calculating saturations. In addition to this, resistivity measurements were used as an additional method of hydrate detection. Figure 4.1.1 shows an example of a hydrate formation performed in this thesis. It is presented as the cumulative volume methane consumed, electrical resistivity measured through the core and the temperature at the core surface. The initial increase in gas consumption and resistivity is a direct result of the cooling process. This was followed by a period of induction time, which is the time span from when the system reaches the hydrate stability region until a detectable amount of hydrate is observed (chapter 1.1.5). During the period of induction time, no methane is therefore consumed. The starting point of the hydrate formation was detected as a rapid increase in gas consumption. A small increase in temperature as well as a drop in resistivity was also observed in several of the experiments. This is further discussed in chapter 4.1.2. The rate of hydrate formation was initially high and decreased over time as water was consumed in the process. Eventually, the consumption curve flattened out and the formation was completed. The gas consumption could then be used to calculate fluid saturations by using the hydration number, introduced in equation (1.1). The methane consumption during cool down and as a result of leakages was deducted in the calculations. The gas consumption curves for the hydrate formations performed in this thesis are presented in Figure 4.1.5 for the experiments with low initial water saturation (S_{wi} ~ 0.4) and Figure 4.1.4 for the experiments with a high initial brine salinity (3.5 wt%).

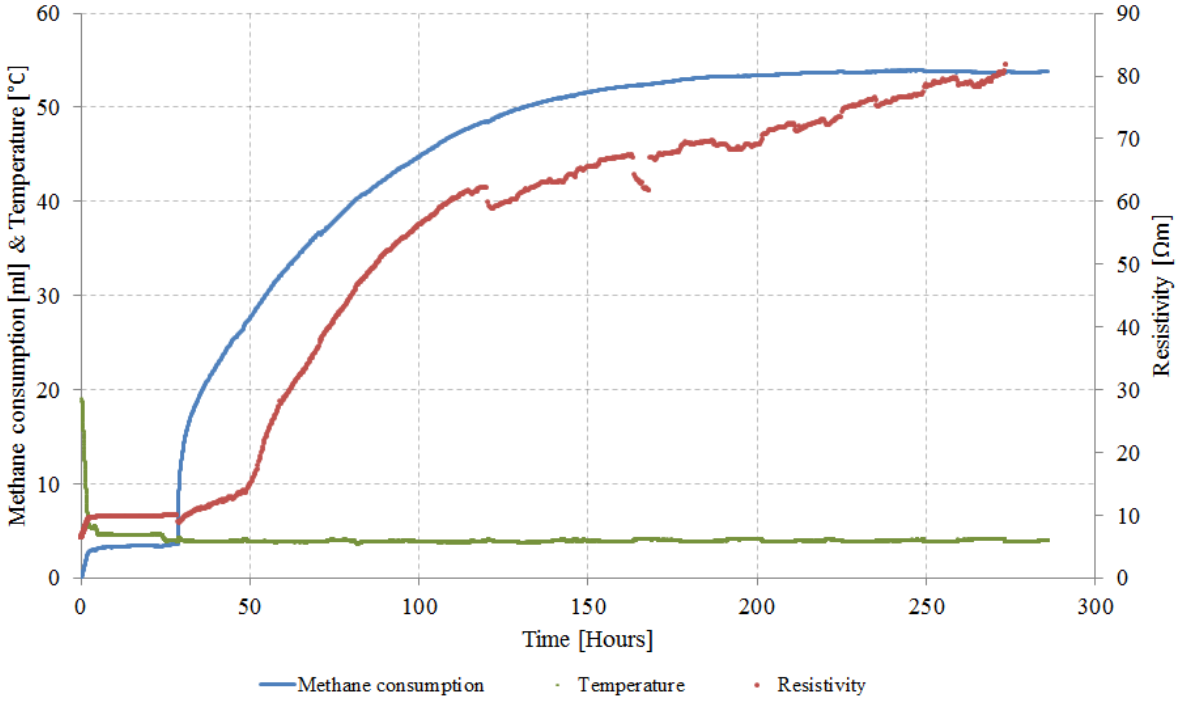

Figure 4.1.1 – Hydrate formation curve for HR 50 showing methane consumption, resistivity and temperature. Pump delivering constant pressure at 8.3 MPa and temperature reduced to 4 ± 0.6 °C to initiate hydrate formation. Initial water saturation at 0.646 and 3.5 wt% brine salinity

4.1.1 Effect of water saturation on hydrate formation

Methane hydrate was successfully formed in sandstone cores at various initial water saturations, resulting in final water saturations up to 50 %. Note that these systems are actually excess gas systems with free water present. Table 4.1 presents both initial water saturation and final hydrate saturation for the experiments conducted in this thesis. The hydrate saturation was found to be highest in experiments conducted at intermediate initial water saturations (S_{wi} ~ 0.5-0.6). At low initial water saturations, the hydrate formation seemed to be constrained by water availability and salinity, while at fairly high initial water saturations (S_{wi} > 0.7), the hydrate formation seemed to be limited by the available contact surface between water and gas. This may happen as the water reduces the available pore space for gas to occupy. However, HR52 and HR53 both contained fractured cores, held open by a spacer. If hydrate initially formed near the fracture, it could reduce the gas supply to the areas further away from the fracture. In Figure 4.1.2, the final hydrate saturation is presented as a function of initial water saturation for a series of experiments performed at the University of Bergen, including the experiments conducted in this thesis. The data is acquired from the in-house database, presented in Appendix B. Large variations within the final hydrate saturation can be observed for experiments conducted at similar initial water saturation. However, the hydrate saturation trend line seems to increase with initial water saturation until it reaches its maximum (S_{wi} ~ 0.5-0.6) where it starts to decrease.

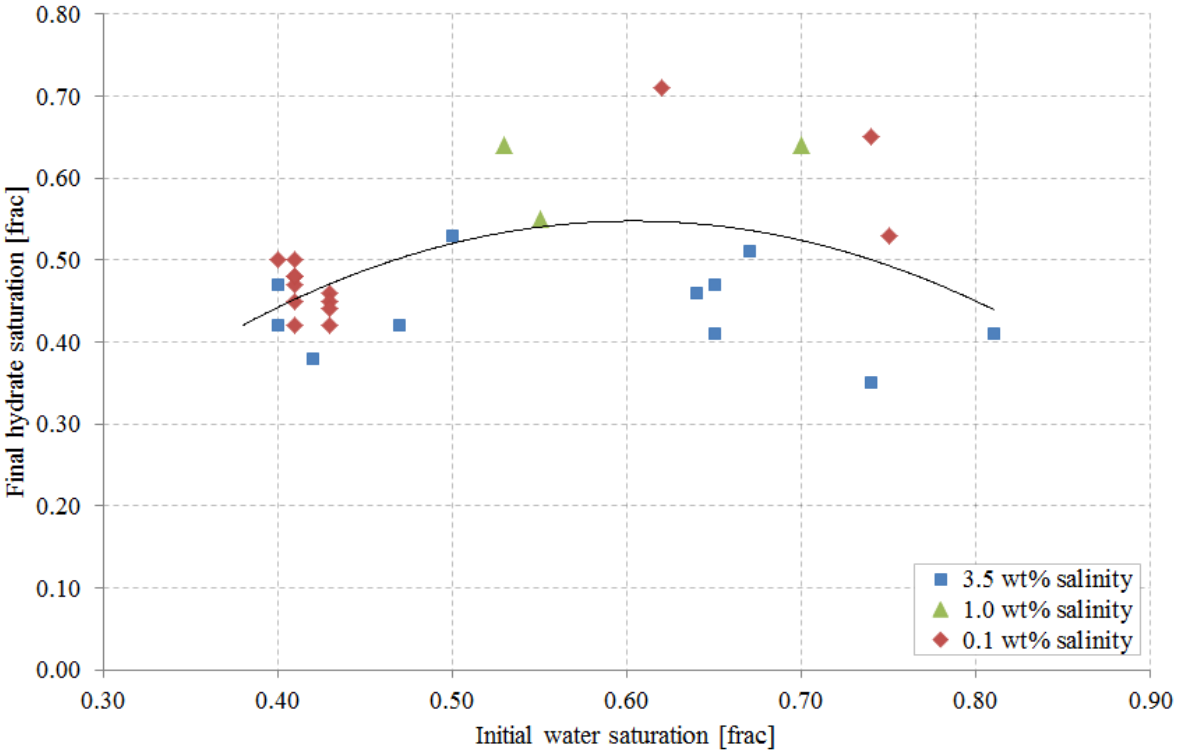

Figure 4.1.2 – Final hydrate saturation as a function of initial water saturations for a series of experiments performed at the University of Bergen, included the experiments conducted in this thesis. Data acquired from in-house database (Hauge, 2013). 2nd order polynomial trend line displayed for all experiments

In Figure 4.1.3, the final water saturation is presented as a function of the initial water saturation for the same experiments presented in Figure 4.1.2. The results demonstrate that the amount of water in excess after hydrate formation increases with initial water saturation. Similar results was also obtained by Hauge et al. (2012). It seems like increasing water saturation reduces the available contact interface where hydrate may form and thereby increase the amount of water in excess after hydrate formation. The majority of the excess water will then be present as metastable pore water (chapter 1.3.5). In the experiments with low initial water saturations however, most of the water is consumed in the hydrate formation. The residual water will therefore consist mainly of equilibrium pore water (chapter 1.3.5) where further hydrate formation is constrained by salinity. CSMGem calculations have showed that hydrate formation is inhibited at salinities above 14 wt% at the current experimental conditions. It can be observed that the final water saturations are generally higher for experiments conducted at 3.5 wt% brine salinity. Note that the final water saturation reaches zero for some of the low salinity experiments. This is probably a result of uncertainties related to leaks and assumptions made in the calculations. The uncertainties are presented and discussed in chapter 4.6. CO_2 may form additional hydrate with both metastable- and equilibrium pore water because it is the preferred guest molecule compared to methane at the current conditions. However, risk of additional hydrate formation and loss of injectivity will be more comprehensive at higher final water

saturations. The largest fraction of excess water was obtained in HR53, with a final water saturation of 0.50 and a hydrate saturation of 0.41. For comparison, the water saturation in Ignik Sikumi was estimated to be approximately 0.25, based on well logs (Schoderbek et al., 2012).

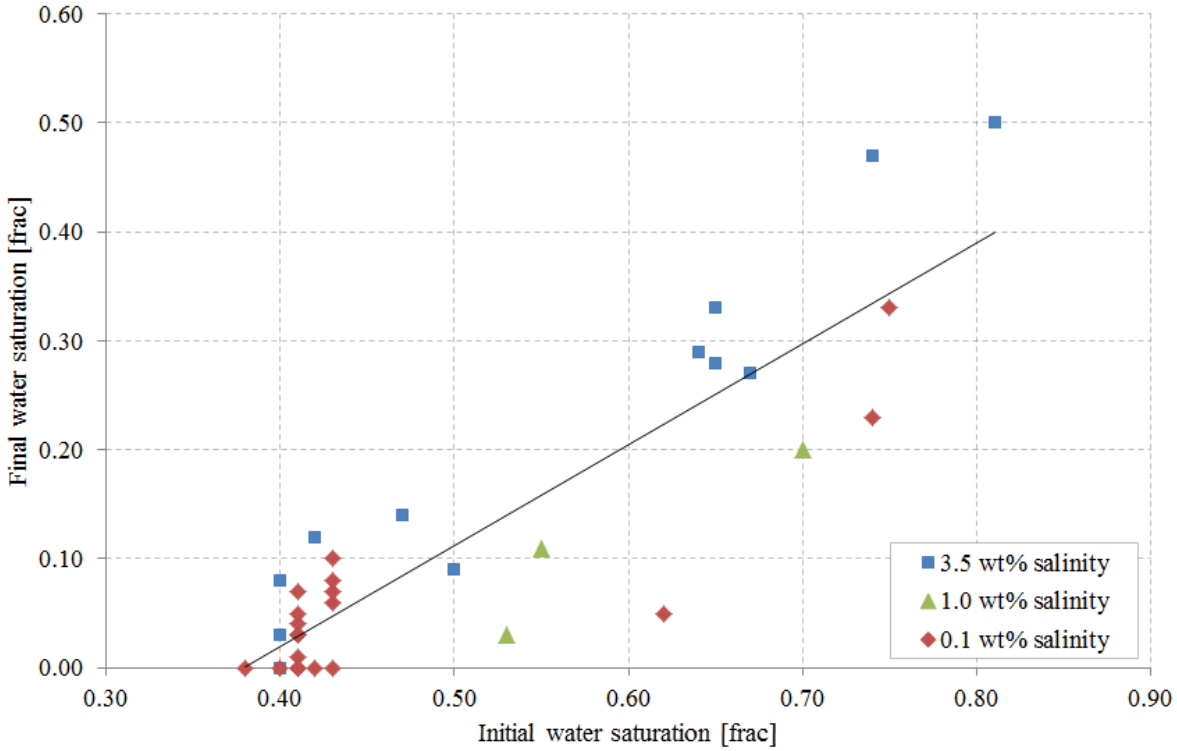

Figure 4.1.3 – Final water saturation as a function of initial water saturation for a series of experiments performed at the University of Bergen, included the experiments conducted in this thesis. Data acquired from in-house database (Hauge, 2013). A linear trend line is displayed for all the experiments

Figure 4.1.4 shows methane consumption as a function of time for the experiments conducted with 3.5 wt% initial brine salinity. The majority of the formation curves start out at a high consumption rate that decreases over time. The exception is HR51, where the consumption rate decreases until approximately 40 hours, where it starts to increase again. The same phenomena was observed by Birkedal (2009) in an experiment with high initial water saturation (~0.6). He explained it by methane diffusion through the core during the experiment, resulting in improved gas distribution and thereby increased reaction interface. This could be a result of an initial heterogeneous water distribution. Hauge et al. (2012) did also investigate this phenomena and found that it was more prominent at low brine salinities (0.1 wt% NaCl). Daily temperature variations resulted in fluctuations in gas consumption for some of the experiments. This was especially prominent in HR53 (Figure 4.6.1).

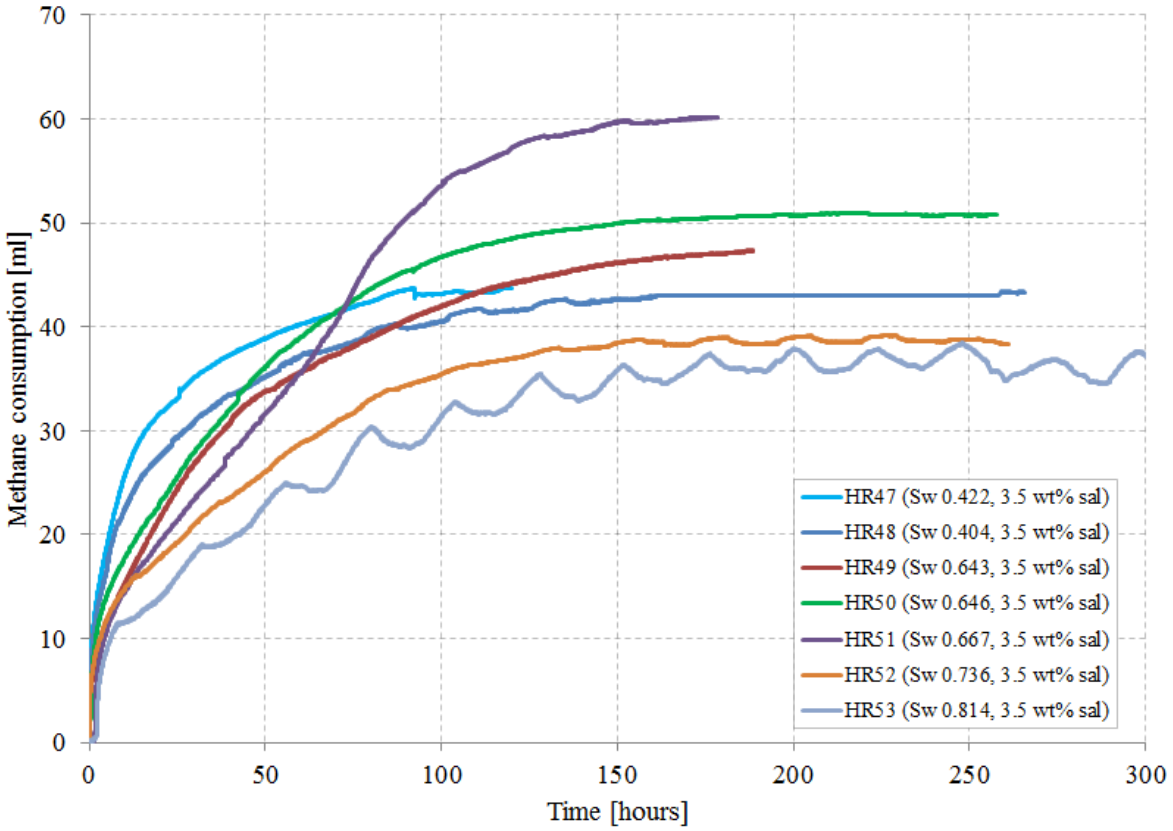

Figure 4.1.4 – Methane consumption as a function of time during hydrate formation in the experiments featuring high initial brine salinity (3.5 wt% NaCl initially). The experiments were performed at varying initial water saturations. The fluctuations in methane consumption for HR53 is a result of variations in room temperature

4.1.1 Salinity impact on hydrate formation

The effect of brine salinity on hydrate formation in Sandstone has previously been investigated by Ersland (2008), Husebø (2008) and Birkedal (2009). They found out that hydrate forms faster at lower brine salinities and that the induction time increases with brine salinity. They also found that the salinity limits the hydrate formation if it becomes high enough. In this thesis, the experiments were performed at respectively 0.1 wt% and 3.5 wt% NaCl brine. Figure 4.1.5 shows methane consumption as a function of time during hydrate formation in the experiments featuring low initial water saturation (< 0.5). HR47 and HR48 had an initial brine salinity of 3.5 wt% NaCl, while DEP 5, CO2-20 and CO2-25 had 0.1 wt% NaCl. It can be observed that both the initial methane consumption rate and the total consumption are higher for the low salinity experiments. The general shape of the consumption curves is also affected by salinity. In the low salinity cases, the consumption increases rapidly before it flattens out, creating a sharp angle in the curves. For the high salinity cases, the slope of the curves decreases more uniformly. However, it should also be noted that DEP 5 is a single experiment, consisting of four hydrate formations and

dissociations, and should not be evaluated as four individual experiments. Still, there is a good agreement between the formation curves in DEP 5, CO2-20 and CO2-25.

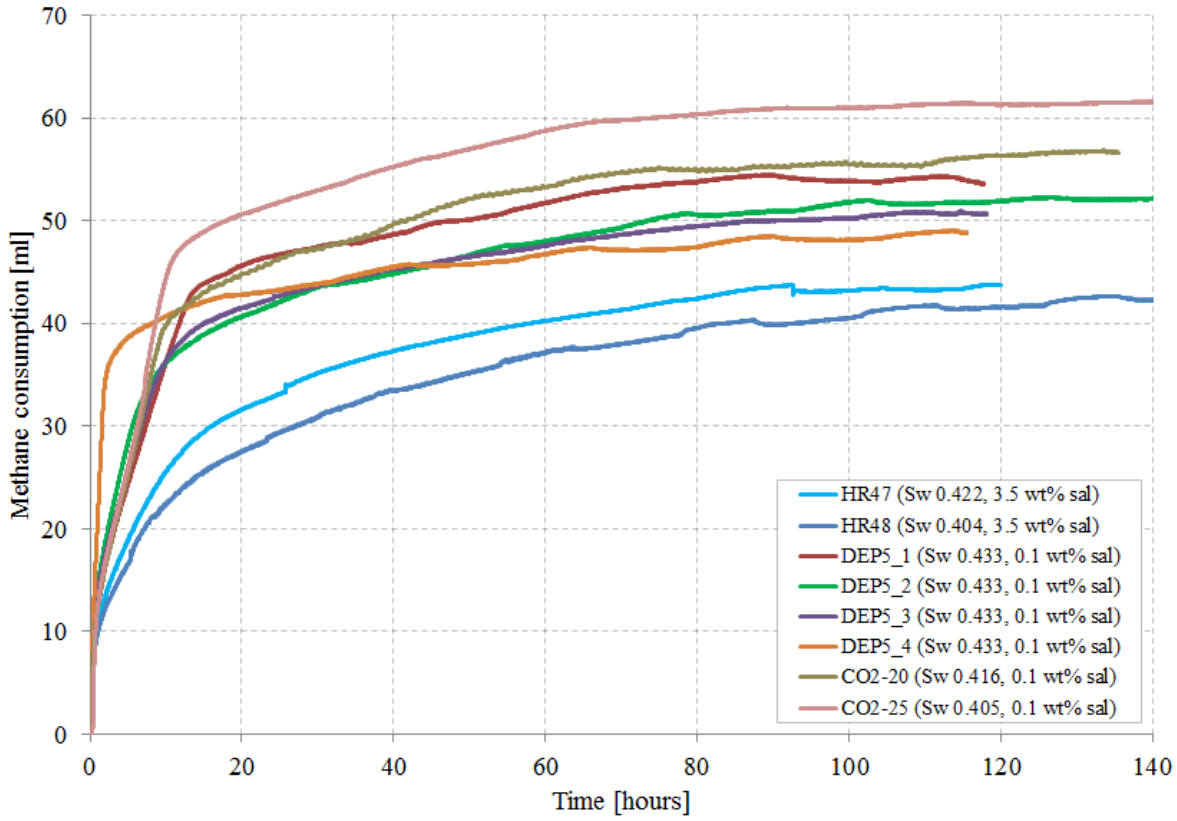

Figure 4.1.5 – Hydrate formation curves for the experiments featuring low initial water saturation. The formation is showed as methane consumed as a function of time. DEP5 is a single experiment including four hydrate formations and dissociations

The average residual brine salinity was obtained from mass balance calculations. As discussed earlier, hydrate formation may be constrained by the salinity of the residual brine, i.e. 14 wt% NaCl at the current experimental conditions. This brine is referred to as equilibrium water, i.e. inactive water. For the experiments conducted at low initial water saturations, the final brine salinity reached 14 wt%, indicating that most of the residual water was present as equilibrium water at the end of the hydrate formation. Table 4.2 shows the salinity before and after hydrate formation for the experiments featuring high initial water saturations (S_{wi} > 0.6). In these experiments, the final water saturations reached values between 0.27 and 0.50 with final salinities in the range of 5.5-8.5 wt% NaCl. This implies that the excess water was primarily metastable pore water, i.e. active water. In addition, the calculated salinities are average values, which implicates that the salinity could be higher in some areas, while lower in others. Knowledge about the final water saturation is important because it may result in loss of injectivity due to hydrate plugging when exposed to CO_2. This is discussed in chapter 4.2.2.

Table 4.2

Brine salinity before and after hydrate formation for the experiments featuring high initial water saturation. Low final salinity and high final water saturation indicates excess water

Name	Initial salinity [wt%]	Final salinity [wt%]	Swi [frac]	Swf [frac]	Sh [frac]
HR49	3.5	7.7	0.64	0.29	0.46
HR50	3.5	8.0	0.65	0.28	0.47
HR51	3.5	8.5	0.67	0.27	0.51
HR52	3.5	5.5	0.74	0.47	0.35
HR53	3.5	5.7	0.81	0.50	0.41

4.1.2 Resistivity response to hydrate growth

Natural gas hydrate can be considered as an electric isolator compared to the formation water (chapter 1.6.1) in a porous rock. Resistivity measurement is therefore a useful method for detecting hydrate growth in sandstone. As water saturation decreases, the resistivity increases. It can therefore be used to calculate hydrate saturation by using Archie's second law, presented in equation (1.14). In this thesis, the experiments denoted by "HR", included resistivity measurements.

In the early stages of the hydrate growth, the resistivity response is less than the response from the gas consumption. This could be explained by the brine connectivity which remains intact at low hydrate saturations. As hydrate forms in the porous media, it may break the continuous water phase (Figure 1.6.1). At higher hydrate saturations, the resistivity measurements will therefore be more sensitive to changes. This can be observed in Figure 4.1.1, where the resistivity starts to fluctuate after approximately 120 hours. Figure 4.1.6 compares the calculated water saturation from mass balance and resistivity during hydrate formation in HR49. The water saturation obtained from resistivity was calculated by using Archie's second law (chapter 1.6.1). Since the electrical conductivity of brine is a function of salinity, a dynamic R_0 was used, taking into account the increase in brine salinity as hydrate forms. Good compliance between the calculated saturations in Figure 4.1.6 supports the application of resistivity logs in hydrate exploration and characterization.

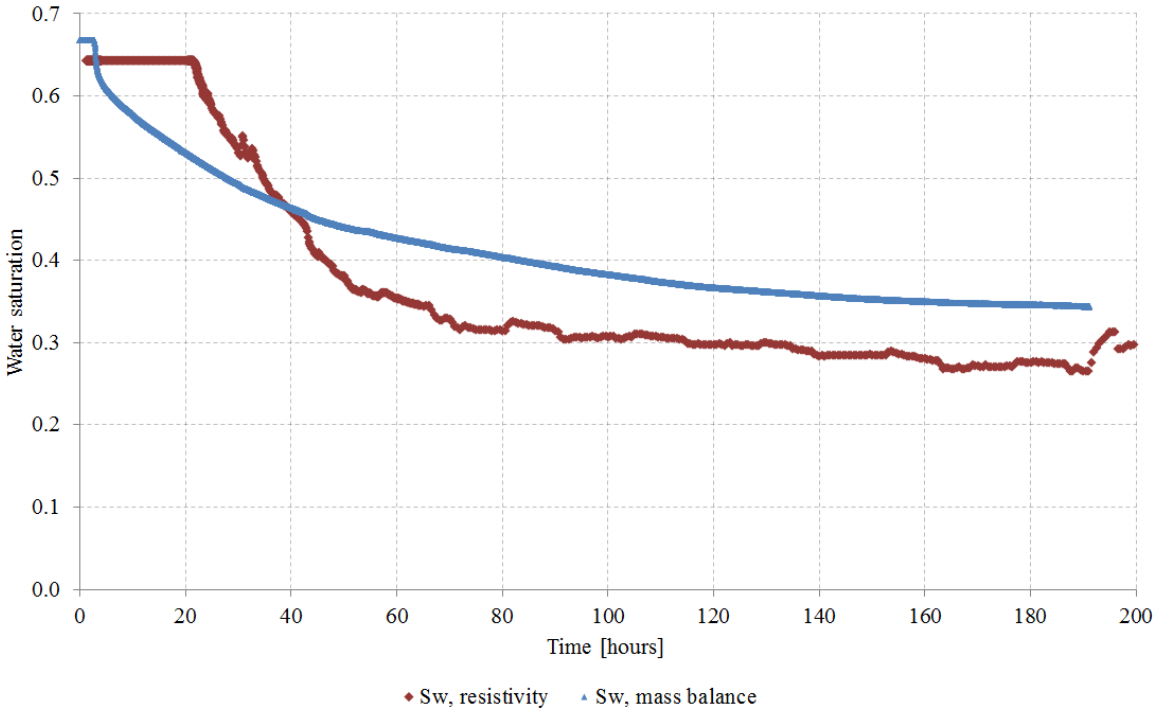

Figure 4.1.6 – Water saturation during hydrate formation in HR49, calculated from both mass balance and resistivity measurements

Figure 4.1.7 shows resistivity measurements as a function of time during hydrate formation in the HR-experiments. The water saturations, before and after hydrate formation, clearly has an effect on the resistivity. It can be observed that the initial resistivity increase is largest in the experiments featuring low initial water saturations (S_{wi} ~ 0.4). This is as expected, because the brine connectivity reduces faster in these experiments than in the experiments featuring higher initial water saturations (S_{wi} > 0.6). In addition, the overall resistivity is lower in the experiments with high water saturations. Another observation that can be made is that most of the resistivity curves continue to increase after hydrate formation. In HR48 however, the curve starts to decrease after the formation is completed. This was a baseline experiment featuring low initial and final water saturations. The same decreasing trend in resistivity can be observed for HR52 and HR53. These experiments featured high initial (S_{wi} < 0.7) and final (S_{wf} > 0.4) water saturations, explaining the overall low resistivity. In addition, the cores used in HR52 and HR53 both contained a fracture, held open by a POM spacer. If hydrate formed near the spacer, it could block the methane supply for hydrate formation further away from the spacer, resulting in a heterogeneous hydrate distribution and low hydrate saturation. Gas hydrates in a porous media is a dynamic system where local dissociation and reformation occur continuously (Kvamme, 2012). This may lead to redistribution of hydrate within the core. This may increase the water connectivity, which could explain the decreasing resistivity behavior. Hydrate redistribution has been observed by Tohidi et al. (2001), using micromodels (Figure 1.3.5) and from X-ray CT images (Rees et al., 2011).

Another important parameter that affects the measured resistivity is the confinement pressure. As discussed in the experimental set-up chapter 3.1.1, the resistivity set-up features a floating end piece system, so when the confinement pressure increases, the end piece is pushed towards the core. This leads to a better connection between the end piece and the core, which again results in a lower resistivity measurement. A drop in confinement pressure would therefore increase the resistivity. To minimize the confinement pressures' effect on resistivity, a buffer was implemented in the confinement system in HR50 and experiments performed subsequently.

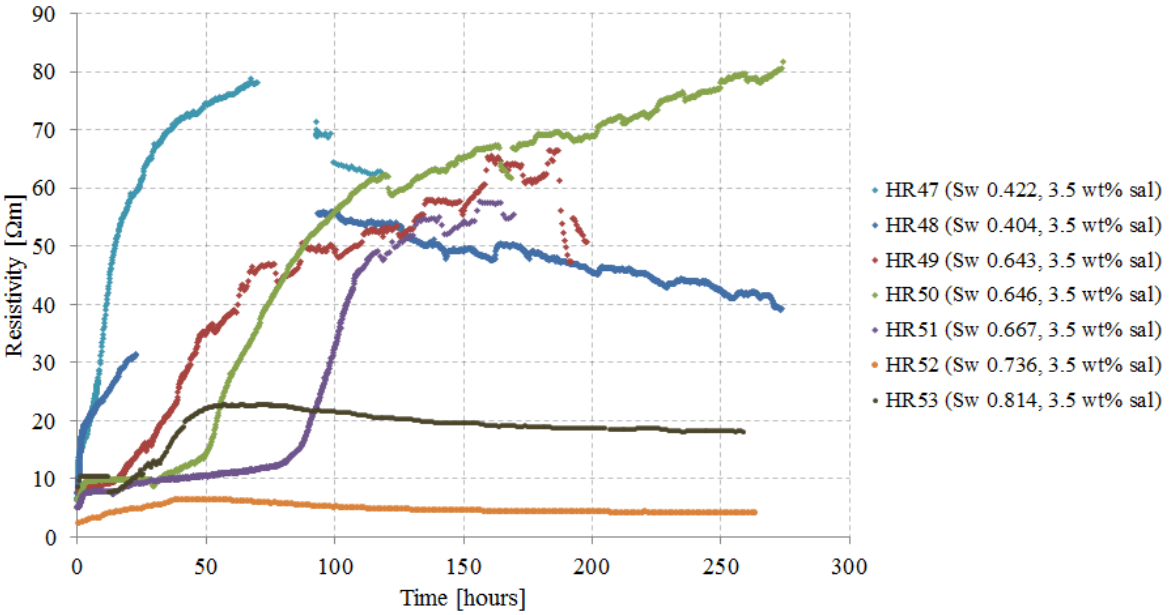

Figure 4.1.7 – Resistivity measurements during hydrate formation. Resistivity is calculated from measured resistance by using equation (1.15). The gap in the HR48 curve is a result of technical difficulties with the LCR meter, while the gap in the HR47 curve is due to loss of confinement pressure

In Figure 4.1.1, a sudden drop in resistivity can be observed as the hydrate growth begins. This drop was observed in all of the experiments featuring resistivity measurements, as well as in earlier studies where hydrate formation has been monitored using resistivity (Birkedal et al., 2011). Birkedal et al. explained the phenomena by the increase in salt concentration at the water-hydrate interface as the hydrate formation begun. However, hydrate formation is an exothermic process, resulting in increased local temperature within the core. This could also contribute to the drop in resistivity and has been observed in the temperature logs in several of the experiments. The temperature and resistivity at the point of initial hydrate growth is presented in Figure 4.1.8 for HR53, where the hydrate formation begun after 12.7 hours, according to the gas consumption logs. At this point, a temperature increase of 0.2 °C and a resistivity drop of 2.82 Ωm were observed. The corresponding changes in temperature and resistivity during cooling were an increase of 3.04 Ωm in resistivity as the temperature decreased with 17 °C. It can therefore be argued that a temperature increase of 0.2 °C does not affect the resistivity significantly. However, it should also be noted that the temperature

is measured at the core surface from the outlet side of the core. A local temperature increase could therefore be higher than the measured value of 0.2 °C.

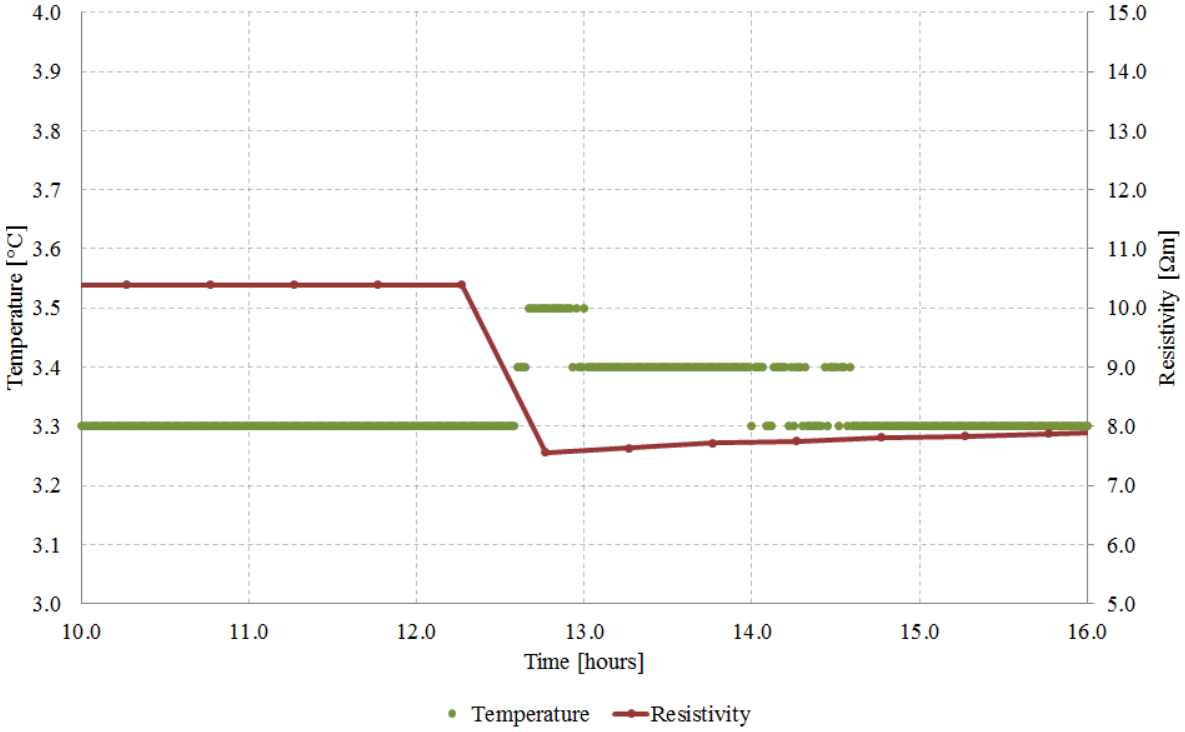

Figure 4.1.8 – Resistivity drop and temperature increase as hydrate formation begins in HR53. Temperature and resistivity as function of time. Hydrate formation begins at 12.7 hours

4.1.3 The "memory effect"

DEP5 consisted of four subsequent hydrate formations and dissociations. The methane consumption curves are displayed in Figure 4.1.9 for the first 20 hours of formation. It shows that the consumption rate is higher in the fourth hydrate formation. This is known as the "memory effect" and is based on the theory that hydrate may form easier from components obtained from hydrate dissociation (Sloan and Koh, 2008). Two opposing explanations have been used to describe this phenomenon: (1) The hydrate structure remains in solution for a time period after the hydrate has been dissociated (Buchanan et al., 2005) and (2) The gas from the hydrate remains in water solution after the hydrate is dissociated (Rodger, 2000). The difference between the dissociations in DEP5 is that the two first dissociations involved depressurization, while the third was conducted as a thermal dissociation. The pressure therefore remained at 8.3 MPa between the third dissociation and the forth formation, leaving a larger quantity of methane in water solution as the solubility of methane is more sensitive to pressure than temperature at the current conditions (Zhenhao and Shide, 2006). This is in compliance with the second explanation of the memory effect. A similar effect has been observed by monitoring hydrate formation and dissociation in sandstone, using NMR. These experiments showed that the water distributed more homogeneously after hydrate had dissociated compared to before hydrate formation

(Ersland, 2013). In the second hydrate formation, the hydrate distribution was therefore improved. This effect may also contribute to the rate of formation and dissociation.

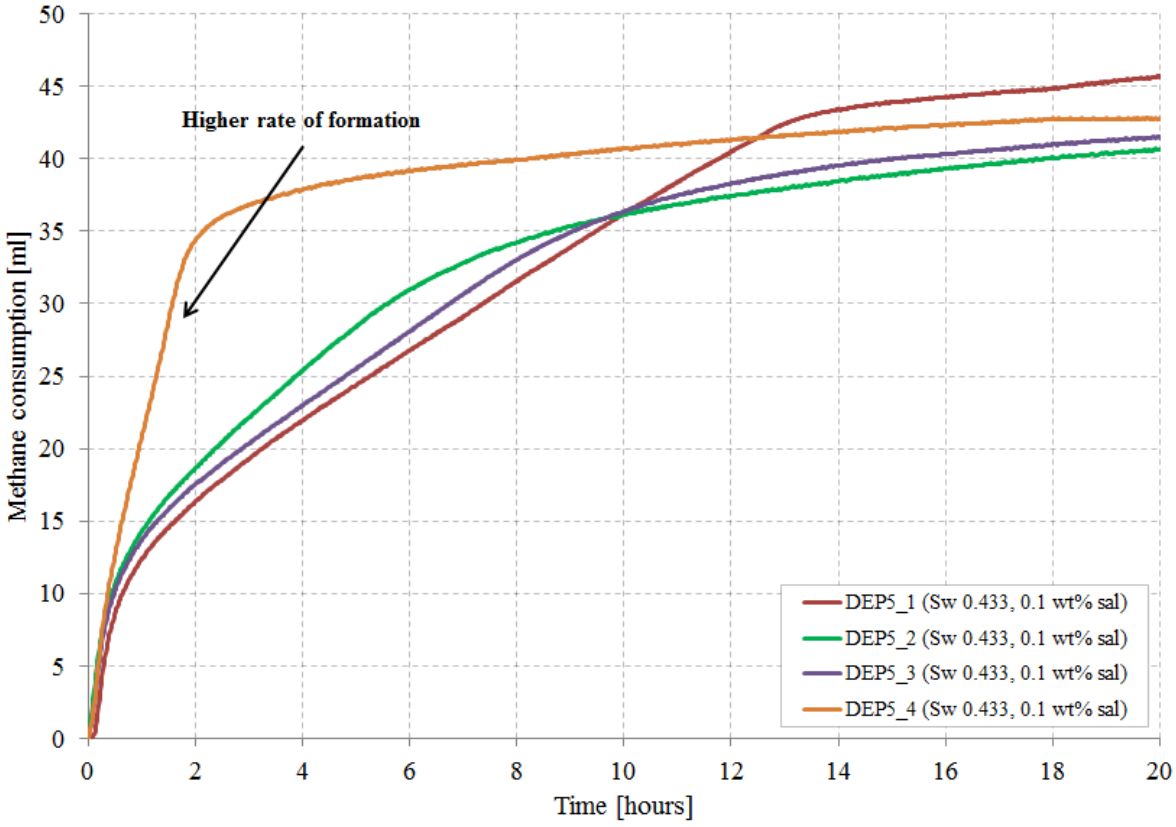

Figure 4.1.9 – Methane consumption as a function of time for the different hydrate formations in DEP5. The rate of consumption is highest for DEP5_4, where hydrate formation was conducted subsequently to a thermal dissociation. The other dissociations were conducted by depressurization

4.2 CO_2 injection into hydrate bearing sandstone

The main goal of this thesis was to investigate how the presence of excess water would affect a production scenario involving CO_2 injection into hydrate bearing sediments, with respect to both injectivity and processes affecting CH_4 recovery and CO_2 sequestration. As discussed earlier, excess water may exist as both metastable- and equilibrium pore water in sandstone containing methane hydrate (chapter 1.3.5). The metastable pore water would form additional hydrate if it came in contact with the methane, while the equilibrium pore water would not. CO_2 and CH_4 have different physical properties, such as density and viscosity. The flow path of CO_2 could therefore be different than for methane and it could contact the metastable pore water. In addition, CO_2 is a better hydrate former than methane at the given experimental conditions (8.3 MPa, 4°C and 0.1-3.5 wt% salinity) and could form additional hydrate with the equilibrium pore water as well. Significant loss of injectivity was therefore expected when CO_2 was injected into hydrate bearing sandstone.

The experiments presented in this chapter were conducted at different initial water saturations in order to investigate how excess water would affect the injection process. It was discovered that the injection of CO_2 into systems with high final water saturation resulted in additional hydrate formation and loss of injectivity. This could be observed by an increase in differential pressure. In some of the experiments, the injectivity was reduced to a point where CO_2 injection was no longer possible and the core was referred to as plugged. To address this issue, nitrogen gas was injected along with the CO_2, working as a hydrate inhibitor at the current thermodynamic conditions. This injections scheme is similar to the full scale reservoir test performed at the Alaska North Slope (Schoderbek et al., 2012).

4.2.1 Injection of CO_2 into systems with low initial water saturation

Five baseline experiments were conducted at initial water saturations around 0.4 and brine salinity of 0.1-3.5 wt% NaCl for comparison. These experiments ended up with final hydrate saturations in the range of 0.38-0.53 and final water saturations between 0.04-0.12. The CO_2 injection was performed as a continuous injection with pure CO_2 in whole sandstone cores. Resistivity was measured during injection in two of the experiments and the Gas Chromatograph (GC) was used to measure the mole fraction of the produced fluids in all of the experiments. One of the experiments contained a mass flow meter (MFM).

Figure 4.2.1 presents the results from the CO_2 injection in HR48. The core had an initial water saturation of 0.404 and an initial salinity of 3.5 wt% NaCl. During the first 24 hours of CO_2 injection, an increase in resistivity can be observed. This could due to additional hydrate formation as CO_2 contacted the excess water. As CO_2 hydrate forms, the brine connectivity is reduced and the resistivity increases. After 24 hours the resistivity started to decrease and continued to do so until the end of the injection. This indicates either hydrate melting or redistribution. The resistivity followed the same trend as in the end of the hydrate formation, showed in Figure 4.1.7. The resistivity seemed to stabilize at approximately 20 Ωm. Based on the argument of hydrate redistribution, this will occur as the water reaches a maximum connectivity at the given saturation. The injection pressure was stable during the entire injection, indicating adequate permeability, while the temperature graph contained some minor fluctuations as a result of changes in room temperature.

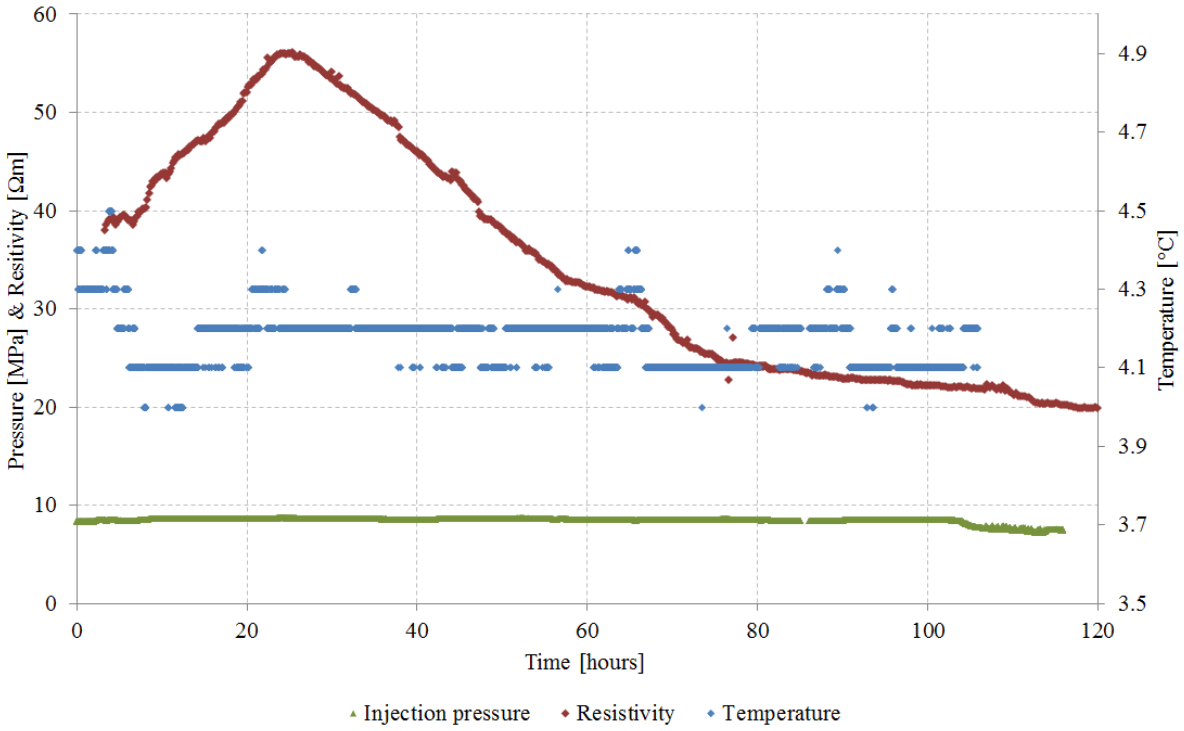

Figure 4.2.1 – Temperature, injection pressure and resistivity as a function of time during CO_2 injection in the baseline experiment HR48, featuring initial water saturation of 0.404 and initial salinity of 3.5 wt% NaCl.

The effluent gas composition during CO_2 injection was measured using the Gas Chromatograph (GC). The GC data from the injection in HR48 are presented in Figure 4.2.2 as mole fraction effluent as a function of pore volumes injected. Production started after approximately 0.1 pore volumes (PV) injected, as the outlet pressure reached the BPV pressure. Mostly CO_2 was produced initially because the inlet and outlet tubing was flushed with CO_2 prior to injection. The methane composition increased with time until it reached a maximum value after approximately 0.35 PV injected. The same behavior can be observed for the nitrogen. Since the only nitrogen present in the system was from the air originally in place in the core, this indicates methane production from the core. The injection continued for approximately 100 hours.

In the experiment CO2_20, the CO_2-injection was performed at 9.4 ± 0.6 °C to investigate the effect of temperature on the exchange process. This has previously been studied by Bringedal (2011) who found that the exchange process was more favorable at 10 °C than at 4 °C. In CO2_20, pure CO_2 was injected at a constant rate of 1.2 ml/h using a high pressure pump. However, during the injection, the refrigerator bath stopped and caused the hydrate to dissociate. The injection could therefore not be completed and the experiment was terminated.

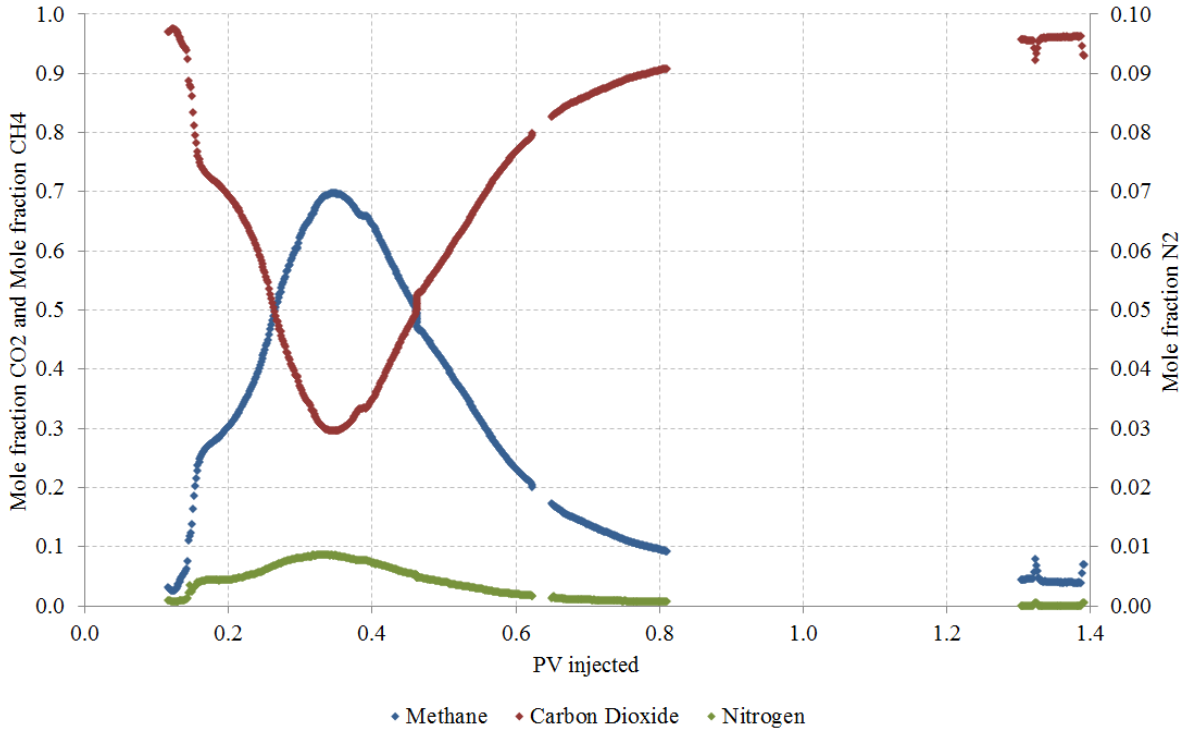

Figure 4.2.2 – Mole fraction of CH_4, CO_2 and N_2 during CO_2 injection in HR48. The GC connection was lost between 0.8 and 1.3 PV injected. Note that the mole fraction of N_2 is presented on the secondary axis and is very low compared to the fractions of CH_4 and CO_2. The GC data starts at 0.1 PV injected at the time when the outlet pressure reached the BPV pressure and production started

CO2-25 was conducted as a baseline experiment at an initial water saturation of 0.41 and 0.1 wt% NaCl. In this experiment, both mass flow and composition were measured. The GC data from CO2-25 are presented in Figure 4.2.3 as a function of pore volumes CO_2 injected. The rear side of the system was flushed with CO_2 prior to injection, explaining the initial high CO_2 mole fraction. The associated N_2 production indicates that free gas from the core is produced. After approximately 0.7 PV injected, the methane mole fraction flattens out at 0.15 and continues to decrease at a lower rate instead of dropping down to zero. This may be explained by methane production as a result of CO_2 exchange. Technical problems with the pressure regulating valve resulted in a gap in the GC data after approximately 1.7 PV injected.

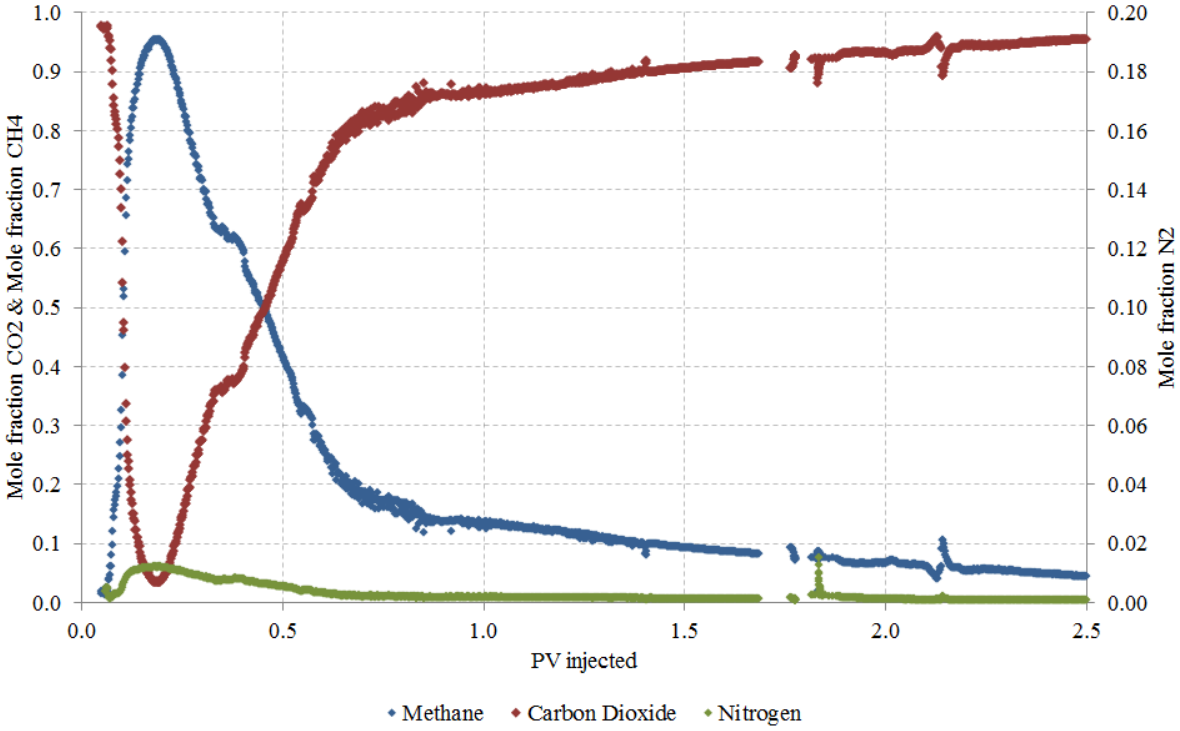

Figure 4.2.3 – Mole fraction of CH_4, CO_2 and N_2 during CO_2 injection in CO2-25. There is a gap in the curve at 1.7 PV injected as a result of troubles with the pressure regulator valve. BPV breakthrough occurred after 0.05 PV injected. Note that the N_2 mole fraction is presented on the secondary axis

HR48 and CO2-25 were experiments conducted at similar conditions, e.g. initial water saturation (S_{wi} ~ 0.4), pressure (8.3 MPa) and temperature (4 ± 0.1 °C). The CO_2 injection was also performed as a continuous injection at 1.2 ml/h in both experiments. However, the salinity of the brine was different between the two. A comparison of HR48 and CO2-25 could therefore provide useful information about how salinity affects the methane production. Figure 4.2.4 shows the mole fraction of CH_4 during the first 1.4 PV injected in HR48 and CO2-25. Good agreement between the curves can be observed. However, the graph for CO2-25 increases quicker and reaches a higher value than HR48. This could be a result of salinity, either from the salinity impact on the hydrate saturation and distribution or as a direct effect on the exchange process. Another explanation could be that CO_2 reacts with the excess water and form additional hydrate because the final water saturation is higher in HR48 than in CO2-25 due to higher salinity.

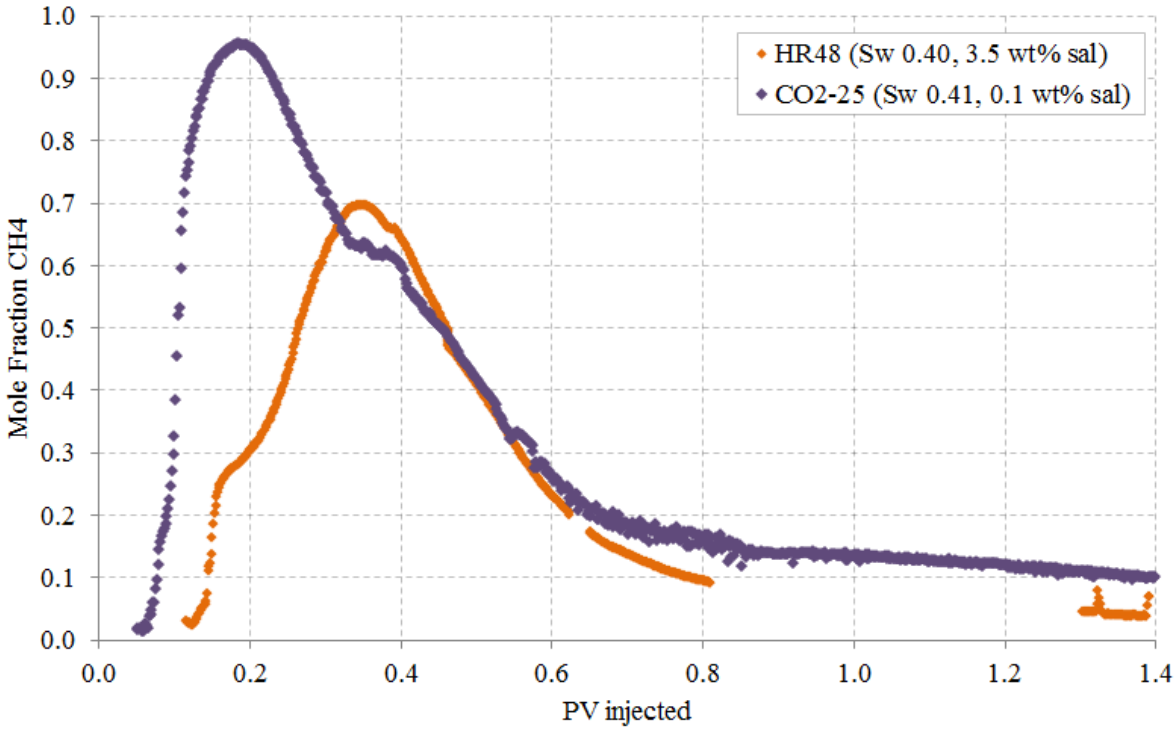

Figure 4.2.4 – Comparing mole fraction of CH_4 produced during the first 1.4 PV CO_2 injected in HR48 (0.40 S_{wi}, 0.42 S_H, 0.08 S_{wf}, 3.5 wt% sal) and CO2-25 (0.41 S_{wi}, 0.51 S_H, 0.05 S_{wf}, 0.1 wt% sal)

4.2.2 Hydrate plugs as a result of CO_2 injection

CO_2 injection in hydrate bearing sandstones could lead to additional hydrate formation with the excess water. This could result in loss of injectivity and plugging of the core. If water is present in the end piece tubings, hydrate plugs could also form within the tubing or at the end piece surfaces. Plugging can be detected as an increase in differential pressure during injection, as the flow through the core is constrained by the plug, resulting in a pressure increase at the inlet side. Differential pressure is defined as the difference between the inlet pressure and the outlet pressure. It is however hard to distinguish between a plug in the tubing and a plug in the core. Resistivity measurement is a way to distinguish between these two. Hydrate formation within the tubing will not alter the resistivity, because the steel tubing is a very good conductor compared to the brine. Formation in the core however, results in an increase in resistivity as the brine connectivity is expected to be low. Another method that can be used to determine the location of a hydrate plug is the pressure logs. The pressure build up would be slower for a plug situated within the core or the outlet tubing than at the inlet.

HR47 was a baseline experiment with an initial water saturation of 0.42 and an initial salinity of 3.5 wt% NaCl. After hydrate formation was completed, continuous injection of pure CO_2 was conducted at a rate of 1.2 ml/h. After the injection had started, the differential pressure increased until the safety pressure of the pump was reached, indicating plugging. It was assumed that the plug was located within the tubing. Several attempts to dissociate the

plug using thermal heating were performed, without success. CO_2 injection could therefore not continue and the experiment was terminated.

DEP5 was another experiment that resulted in plugging. It consisted of four hydrate formations and dissociations in a sandstone core featuring an initial water saturation of 0.43 and an initial brine salinity of 0.1 wt% NaCl. After the forth hydrate formation, CO_2 injection was conducted. This was carried out as a "diffusion driven injection", described in the experimental procedures, chapter 3.2.5. Figure 4.2.5 shows the pressure- and temperature log for the injection. CO_2 was injected at a constant rate of 30 ml/h. Both injection- and production pressure increased simultaneously until the pressure of the BPV was reached. The differential pressure remained low until around 0.8 hours elapsed. Then the injection pressure started increasing, indicating plugging of the core. The injection rate was reduced, but the injection pressure continued to increase. As the differential pressure reached approximately 1 MPa, the injection was stopped and the pump was set to maintain 9.5 MPa on the inlet side in attempt to re-establish flow through the core. After some time, the pressure support at the injection side was removed by closing the inlet valve. As a result of this, the injection pressure decreased and ceased at the production pressure. An explanation to this behavior could be that when the pump was either injecting or maintaining pressure on the inlet side, the hydrate in the pores was pushed towards the pore throats, blocking the flow path. As the pressure support was removed, the hydrate could move away from the pore throat, regaining the relative permeability of the gas.

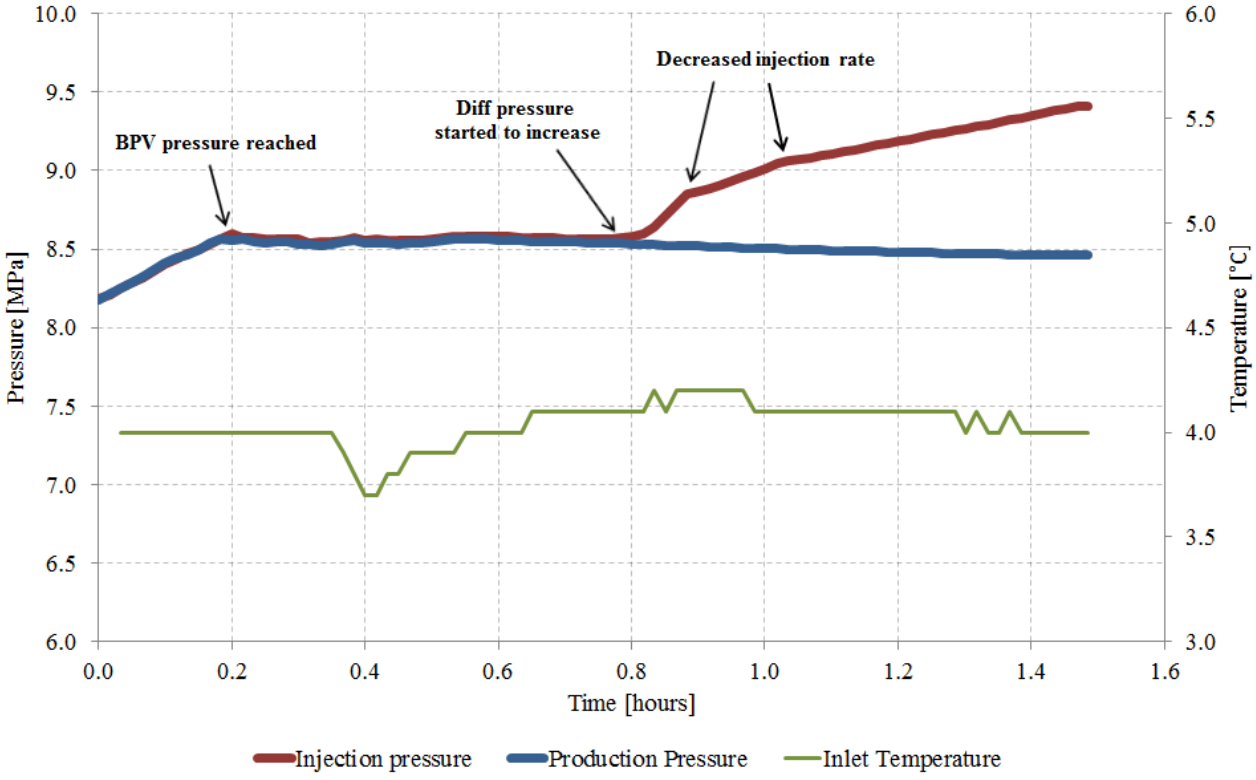

Figure 4.2.5 – Injection pressure, production pressure and inlet temperature during the first CO_2 flush in DEP5. After 1.5 hours, the differential pressure had reached 1.0 MPa and the injection was stopped

When the differential pressure had equalized, a second CO_2 flush was conducted. Both inlet and outlet pressure was reduced to 8.45 MPa before the injection started. The injection- and production pressure, as well as the volume CO_2 injected are presented in Figure 4.2.6. CO_2 was injected at a constant rate of 12 ml/h and kept going for approximately 20 minutes before the differential pressure started to increase. The injection was stopped as it kept increasing. The inlet valve was closed, and the injection pressure dropped immediately, similar to the behavior in the first flush. The injection was started for the second time, at a lower rate, but the differential pressure increased at once. After 1.53 hours elapsed, the injection was stopped and the inlet valve was shut. Like in the previous attempts, the differential pressure dropped to zero. In a third attempt of injecting CO_2, the injection kept going until the inlet pressure reached 9.10 MPa. The outlet valve was closed and the pump was set to keep the pressure constant in order to see if the production pressure increased. No significant change in production pressure was observed during this time period. After approximately 2.6 hours elapsed, the inlet valve was shut and the injection pressure started to decrease immediately. However, this time it decreased slower than previously.

The data in Figure 4.2.6 supports the hypothesis that the movement of hydrate within the pores affects the relative permeability of the gas. However, the theory assumes that the hydrate is plugging the core, not the tubing. In this experiment there are no resistivity measurements, and it is therefore difficult to determine whether the hydrate is plugging the core or the tubing. Still, the CO_2 injection was running for some time before the initial increase in differential pressure was observed. In addition, the pressure build up is relatively slow at such high injection rate (30 ml/h). These arguments support the theory that CO_2 gradually form hydrate with the excess water, which eventually lead to plugging of the core.

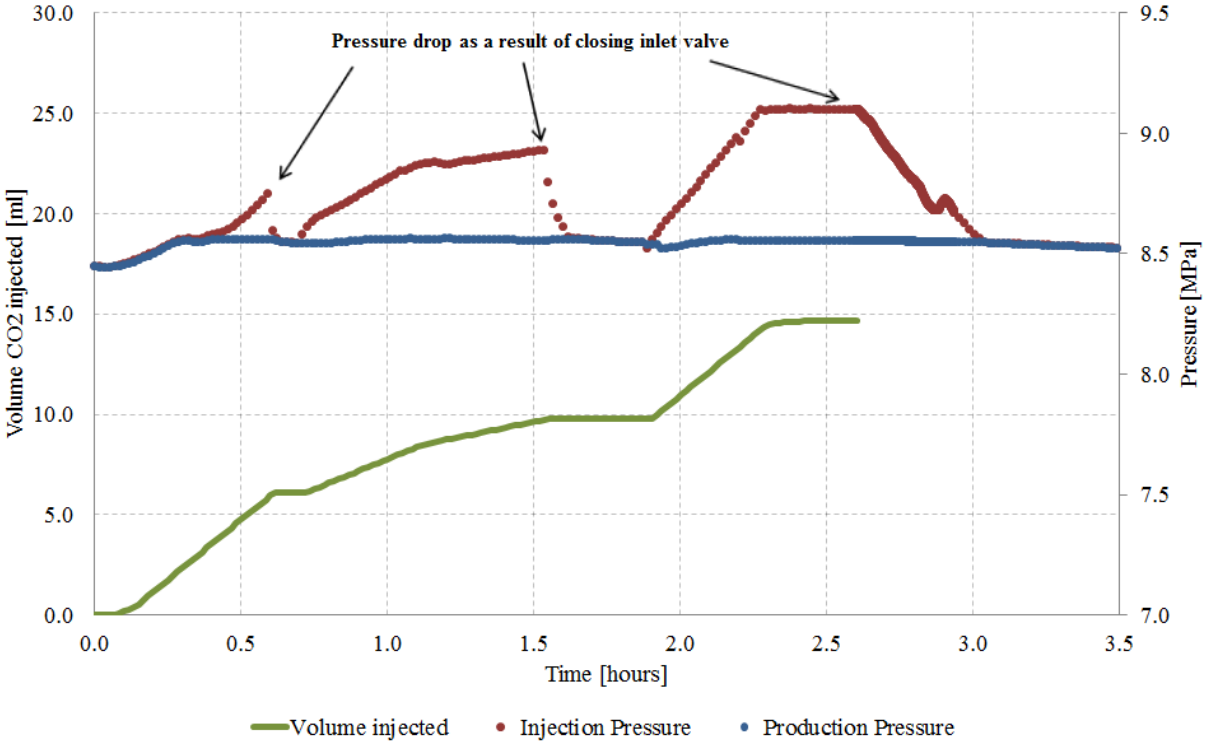

Figure 4.2.6 – Injection pressure, production pressure and volume CO_2 injected in the second CO_2 flush in DEP 5. The injection was performed to investigate the decrease in differential pressure as the pressure support was removed

After the system had been taken down, it was discovered that the CO_2 had damaged the sleeve, which may have resulted in leakage of confinement oil into the core or gas into the confinement volume. However, no traces of confinement oil were observed at the core surface. When the confinement oil was drained after the experiment was terminated, a significant amount of gas was released from the oil, indicating that leakage of gas into the confinement volume had occurred. In addition, the core was broken across the middle, as showed in Figure 4.2.7. The fracture was not likely caused by the confinement pressure, because the orientation of the fracture was perpendicular to the stress exerted by the confinement oil. Local differential pressure as a result of hydrate plugging the core offers a plausible explanation to this phenomenon. The fracture could also be a result of multiple hydrate dissociations or physical stress as the core was removed from the core holder.

Figure 4.2.7 – Broken core in DEP5. Local differential pressures due to hydrate plugging offers a plausible explaination for the fracture

Another example where hydrate plugging prevented injection was HR53, which consisted of a fractured core, held open by a POM spacer, featuring high initial water saturation (S_{wi} - 0.81). The core contained a relatively large amount of excess water. When CO_2 injection started, the differential pressure increased immediately. The resistivity, injection- and production pressures are presented as a function of time in Figure 4.2.8. The injection rate was reduced from 0.50 ml/h to 0.25 ml/h after 0.08 hours in attempt to reduce the differential pressure. It can be observed that the production pressure started to increase slowly beyond this point. In addition, the resistivity increase ceased. However, the injection pressure continued to increase, and after 0.3 hours the injection was stopped and the inlet and outlet valves were shut. After 0.6 hours, the production pressure evened out and the resistivity started to increase again, probably due to further plugging. Since HR53 contained a spacer, it is not likely that the plug was situated within the core. The quick response in injection pressure indicate plug at the inlet side. However, the increase in resistivity indicates that the plug was not located in the tubing either. It is therefore reasonable to argue that hydrate formed at the inlet end piece surface, blocking both fluid flow and electrical communication. This may be due to the high initial water saturation that could have resulted in water adsorption on the end piece surfaces.

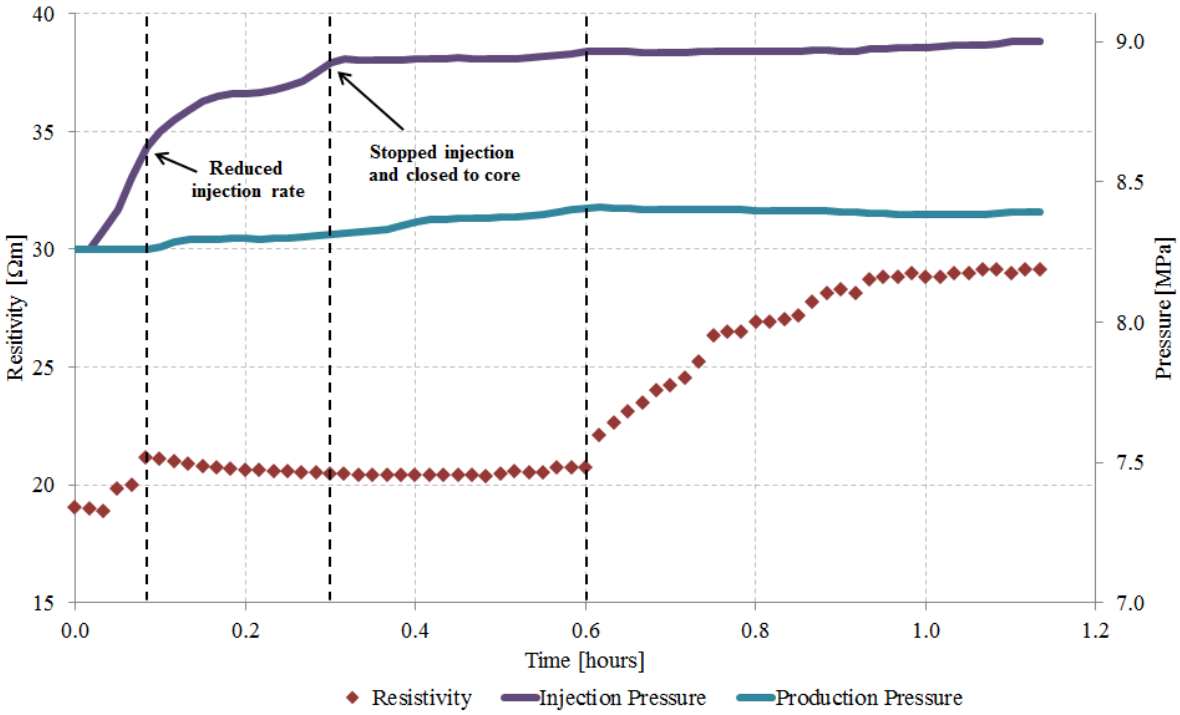

Figure 4.2.8 – Hydrate plug during CO_2 injection in HR53. Resistivity, injection- and production pressure as a function of time

4.2.3 Re-establishing flow in a plugged core by injecting nitrogen

In the following experiments, the initial water saturations were increased ($S_{wi} > 0.6$) in order to achieve higher final water saturations (S_{wf}). The hydrate formations were conducted according to procedures within Bentheim sandstone cores and resulted in final water saturations between 0.28-0.50. As mentioned earlier, excess water is generally present in hydrate bearing sediments found in nature. These experiments could therefore be more representative to real reservoir production scenarios. However, loss of injectivity was expected as a result of additional hydrate formation between the injected CO_2 and the excess water.

HR49 was the first experiment conducted with a significant amount of water in excess (S_{wf} – 0.29). Pure CO_2 was injected at a constant rate in order to review the injectivity of the system. Differential pressure and resistivity is presented in Figure 4.2.9 for the first 250 hours. The figure is divided into a period of CO_2 injection represented by the green line, and a period of N_2 injection represented by the blue line. A rapid increase in differential pressure can be observed during the first couple of hours of injection, indicating loss of injectivity due to CO_2 hydrate formation with the excess water. The inlet pressure exceeded the safety pressure and the injection was stopped. After approximately 66 hours, the CO_2 injection was resumed, resulting in another pressure build up on the inlet side. The outlet valve was shut and the pressure was maintained at 9.0 MPa on the inlet side in order to review the permeability of the core. A significant increase in resistivity can be observed

during this time period, indicating further hydrate formation. This could be a result of both enhanced CO_2 availability and altered driving force due to the increased pressure.

After approximately 142 hours, pure nitrogen was injected in attempt to dissociate hydrate and regain injectivity. Previous experimental results have showed that nitrogen can be used to dissociate hydrate in a plugged core (Masuda et al., 2008, Birkedal, 2009). The pressure was maintained on the inlet side, while the differential pressure was monitored. The core was exposed to nitrogen through three pressure build up tests. A gradually increasing response in differential pressure can be observed for each pressure build up, indicating re-established permeability. These results confirm that nitrogen can be used to regain injectivity in a plugged core.

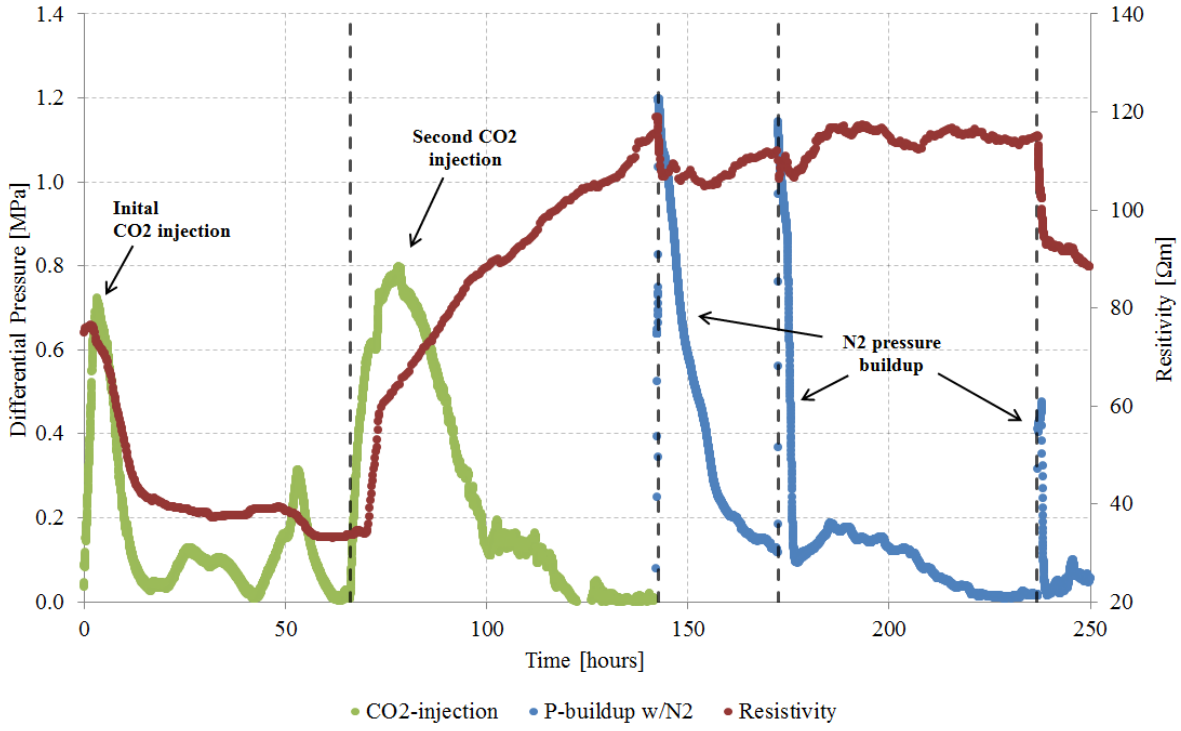

Figure 4.2.9 – Differential pressure and resistivity measurements during the first 250 hours of injection in HR49. The vertical dashed lines represent important events during the injection. The green line represents the differential pressure during CO_2 injection and the blue line during N_2 injection.

To avoid further permeability reduction, the injection was continued with a binary mixture of CO_2 and N_2. The mixture consisted of 75 mole% N_2 and 25 mole% CO_2 and was injected at a total rate of 1.2 ml/h using two high pressure pumps. The co-injection started at 264 hours and kept going for approximately 100 hours. Figure 4.2.10 shows differential pressure and resistivity measurements during the co-injection. The differential pressure, represented by the orange line, remained stable during the entire injection, indicating adequate permeability. The decrease in resistivity is in compliance with the other CO_2 injections performed in this thesis. After the co-injection was completed, an attempt to inject pure CO_2 was performed. This is represented by the green line in Figure 4.2.10 and resulted in a

major increase in differential pressure and resistivity, indicating hydrate formation and loss of injectivity.

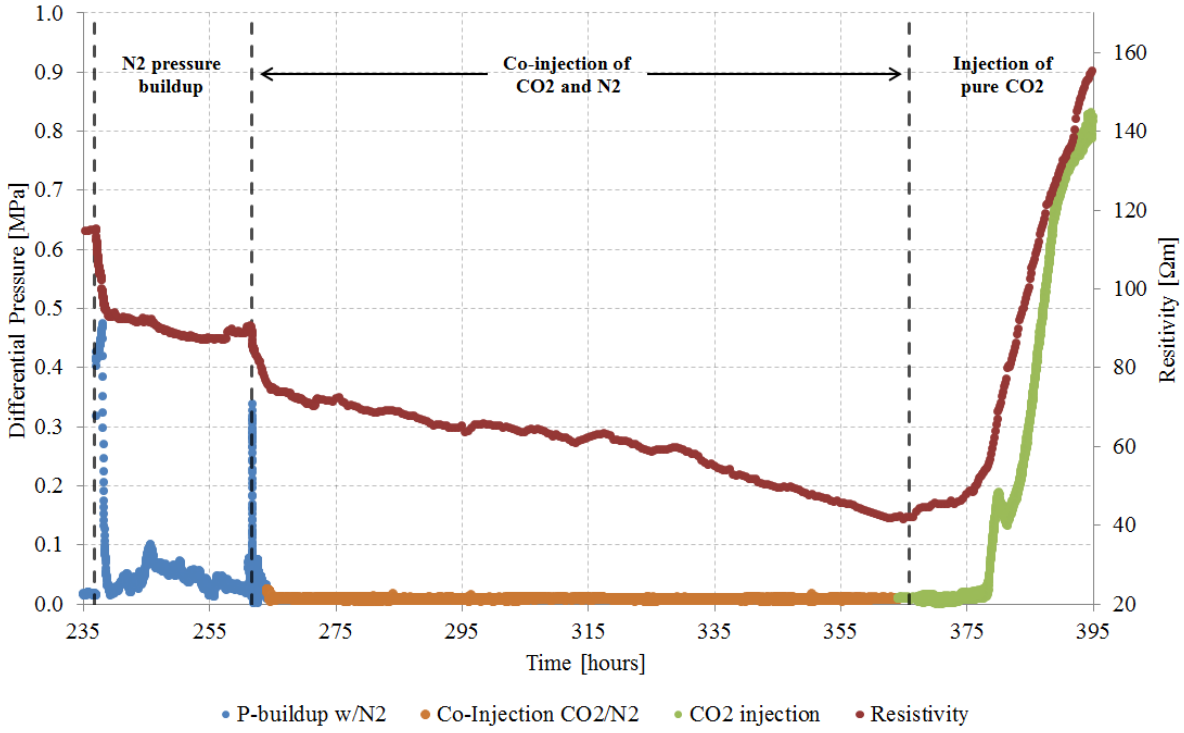

Figure 4.2.10 - Differential pressure and Resistivity measurements between 235-395 hours of the injection in HR49. The vertical dashed lines represent important events during the injection. The orange line represents the differential pressure during Co-Injection of CO_2 and N_2.

Figure 4.2.11 presents GC data from the co-injection of CO_2 and N_2 in HR49. The mole fraction of the effluent is presented as a function of pore volumes injected. Production begun after 0.5 PV injected as the outlet pressure reached the BPV pressure. In addition, the injected mole fractions of CO_2 and N_2 are represented by the horizontal dashed lines.

It can be observed that the mole fraction of nitrogen is initially relatively high, most likely due to the pressure build up performed with pure nitrogen prior to the co-injection. The methane breakthrough occurs after approximately 1.0 PV injected with a simultaneously increase in CO_2 fraction. The mole fraction of methane fluctuates during the entire co-injection. This could be a result of nitrogen induced dissociation, improving methane production and increasing the amount of water available for CO_2 sequestration. After approximately 2.9 PV injected, the co-injection was stopped and the injection of pure CO_2 was initiated in order to review the injectivity. This explains the rapid increase in CO_2 mole fraction at the end of the experiment. However, there is a time span between the start of the injection until it is observed in the GC data. The differential pressure and resistivity, presented in Figure 4.2.10, also remains low for a time period before it increases. This implies that the CO_2 flows through the core and gradually form hydrate with excess water, which eventually plugs the core. The reason for the delay time could be that the CO_2 must

displace a certain amount of nitrogen before it can form hydrate, since nitrogen work as a hydrate inhibitor at the current conditions (chapter 1.1.4).

The mole fraction of methane is relatively high as co-injection ceases. This implies that further methane production could have been achieved by continuing the co-injection of CO_2 and N_2. It can also be observed that the produced fraction of CO_2 remains below the injected CO_2 fraction during the entire co-injection. This indicates that a certain amount of CO_2 remains in the core during the injection.

The experimental results presented above demonstrate that the injection of CO_2 into hydrate bearing sediments with excess water may lead to additional hydrate formation and loss of injectivity. In addition, nitrogen can be used to dissociate hydrate in a plugged core, or co-injected with CO_2 to prevent hydrate formation. These results are in compliance with recently conducted experimental and full scale reservoir tests (Schoderbek et al., 2012, Kneafsey et al., 2013).

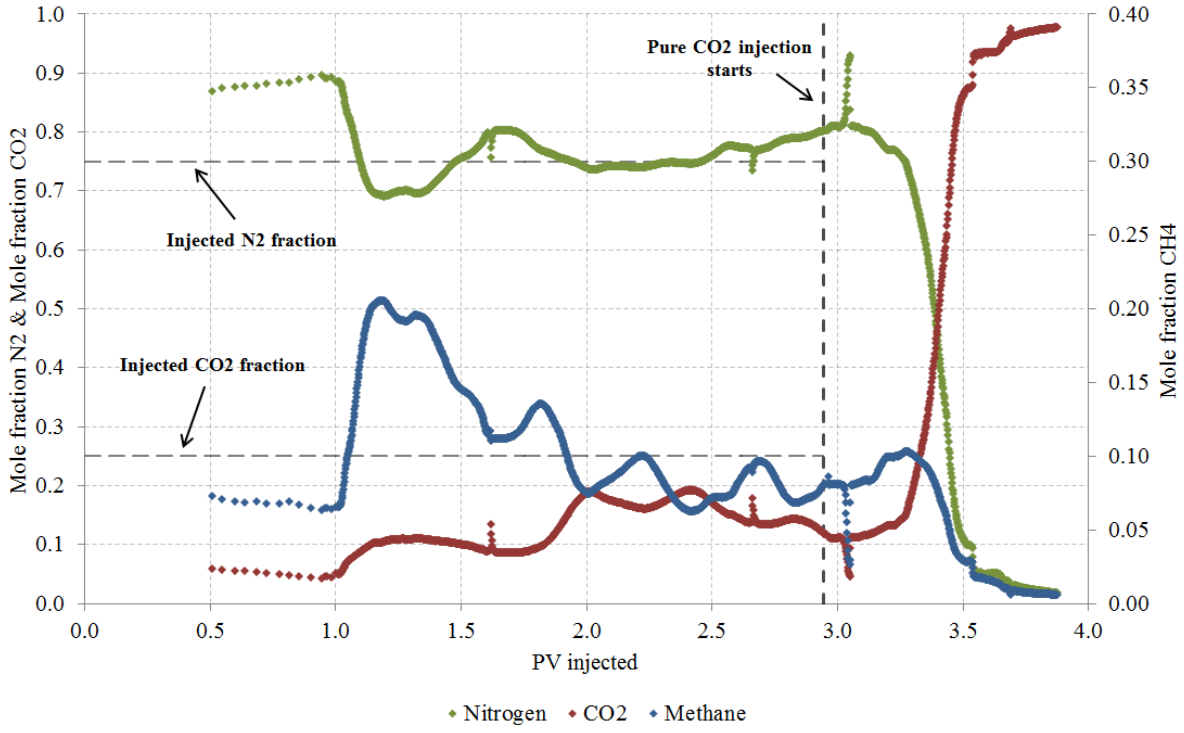

Figure 4.2.11 – GC data from co-injection of CO_2 and N_2 in HR49 showing mole fraction of N_2, CO_2 and CH_4 produced as a function of total pore volumes injected. The CH_4 mole fraction is presented on the secondary axis. The outlet pressure reaches the BPV pressure after 0.5 PV injected. The injected fractions of CO_2 and N_2 are represented by the horizontal dashed lines. Note that the figure does not include the initial CO_2 injection and N_2 pressure buildups presented in Figure 4.2.9 as no production occurred during that time period.

4.2.4 Co-injection in systems with high initial water saturation

After a successful CO_2/N_2 co-injection in HR49, a new experiment was conducted at similar conditions, but with co-injection from the beginning. The injection in HR51 was conducted with the same composition of the injected mixture (75 mole% N_2 and 25 mole% CO_2) as in HR49. It consisted of a whole Bentheim sandstone core with an initial water saturation of 0.64 and a brine salinity of 3.5 wt% NaCl. HR51 included both MFM and GC, making it possible to measure the amount of moles of each component in the effluent. A new Back Pressure Valve (BPV) was implemented and tested in this experiment, which resulted in several problems with the pressure.

A flow control valve was located downstream from the GC in order to maintain a steady flow through the MFM. Injection pressure, production pressure and resistivity are presented in Figure 4.2.12 for the co-injection in HR51. During the first hours of injection, the differential pressure increased. After 6 hours, the injection was stopped and the BPV was closed. The nitrogen pump was set to maintain 9.0 MPa on the inlet side in order to re-establish flow through the core. At around 25 hours, the inlet and outlet pressures had equalized and the BPV was opened. The pressure dropped to 8.5 MPa and the co-injection was resumed. The differential pressure increased during the first hours of injection, before it dropped to zero. During this time period, the resistivity increased as well, indicating additional hydrate formation. This was followed by an increase in pressure on both inlet and outlet side. This happened due to problems with the BPV, which were supposed to open at 8.5 MPa. At approximately 67 hours, the BPV opened and the pore pressure dropped from 9.71 MPa to 7.76 MPa. The injection continued and the pore pressure equalized at 8.5 MPa. Additional problems with the BPV occurred after approximately 94 hours, where the pore pressure dropped from 8.5 MPa to 6.6 MPa. The pressure increased to 8.5 MPa again, and maintained throughout the injection. Despite pressure fluctuations due to problems with the BPV, the differential pressure remained low during the entire co-injection, indicating good permeability. The resistivity followed the similar declining trend which was observed in the other experiments.

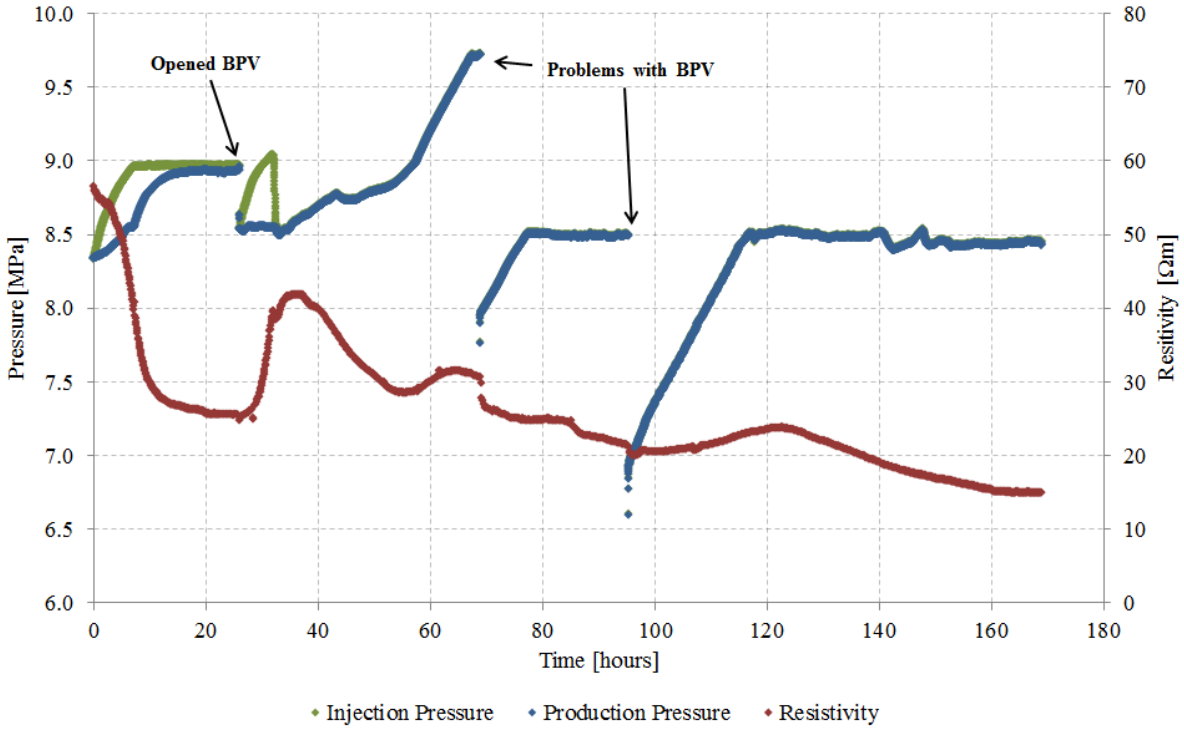

Figure 4.2.12 – Injection pressure, production pressure and resistivity during co-injection of CO_2 and N_2 in HR51. The increase and drop in pressure is a result of problems with the BPV

The GC data from the co-injection in HR51 are presented in Figure 4.2.13. No GC data were available between 32 and 115 hours elapsed because the GC connection was lost. The data points within this time interval are therefore interpolated. Initially, the mole fraction of nitrogen in the effluent is relatively high because the rear side of the system was flushed with nitrogen prior to the injection. A rapid increase in methane production can be observed after approximately 20 hours. The mole fraction of methane was still increasing as the GC connection was lost, suggesting that the interpolated values could be underestimated. In addition, the mole fraction of methane was approximately 0.24 at the end of the injection, indicating that even more methane could be produced if the injection had continued. The CH_4 recovery and CO_2 storage are presented in chapter 4.4 and 4.5.

This experiment confirms the results from HR49. The injection of N_2 together with CO_2 can inhibit formation of CO_2 hydrate with the excess water and thereby reduce injectivity problems. In addition, the implementation of the mass flow meter together with the GC made it possible to calculate the produced amount of each component in the effluent.

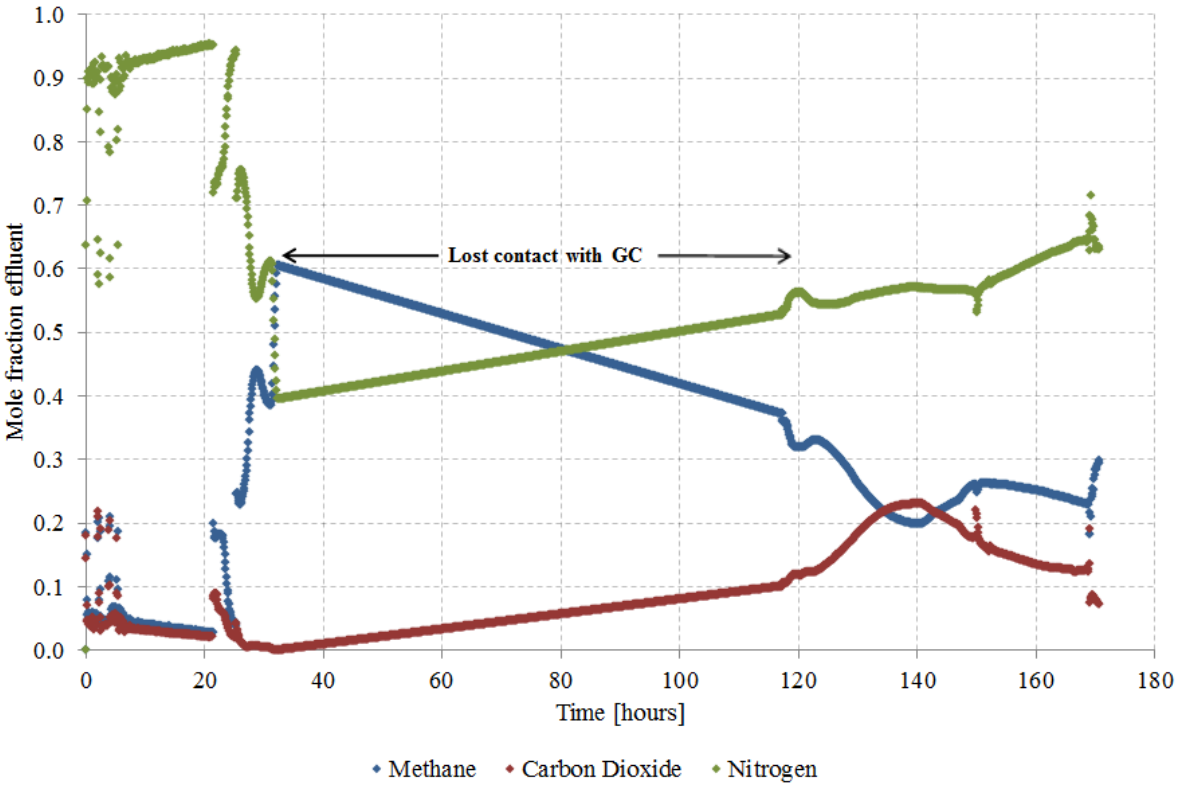

Figure 4.2.13 – GC data from co-injection of CO_2 and N_2 in HR51. The connection to the GC was lost between 32 and 115 hours elapsed. The data points within this time interval is therefore interpolated

4.2.5 CO_2 injection in hydrate bearing sandstones with fracture

The previous experiments were conducted at relatively high initial water saturations (S_{wi} ~ 0.65). Since CO_2 injection was successfully completed in several of these experiments, it was decided to increase the initial water saturations even further. However, based on the previous experiments, loss of injectivity due to additional hydrate formation was expected at such high water content. In order to minimize these problems, fractured cores were used. A Bentheim sandstone core was cut lengthwise into two halves to simulate a fracture, with a POM spacer situated between the two core sections in order to keep the fracture open and to provide a flow path for the injected fluids. The core was saturated with 3.5 wt% NaCl and methane hydrate was formed at 8.3 MPa and 4 °C. One of the goals of conducting fracture experiments was to increase the driving force for the CO_2-CH_4 exchange due to the high CO_2 concentration in the fracture. In addition, it was desired to investigate if the water could provide as a transport channel for CO_2 and CH_4 and thereby accelerate the reaction, which was observed by Ersland (2008). The CO_2 injection was conducted as a diffusion driven injection, consisting of multiple CO_2 flushes (chapter 3.2.5). Approximately one pore volume of CO_2 was injected at a high rate (15-60 ml/h). Then the system was left alone for about one week for the exchange process to take place. This sequence was repeated several times. The first flush was performed in order to produce the free methane present in

the spacer and the pore volume, while the subsequent flushes produced methane from the exchange process. This method is promising because the CO_2 utilization is better than for a continuous injection.

The composition of the effluent was measured with the GC during the first flush and is presented in Figure 4.2.14 as a function of PV injected. The nitrogen mole fraction is displayed on the secondary axis because the only nitrogen present in the system was the air in the core prior to hydrate formation. The increase in nitrogen mole fraction therefore indicates that the free gas from the core is being produced. At the start of the injection, the effluent consists of almost pure CO_2, because the rear side of the system was flushed with CO_2 prior to the injection. The methane breakthrough occurs after approximately 0.2 PV injected and increases rapidly. The methane produced from the first flush is assumed to be mainly free gas from the spacer and pore volumes. This explains the high mole fraction of methane in Figure 4.2.14.

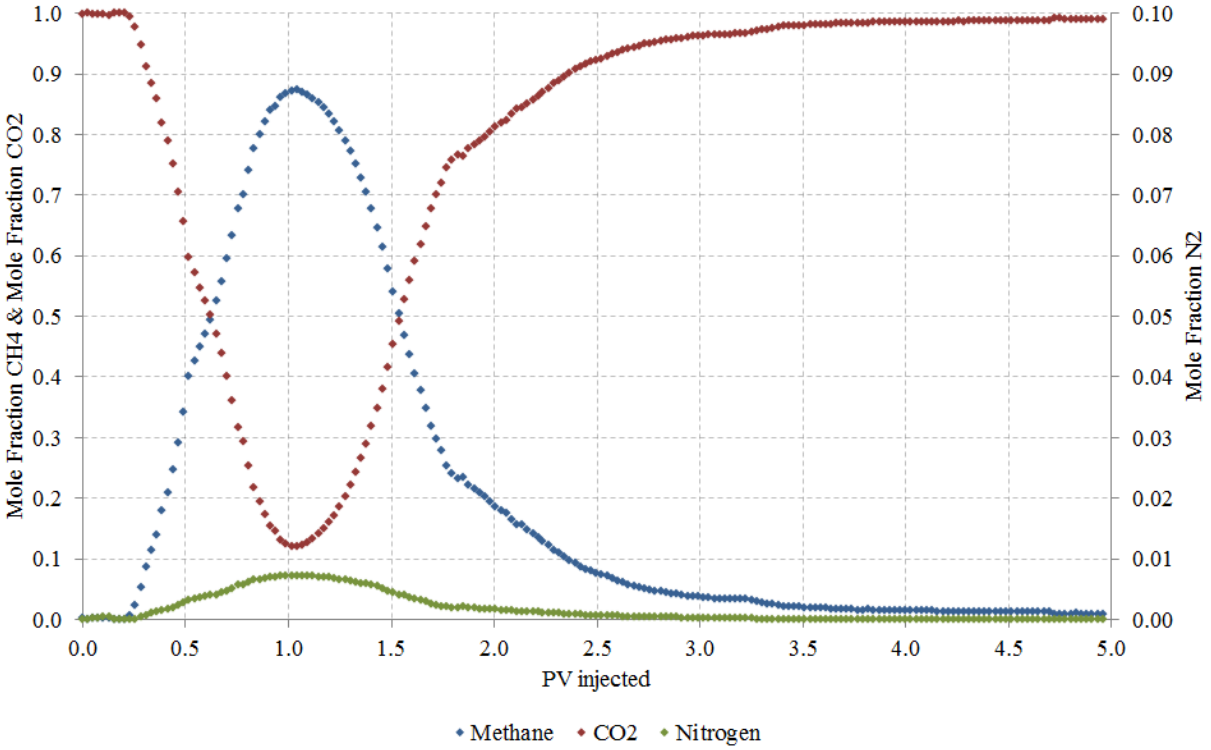

Figure 4.2.14 – GC data from the first CO_2 flush in HR52. Note that the N_2 mole fraction is presented on the secondary axis

Figure 4.2.15 shows the production pressure, temperature and resistivity during and after the first CO_2 flush in HR52. CO_2 was injected at 15 ml/h for the first 5 hours. Then the pump was set to maintain the pressure at 8.55 MPa. Approximately 23 ml CO_2 was consumed from the pump in the time period where the pressure was kept constant, indicating formation of CO_2 hydrate with the excess water (Figure 4.5.1). After 23 hours, the inlet- and outlet valves were shut, because the pump was required in another experiment. This resulted in a pressure decrease, most likely due to further hydrate formation. The pressure drop could also be a result of a leakage, but since the pressure

converges towards 7.5 MPa, hydrate formation is the most reasonable explanation. The fluctuations in temperature follow the daily changes in room temperature. The temperature measurements presented in Figure 4.2.15 are measured at the core surface. The pressure fluctuations seem to follow the temperature variations. The resistivity remains stable during the entire flush. In addition, the resistivity is very low compared to the other experiments performed in this thesis. This is most likely because the final water saturation was relatively high (S_{wf} - 0.47). As discussed earlier, resistivity measurements are most sensitive at low water saturations.

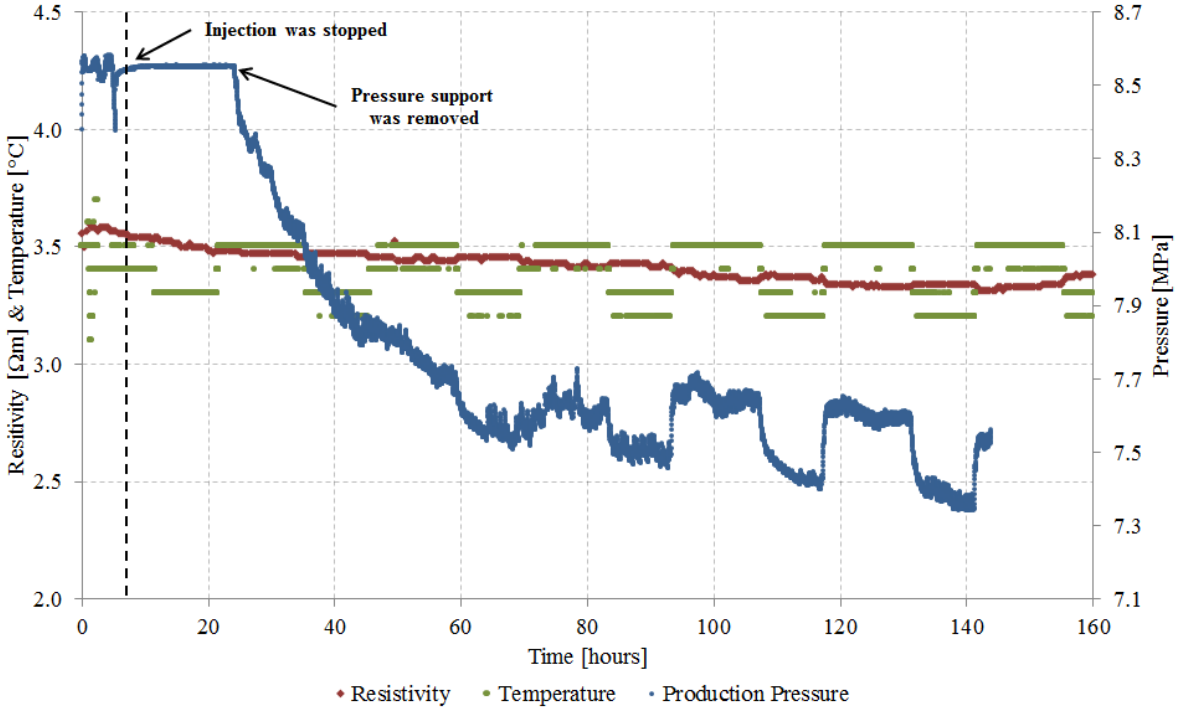

Figure 4.2.15 – Resistivity, production pressure and core temperature during and after the first CO_2 flush in HR52. The fluctuations in pressure after 60 hours seem to follow the temperature fluctuations. Pressure support was removed after 23 hours

After approximately one week, the core was repressurized with CO_2 from both sides to 8.3 MPa and a second flush was conducted in the same manner as the first one. The production pressure, temperature and resistivity from the second flush are displayed in Figure 4.2.16. The injection pressure was equal the production pressure at all time, due to the spacer. The initial increase in pressure is from repressurizing the core. Approximately one pore volume of CO_2 was injected in two hours before the injection was stopped. Then the system was left alone for another week. The production pressure followed the same declining trend as in the first flush, with fluctuations in compliance with the temperature. The resistivity remained fairly stable, with a slight increase, indicating hydrate formation. The purpose of the second flush was to replace the produced methane from the CO_2-CH_4 exchange and supply additional CO_2 to continue the exchange process.

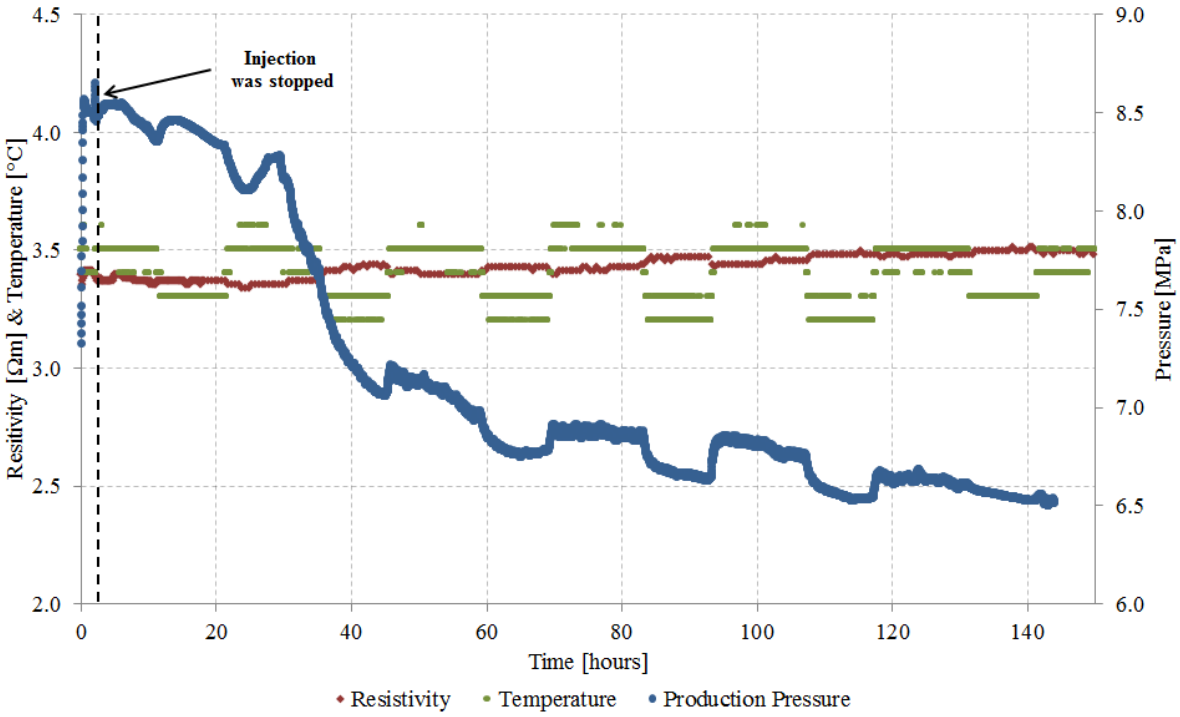

Figure 4.2.16 - Resistivity, production pressure and core temperature during and after the second CO_2 flush in HR52. The fluctuations in pressure follow the temperature fluctuations. The initial increase in pressure is from the repressurization after the first flush

Both composition and mass flow of the effluent was measured during the second CO_2 flush. The GC data is presented in Figure 4.2.17. Note that the mole fractions of CH_4 and N_2 are presented on the secondary axis. Since most of the free gas had been replaced with CO_2 in the first flush, a smaller CH_4 production was expected in the second flush. A maximum CH_4 mole fraction of approximately 9 % can be observed after 0.36 PV injected. The high initial N_2 fraction could be explained by air that was situated in the GC tubing prior to the flush.

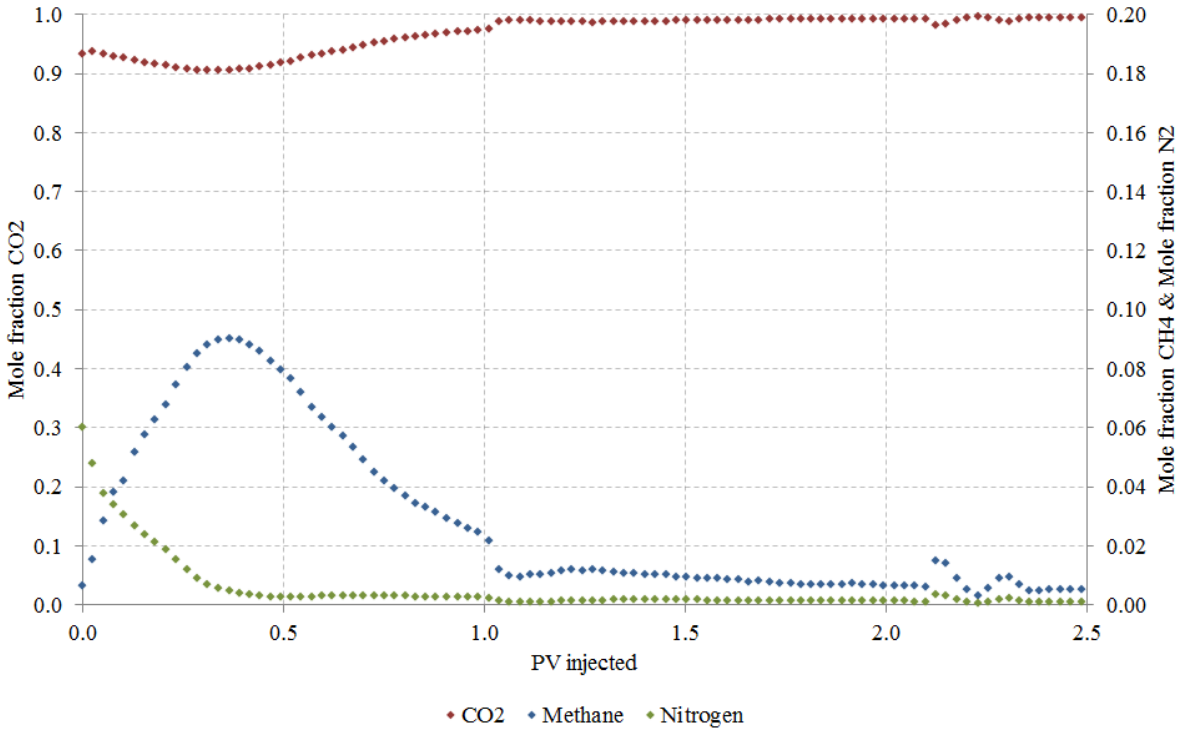

Figure 4.2.17 – GC data from the second CO_2 flush in HR52. Note that the mole fractions of CH_4 and N_2 are presented on the secondary axis

After one week, the pore pressure had reached 6.5 MPa. In order to perform a third CO_2 flush, the system was repressurized to 8.5 MPa from both sides. Then the bypass valve was closed and CO_2 injection started. This resulted in a rapid increase in differential pressure, indicating hydrate plugging either the inlet or the outlet of the system. Several attempts of dissociating the hydrate plug with nitrogen was performed, but without success. It was therefore not possible to continue with CO_2 injection. However, the time of N_2 exposure was probably too short in order to dissociate the plug. Since the core contained a fracture, the hydrate plug was most likely situated in the tubing or at the end piece surfaces. The system was therefore dissociated and the experiment terminated.

4.3 Methane production by hydrate dissociation

Production by dissociation seems to be the most promising method of producing gas hydrates found in nature (Moridis et al., 2009). This is done by moving the reservoirs thermodynamic conditions outside the hydrate equilibrium zone, either by increasing the temperature, decreasing the pressure or altering the hydrate equilibrium curve by introducing an inhibitor. This is further discussed in chapter 1.4.1. In this thesis, most of the experiments were conducted in order to investigate production scenarios involving CO_2 injection. However, after the CO_2 injection was completed, the mixed gas hydrate was produced by dissociation in order to obtain additional information about the hydrate. The

hydrate was dissociated either as a *single step depressurization*, *multiple steps depressurization* or by *thermal dissociation*. The depressurization methods involved maintaining the temperature, while reducing the pressure. By thermal dissociation, the pressure was kept constant and the temperature was increased. The procedures for these production methods are presented in chapter 3.2.6.

4.3.1 Production by multiple steps depressurization

The dissociation pressure of pure methane hydrate is 4.5 MPa at 4° C and 3.5 wt% brine salinity, according to CSMGem calculations. If a fraction of the methane molecules within the hydrate are replaced with CO_2, the dissociation pressure will be reduced. The goal of conducting a multiple steps depressurization was to obtain a dissociation pressure for the mixed CO_2/CH_4 hydrate after CO_2 exchange. The dissociation pressure would thereby give an estimate of the amount of CO_2 sequestrated within the hydrate.

After the CO_2 injection was completed, the core was flushed with CH_4 at a high rate (~ 60 ml/h) in order to displace the free CO_2 present in the core. This was done because CH_4 has a higher dissociation pressure than CO_2 and would therefore reduce problems with hydrate reformation during depressurization. After the free CO_2 had been replaced with CH_4, the pressure was reduced from 8.3 MPa to a pressure near the equilibrium curve for pure CH_4 hydrate. Then the pressure was reduced stepwise with pressure steps of approximately 69 kPa. The gas volume received was measured for each step. The dissociation could be observed as a significant increase in gas production.

The multiple steps depressurization in HR48 is presented in Figure 4.3.1, where the dissociation seemed to start at 3.17 MPa. However, reformation occurred due to fluctuations in temperature, resulting in a decrease in the gas consumption curve at 3.17 and 3.10 MPa. This is presented in Figure 4.3.2 for the 3.10 MPa pressure step. The gas consumption then increased for each pressure step, until it reached a maximum at 2.76 MPa. Note that the produced volumes correspond to the individual pressure steps. Since the hydrate consisted of both CO_2 and CH_4 in a heterogeneous mixture, the dissociation occurred at different pressures. In HR48, the hydrate dissociation occurred between 3.17 and 2.69 MPa. The corresponding mixed hydrate compositions were calculated using CSMGem. 3.17 MPa correspond to a mixed hydrate composition of 60.1 % CH_4 and 39.9 % CO_2, while 2.69 MPa corresponds to 32 % CH_4 and 68 % CO_2. However, this only gives an indication on the composition of the hydrate, because it is most likely varying throughout the core. Pure methane hydrate may exist in some areas that have not been contacted by CO_2, while pure CO_2 hydrate may exist in areas where it has formed hydrate with the excess water.

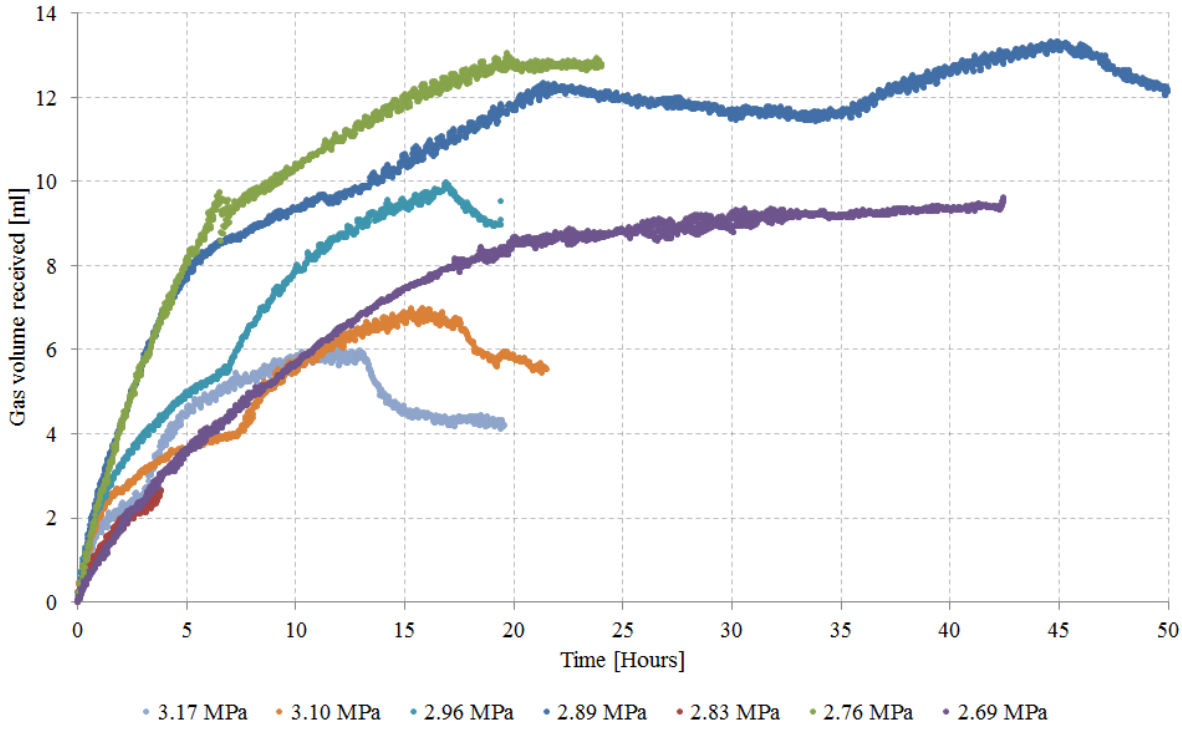

Figure 4.3.1 – Gas production for different pressures during stepwise depressurization in HR48. Note that the volume consumed at each step corresponds to the specific pressure for that step

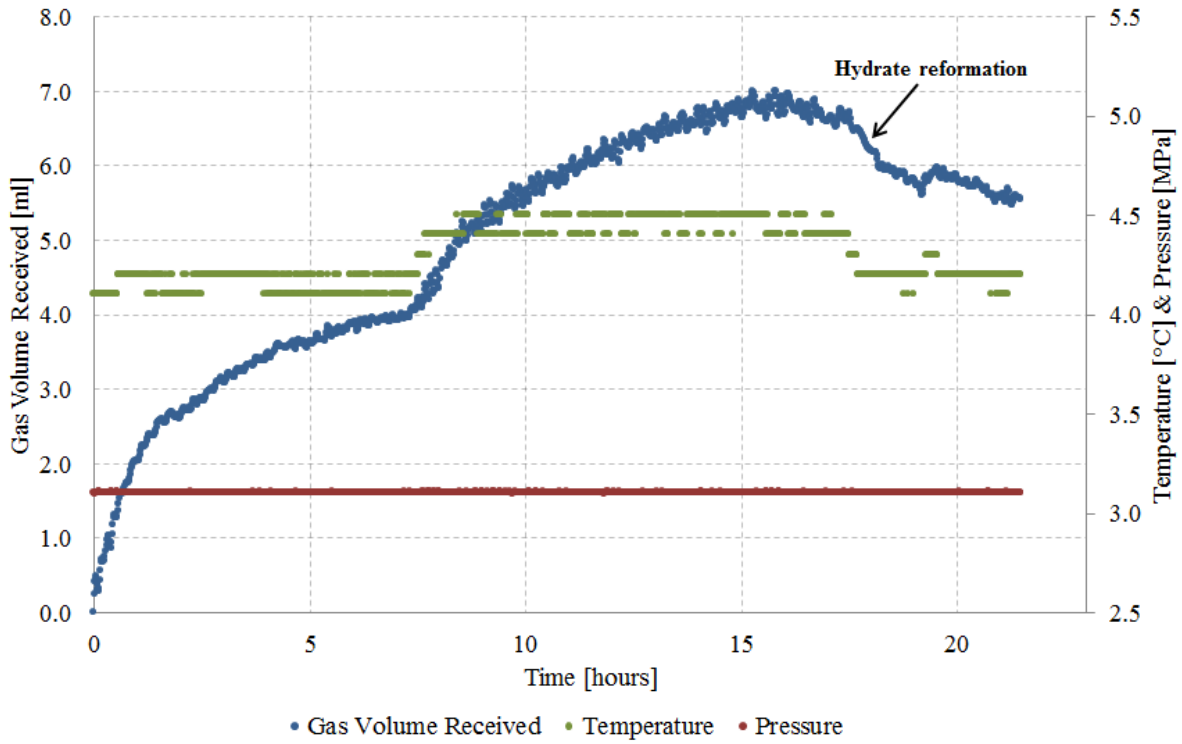

Figure 4.3.2 – Hydrate reformation as a result of temperature variations during depressurization for the 3.10 MPa pressure step in HR48

The core from HR48 was also used in HR49, but with a different initial water saturation and co-injection of CO_2 and N_2 instead of pure CO_2. The depressurization in HR49 was also conducted as a stepwise depressurization, but using N_2 instead of CH_4 as the free gas in the system. The data from the depressurization is presented in Figure 4.3.3. In HR49, hydrate dissociation seemed to occur between 3.45 MPa and 3.03 MPa, which is higher than in HR48. This is probably because N_2 was used for the depressurization instead of CH_4, affecting the hydrate dissociation pressure. It can also be observed that most of the gas consumption curves in Figure 4.3.3 are still increasing at the end of the curve. This indicates that the pressure steps were too short.

The corresponding mixed hydrate compositions were calculated in the same way as in HR48. 3.45 MPa corresponds to a mixed hydrate containing 71.5 % CH_4 and 28.5 % CO_2, while 3.03 MPa corresponds to 53.5 % CH_4 and 46.5 % CO_2. However, since nitrogen was used in the depressurization, this would affect the dissociation pressure.

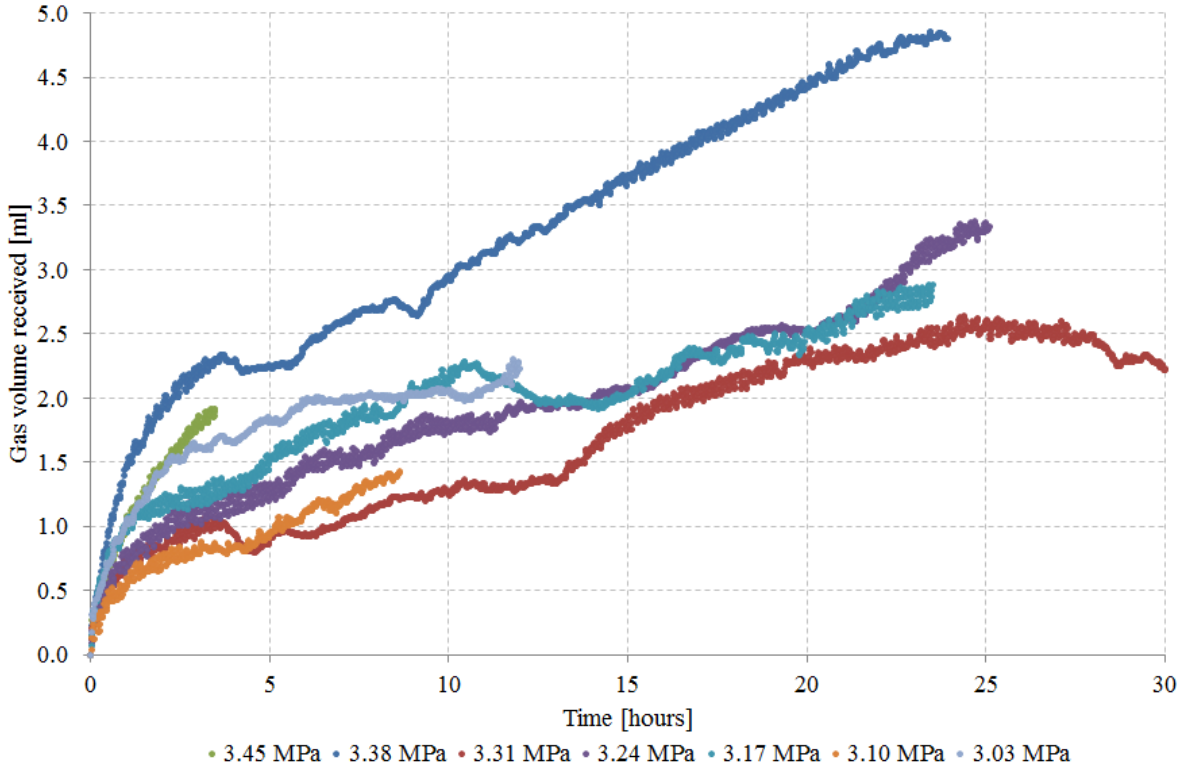

Figure 4.3.3 – Gas volume received for different pressures during stepwise depressurization in HR49. Note that the volume consumed at each step corresponds to the specific pressure for that step. The depressurization was performed using N_2

4.3.2 Production by single step depressurization

A multiple step depressurization could take more than a week to perform. In order to make the process more effective, the method of single step depressurization was applied. This method was less time consuming than the multiple step depressurizations, but did not provide any values of the dissociation pressure of the hydrate. The method is described in chapter 3.2.6. In DEP5, the single step depressurization was conducted in order to provide data for numerical simulations.

DEP5 consisted of four hydrate formations and dissociations where two of the dissociations were performed as single step depressurizations. Both of the dissociations were performed with only methane hydrate present. The first depressurization is presented in Figure 4.3.4 as the gas consumption as a function of time after the pressure had reached 3.17 MPa. Even though some methane hydrate probably dissociated during pressure reduction, it is not included in the figure, because it is difficult to distinguish between the amount dissociated from hydrate and the amount as a result of the pressure reduction. It can be observed that the depressurization curve follows a similar trend as the formation curves, with an initial high consumption rate, decreasing over time. The shape of the curve will depend on the driving forces in the dissociation process, in this case, the pressure difference between the pore pressure and the equilibrium pressure of the hydrate. However, Kneafsey et al. (2007) showed that the rate of hydrate formation and dissociation could also be a function of other physical causes that effects the communication between methane and water when altering pressure and temperature. In DEP5, the pressure was reduced to 3.17 MPa, which is below the dissociation pressure of pure methane hydrate at the given temperature and salinity. After 48 hours, the pressure was further reduced to 1.92 MPa, but no additional dissociation was observed. A slightly fluctuating behavior in the received gas volume can be observed in Figure 4.3.4. This seems to be a result of the daily temperature variations.

One of the main goals of DEP5 was to provide experimental data that could be used in numerical simulations of methane hydrate dissociation in sandstone. Figure 4.3.5 shows a simulation conducted by Birkedal et al. (2013a) using TOUGH+HYDRATE. The numerical simulation was based on the first single step depressurization in DEP5. The figure demonstrates excellent agreement between the empirical- and numerical data. Temperature variations and heat transport proved to be important parameters controlling the dissociation rate.

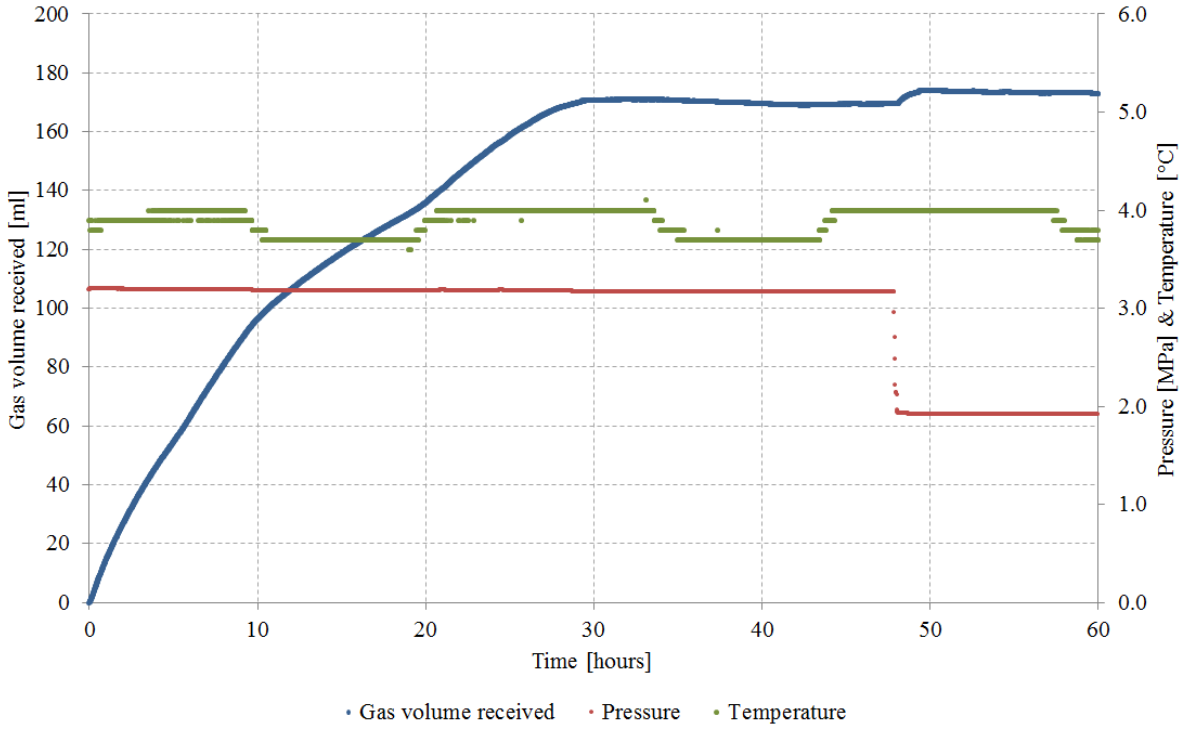

Figure 4.3.4 – Gas volume received, pressure and temperature during the first hydrate dissociation in DEP 5. The inlet and outlet pressure was equal during the process. The temperature was measured at the core surface

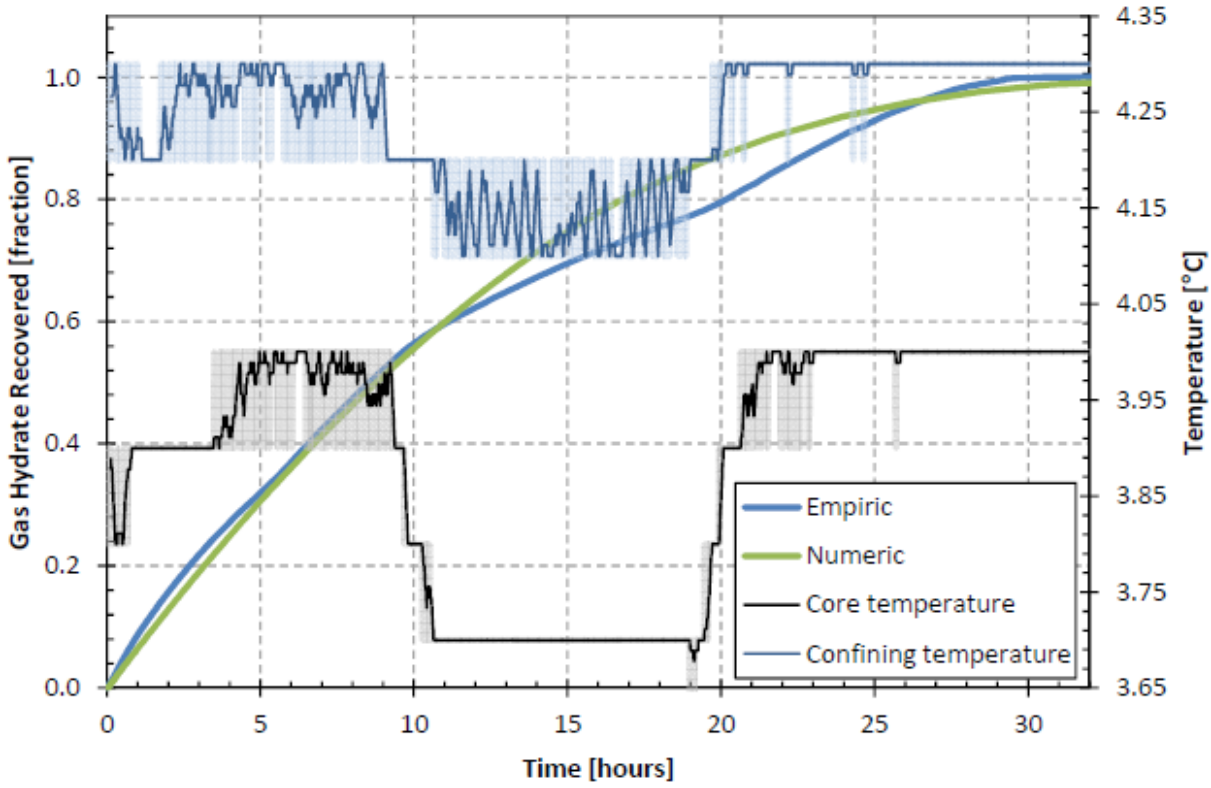

Figure 4.3.5 – Comparison of numerical simulation based on the empiric data from the first hydrate dissociation in DEP5. Simulation was conducted by Birkedal et al. (2013a).

After the first hydrate formation in DEP5, pure methane hydrate was formed for the second time, without removing the core from the core holder. The hydrate formations in DEP5 are presented in chapter 4.1. A second single step depressurization was then performed in the same procedure as the first one and is presented in Figure 4.3.6. The gas consumption curve looks similar to the one in Figure 4.3.4 except that the first depressurization takes approximately 40 hours, while the second one is completed in about 15 hours. In addition, the gas consumption is lower in the second case. This is probably a direct result of the higher dissociation rate leading to a larger amount of methane being dissociated during the pressure reduction time. This volume is not included in Figure 4.3.4 and Figure 4.3.6. A possible explanation to the high dissociation rate could be that the hydrate was redistributed within the pore network, so that the free gas phase became more continuous. A reduction in pressure would therefore be quicker and more responsive throughout the core, compared to a case where the hydrate is more heterogeneously distributed. The main difference between the first and the second dissociation is the time elapsed after the hydrate formation. The first dissociation took place immediately after the formation had been completed, while the second hydrate formation was followed by a waiting period of approximately 27 days before the second dissociation was started. The redistribution of hydrate within the pore network could be a result of microscopic dissociation and reformation during this period of time. Tohidi et al. (2001) observed that gas hydrate in a synthetic porous media micromodel redistributed over a time period of 2 days (Figure 1.3.5). Similar behavior have been observed by Rees et al. (2011) through X-ray CT imaging. Another explanation could be that when the gas hydrate is dissociated for the first time, the water becomes more evenly distributed than originally, resulting in a more homogeneously distributed gas hydrate after the second formation. This has been observed by Ersland (2013), using Magnetic Resonance Imaging. However, this phenomenon could likely cause the second hydrate formation to go faster than the first one. This was not observed in the two first hydrate formations in DEP5. It was also found that the average core temperature was approximately 0.3 °C higher in the second depressurization, which could have a significant effect on the dissociation rate. According to CSMGem, this corresponds to 1.4 MPa difference in dissociation pressure.

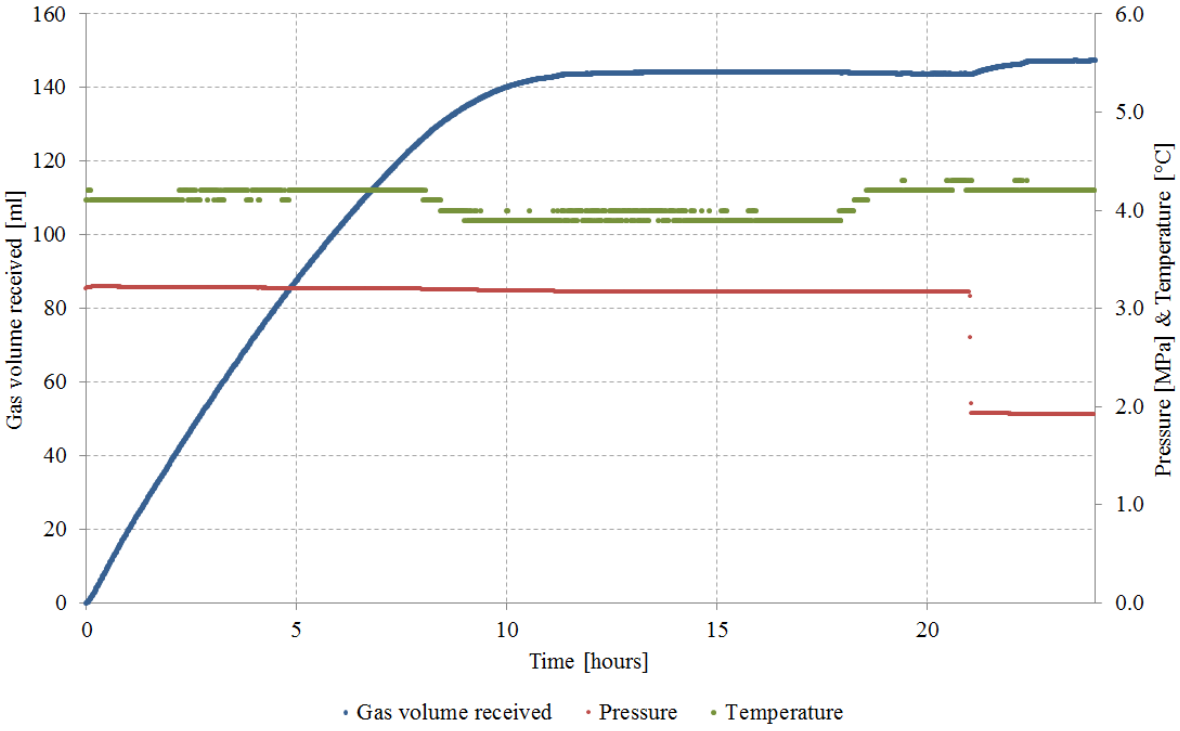

Figure 4.3.6 - Gas volume received, pressure and temperature during the second hydrate dissociation in DEP 5. The pressure was further reduced after 21 hours, without any additional dissociation

4.3.3 Production by thermal dissociation

Thermal dissociation is another method that was applied. The procedure used in this thesis is somehow different from a real reservoir production scenario, where this is mainly performed by injecting a hot fluid into the hydrate bearing porous media (Makogon, 1997). In this thesis, the thermal dissociation was done by increasing the temperature of the refrigerator bath that was circulating antifreeze around the core holder. By doing so, the core was heated from the sides, resulting in a radial temperature gradient in the core. The temperature quickly exceeded the dissociation temperature of the gas hydrate, resulting in dissociation. The cumulative volume gas received by the pump was registered.

The third hydrate dissociation in DEP5 was conducted as a thermal dissociation and is presented in Figure 4.3.7. The figure contains pressure, temperature and gas volume received as a function of time. The process was performed according to the procedures described in chapter 3.2.6. As the temperature of the refrigerator bath and the system was increased, it quickly exceeded the dissociation temperature of the gas hydrate at the current pressure and salinity. The dissociation completed before the temperature had reached 20 °C, most likely because of the temperature sensitivity of the dissociation rate. Another contribution to the rapid dissociation could be that the hydrate was finely distributed within the core, based on the argument that multiple formations and dissociations makes the water more evenly distributed within a porous media (Ersland, 2013). Compared to other experiments conducted at similar initial conditions, DEP5 contained a relatively high

residual water saturation (> 10%). Since water has a higher thermal conductivity than hydrate at the applicable experimental conditions (Gupta, 2007), the hydrate distribution in the core could have an effect on the total thermal conductivity of the core and thereby alter the rate of dissociation. Based on this explanation, the rate of hydrate dissociation could increase with the degree of hydrate distribution. However, hydrate dissociation is an endothermic reaction and thereby counteracts the heating process, resulting in a slower temperature increase.

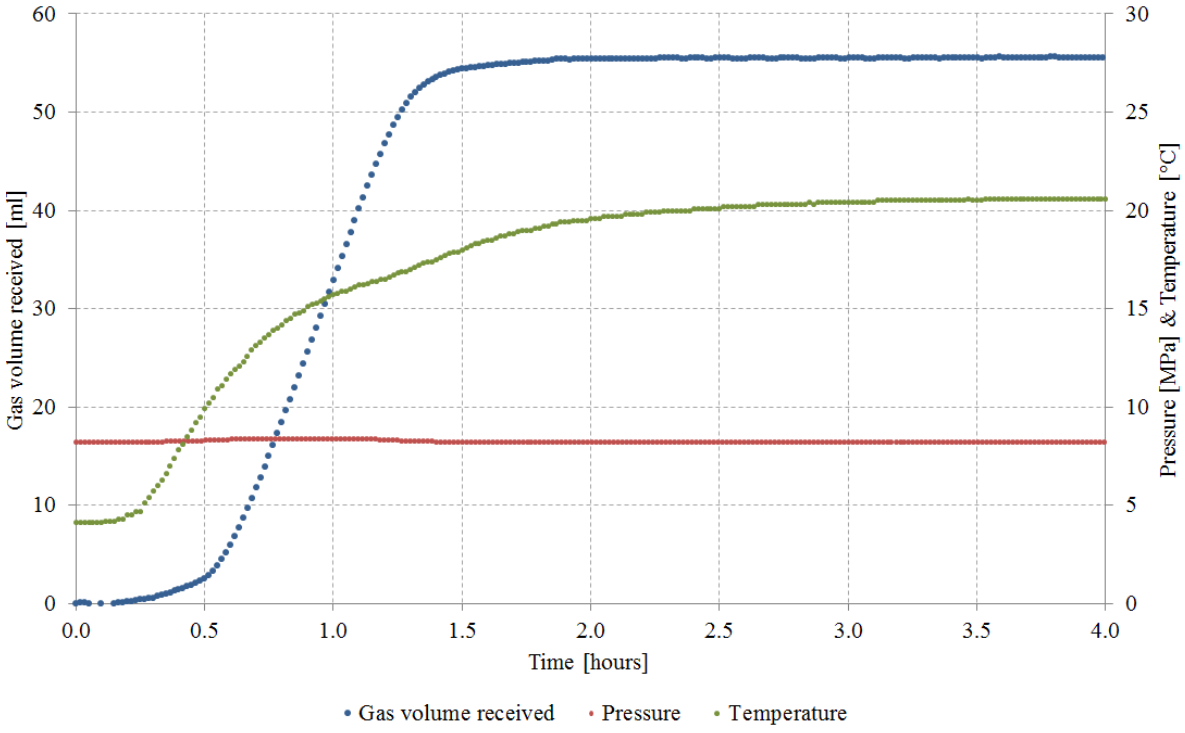

Figure 4.3.7 – Gas volume received, pressure and temperature during the third hydrate dissociation in DEP5. The gas hydrate was thermally dissociated by increasing the temperature to approximately 20 °C with a constant pressure of 8.21 MPa

4.4 Methane recovery

The implementation of the mass flow meter made it possible to calculate the amount of methane produced, and thereby the methane recovery in the experiments conducted. The methane recovery is an important parameter when evaluating the effectiveness of the applied production method and gives information about the fraction of the original reserves that have been produced. One of the goals in this thesis was to investigate if the presence of excess water would affect the methane recovery when injecting CO_2 into hydrate bearing sediments. Previous research has shown indications that excess water may increase the CO_2-CH_4 exchange rate by working as a medium of transportation for the CO_2 and CH_4 molecules (Ersland, 2008). However, it did not seem to affect the total methane recovery.

4.4.1 Calculating methane recovery

The methane recovery (R_{CH4}) is defined in equation (4.1) as the fraction between the amounts of moles methane produced ($n_{CH4,prod}$) and the amounts of moles originally in place in the system ($n_{CH4,tot}$), including free methane. After hydrate formation, methane was present in the core as both free gas and within the hydrate. The amounts of methane in place were obtained from mass balance calculations for both free gas and hydrate phase. These calculations were based on the methane consumption during hydrate formation, corrected for leakages, tubing volume and the volume added as a result of water expansion as hydrate forms. The hydration number N_H, used in equation (1.1), was set to 5.99, which is considered a good estimate for simple structure I methane hydrate (Sloan and Koh, 2008). This was used to calculate hydrate saturation and the amount methane present in the hydrate. The amount of methane produced during injection was calculated from the composition (GC) and mass flow (MFM) of the effluent. The sample intervals on the GC varied between 1-5 minutes, while the MFM measured the mass flow every 1-3 seconds depending on the injection rate of the current experiment. The data for the GC and the MFM was therefore correlated. This was achieved by calculating the cumulative mass produced per GC time interval. Then the amount of moles produced of each component could be calculated by using the composition and the mixed molar mass.

$$R_{CH_4} = \frac{n_{CH_4,prod}}{n_{CH_4,tot}} \tag{4.1}$$

However, in these calculations, leakage was not been taken into account. Even though it is possible to make an estimate of the leakage rate, it is very difficult to identify the locations of the leakages. Since the composition is only measured at the system outlet and the temperature and pressure varies for the different parts of the system, there is currently no method that can be used to include leakages in the production calculations. However, it should be noted that by excluding this, the methane recovery will be underestimated. The reason for this is that the inlet and outlet side of the system was flushed with either CO_2 or N_2 prior to injection, so that any methane leakage would be methane from the core, which would have contributed to the recovery if it had not been lost. When calculating CO_2 storage, leakage would have the opposite effect. This is further discussed in chapter 4.5.

In the experiments conducted before the mass flow meter was implemented (HR48 and HR49), the recovery was calculated by assuming that the volume produced equals the volume injected. This assumption is not correct due to factors such as gas compressibility, solubility, additional hydrate formation, dissociation and exchange of guest molecules.

4.4.2 Comparison of methane recoveries

Figure 4.4.1 shows methane recovery as a function of time in a series of experiments conducted at the University of Bergen, including experiments conducted in this thesis. The

start point of the curves is defined as the point where production started, i.e. when the production pressure exceeded the BPV pressure. The injection was performed as a continuous CO_2 injection in all the experiments except HR49 and HR51, where N_2 was injected along with CO_2 in order to reduce the risk of plugging due to the high initial water saturation. The gaps in the recovery curves are results of problems with the GC or the pressure regulator valve.

It can be observed that there is generally good compliance between most of the recovery curves. However, in the experiments where the mass flow meter was absent (marked by *), the recovery appeared to be lower. Since both the initial conditions and the injection procedures were similar for all the experiments, it seems that the assumption that volume produced equals volume injected leads to an underestimation of recovery in the experiments conducted without mass flow meter. This may be a result of both increased density as CH_4 mixes with the injected CO_2 as well as additional hydrate formation between CO_2 and the excess water. In the experiments where nitrogen is introduced, hydrate dissociation may also occur. In addition, the mixed density will also be a function of nitrogen content. In HR49, the effects of formation, dissociation and density change could be more comprehensive because nitrogen was co-injected with the CO_2 and the system contained a significant amount of excess water. HR49 achieved the lowest methane recovery according to the calculations.

Another observation that can be made is that several of the recovery curves are still increasing towards the end. This implies that the recovery could have been higher if the injection was continued. The highest recovery was obtained in HR51, where CO_2 and N_2 were co-injected. This could be a result of nitrogen dissociating methane hydrate and thereby increasing both recovery and the amount of water available for CO_2 hydrate formation. Kneafsey et al. (2013) observed hydrate dissociation and water formation when injecting a similar CO_2/N_2 mixture into hydrate bearing sediments.

In Figure 4.4.2, methane recovery is presented as a function of final hydrate saturation for the same experiments presented in Figure 4.4.1. There is no obvious trend indicating that the recovery is affected by salinity or final hydrate saturation. More data is therefore required to evaluate if those parameters has an effect on recovery. In addition, several of the experiments had an increasing recovery at the end of the injection (seen in Figure 4.4.1) and the recoveries computed without mass flow data seemed to be underestimated.

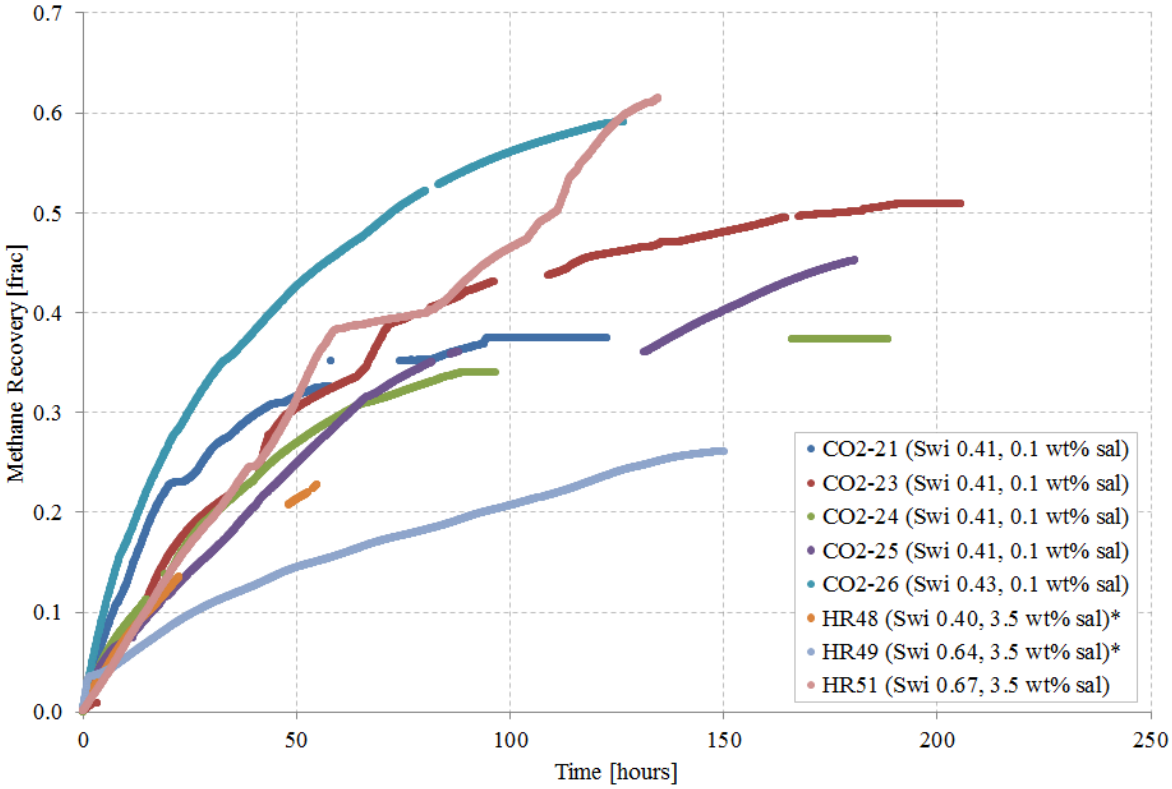

Figure 4.4.1 – Methane recovery as a function of time for a series of experiments conducted at the University of Bergen. Data acquired from in-house data base (Hauge, 2013). (* Mass flow meter was not implemented in the experiment)

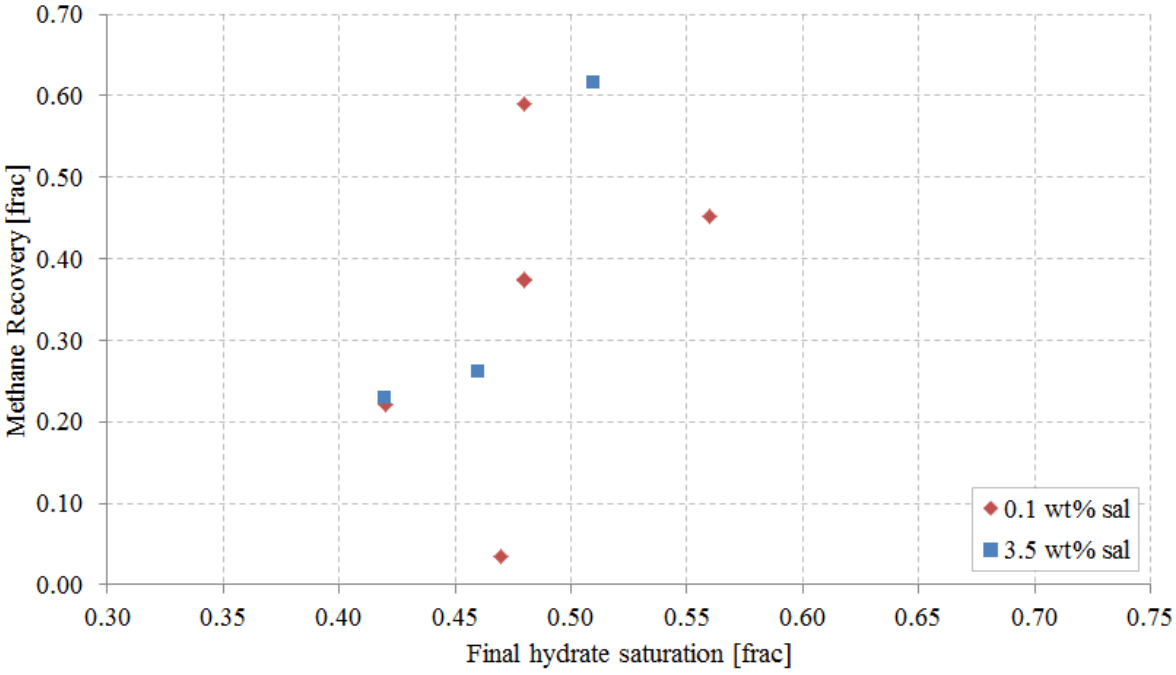

Figure 4.4.2 – Methane recovery as a function of final hydrate saturation for a series of experiments conducted at the University of Bergen. Data acquired from in-house data base (Hauge, 2013)

4.4.3 Methane recovery from diffusion driven CO_2 injection

In HR52, the CO_2 injection was conducted as a diffusion driven injection, containing two CO_2 flushes. The methane recovery for the two flushes is presented in Figure 4.4.3. There was a one week waiting period between the first and the second flush, but for convenience, it was not included in the graph. During the first flush, a relatively high methane production can be observed. The methane is assumed to be primarily free methane from the spacer and the pore volume. However, the spacer may reduce the volumetric sweep efficiency for the displacement process, resulting in residual free methane present in the core after the first flush. The methane could then diffuse into the fracture as a result of the concentration gradient. In the second flush, it was therefore assumed that some of the methane was produced from hydrate and some from the residual free methane. However, it is not possible to distinguish between the two. An attempt to conduct a third CO_2 flush resulted in a hydrate plug, most likely within the tubing or at one of the end piece surfaces. If a third flush had been completed, it would have been easier to discuss the amount of methane produced from hydrate. It is expected that for every flush performed, less free methane is present in the core, resulting in increased driving forces for the CO_2-CH_4 replacement process.

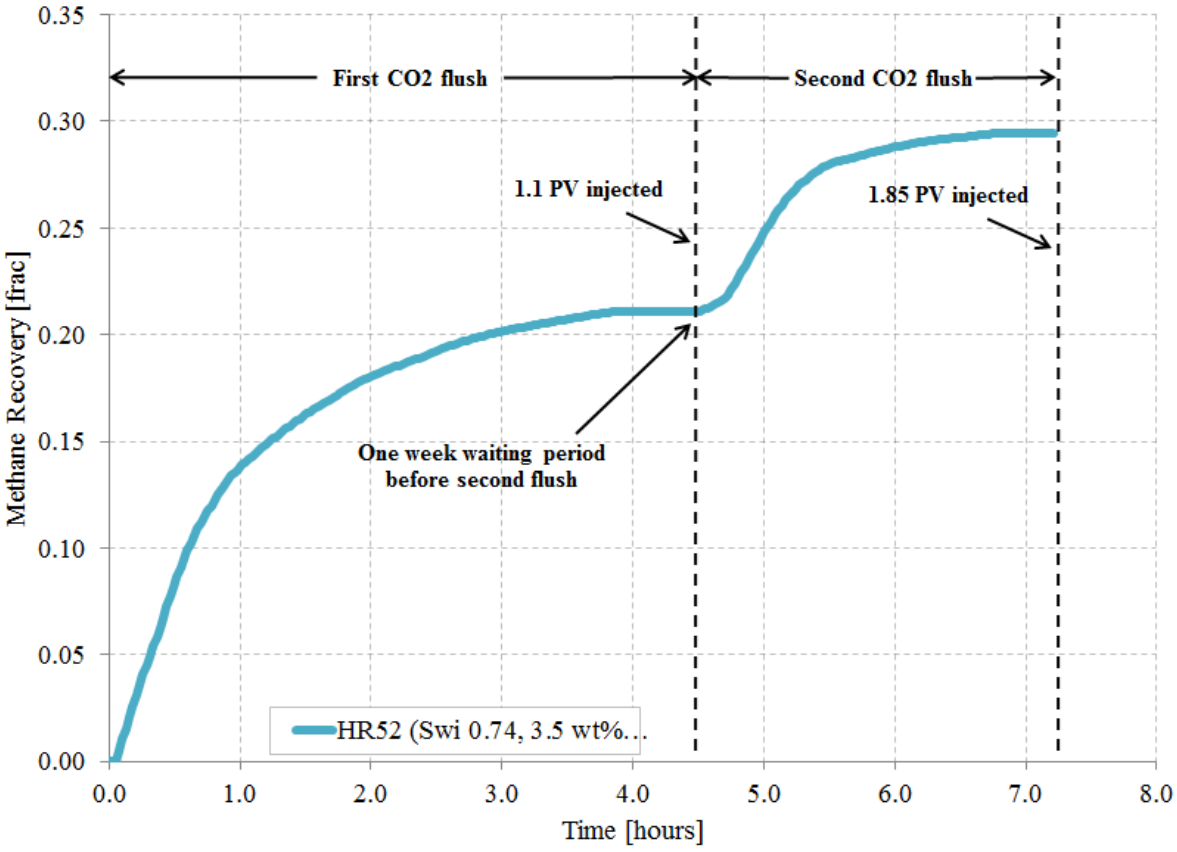

Figure 4.4.3 – Methane recovery for diffusion driven CO_2 injection in HR52, featuring a fractured core. The injection consisted of two flushes with one week waiting period in between. The recovery curves are merged for convenience

4.5 CO_2 sequestration

Injection of CO_2 into hydrate bearing sediments has the advantage of producing methane without dissociating the hydrate. In addition, it provides the possibility of long term CO_2 sequestration. In the experiments performed in this thesis, CO_2 has been injected into Bentheim sandstone cores containing methane hydrate. In such a scenario there are several ways in which CO_2 can be sequestrated: (1) Replacing CH_4 as guest molecule in the hydrate, (2) Forming additional hydrate with the excess water or (3) Remain in the core as free CO_2. The two scenarios where CO_2 is stored within a hydrate phase are considered permanent options. Graue et al. (2006a) have showed that the injection of CO_2 into hydrate bearing sediments may offer as a long term storage option. When discussing CO_2 sequestration, the presence of excess water may increase the storage potential for CO_2, but can also contribute to loss of injectivity.

The potential of CO_2 sequestration was analyzed by several different methods. In the experiments where the mass flow meter was used, both the amount of CO_2 injected and the amount of CO_2 produced were known. The CO_2 storage could then be calculated as the difference between the two. However, it is difficult to include leakages in these calculations. This result in a significant overestimation of the amount CO_2 stored. An example of this is CO2-25, where an attempt to calculate CO_2 storage was conducted. It was found that 95.3 % of the injected CO_2 was stored. This is practically impossible and illustrates that leakages makes it difficult to estimate CO_2 storage. An attempt to include leakages in the calculation was also made. The leakage rate obtained from the pressure tests prior and after hydrate formation was used. Since it was not possible to know the composition of the leakage volumes, it was assumed that it was only CO_2 in order to review the worst-case scenario. These calculations showed that 94.6 % of the injected CO_2 had been stored, which is also practically impossible. This demonstrates that the leakage rate is significantly higher when CO_2 is introduced in the system, which may be due to CO_2 diffusion through the sleeve. In order for this method to be useful, the impact of leaks needs to be minimized and methods for estimating leakage rate with CO_2 in the system needs to be applied.

If CO_2 diffusion through the sleeve was the major cause of leakage, it can be assumed that the leakage of CH_4 was approximately the same as during the hydrate formation. The cumulative amount of CH_4 produced from GC and MFM data could therefore be used to estimate the amount of CO_2 stored, making a few assumptions. It was assumed that all the free CH_4 had been replaced with CO_2 during the injection. In addition the hydration number (N_H) was assumed to be constant, i.e. one mole of CO_2 replaces one mole of CH_4 in the hydrate. This made it possible to calculate the amount of CH_4 produced from the hydrate and thereby the amount of CO_2 stored in hydrate and as free CO_2. The results are presented in Table 4.3. "*CO_2 in hydrate*" is the fraction between the amount of moles CO_2 in the hydrate and the total amount of guest molecules (both CH_4 and CO_2) in the hydrate. The *"CO_2 sequestrated*" is the fraction of the injected CO_2 that remains in the core, either as free CO_2 or in hydrate phase. Note that most of the CO_2 is present as free CO_2. It should

also be noted that the assumptions made in these calculations is inaccurate, because a certain amount of CH_4 will remain as free gas in the core, which means that the amount of CH_4 produced from hydrate and thereby the CO_2 stored in hydrate will be underestimated. The amount of free CO_2 will then be overestimated. The assumption that the hydration number (N_H) is constant is also incorrect and would have an effect on the calculated amount of CO_2 stored in hydrate. In addition, the solubility of the components in the different phases has not been taken into account. However, these assumptions have to be made in order to calculate the CO_2 storage from the data available.

Table 4.3

CO_2 storage estimates in CO2-25 based on produced amount of CH_4

Before CO_2 injection		**After CO_2 injection**			
CH_4 in hydrate [mol]	**CH_4 as free gas** [mol]	**CO_2 stored in hydrate** [mol]	**Free CO_2 in the core** [mol]	**CO_2 fraction in hydrate** [%]	**CO_2 sequestration** [%]
0.301	0.152	0.058	0.631	19.1	21.0

Another method that gives an indication of CO_2 storage potential is the multiple step depressurization, presented in chapter 4.3.1. The mixed hydrate, obtained as a result of CO_2 injection, was depressurized stepwise until hydrate started to dissociate. The dissociation pressure for pure methane hydrate is 4.5 MPa (CSMGem) at the current experimental conditions (4 °C, 3.5 wt% NaCl). When CO_2 replaces CH_4 in a fraction of the hydrate cages, the hydrate dissociation pressure will be reduced. The dissociation pressure could therefore be correlated to a mixed hydrate composition from hydrate equilibrium calculations. However, by using this method, a series of dissociation pressures were obtained due to heterogeneous hydrate composition. In HR48, hydrate dissociation seemed to occur between 3.17 - 2.69 MPa. Based on calculations using CSMGem, this corresponds to CO_2 content between 39.9 - 68 % (chapter 4.3.1). In HR49, dissociation was observed between 3.45 – 3.03 MPa, which corresponds to a CO_2 content of 28.5 – 46.5 %. However, in HR49, nitrogen was used to depressurize the system, which would affect the equilibrium conditions for the hydrate. Also note that the calculations in CSMGem are made on a homogeneous hydrate mixture in bulk. The composition of the hydrate after CO_2 injection in these experiments is most likely varying throughout the core. Still, this method gives an indication that CO_2 sequestration occurs.

In some of the experiments, CO_2 sequestration was observed indirectly. In HR52, the CO_2 injection was performed as a diffusion driven injection (chapter 4.2.5). The injection was stopped after approximately one pore volume of CO_2 injected and the pump was set to keep a constant pressure of 8.55 MPa. Figure 4.5.1 shows the CO_2 consumption during the constant pressure maintenance. It can be observed that the consumption curve looks like a gas consumption curve during hydrate formation. This is clearly and indication that the

injected CO_2 formed hydrate with the excess water. The slope of the curve is initially declining, but starts to increase again after approximately 6 hours, which may be a result of the decrease in temperature which induces further hydrate formation. CO_2 diffusion through the sleeve could also explain this behavior. After 18 hours, the inlet and outlet valves were shut because the pump was required in another experiment. As a result of this, the pressure started to decrease, probably due to further formation of CO_2 hydrate with the excess water. The same behavior was observed during the second CO_2 flush in HR52. The pressure decline curves are presented in Figure 4.2.15 and Figure 4.2.16 and discussed in chapter 4.2.5.

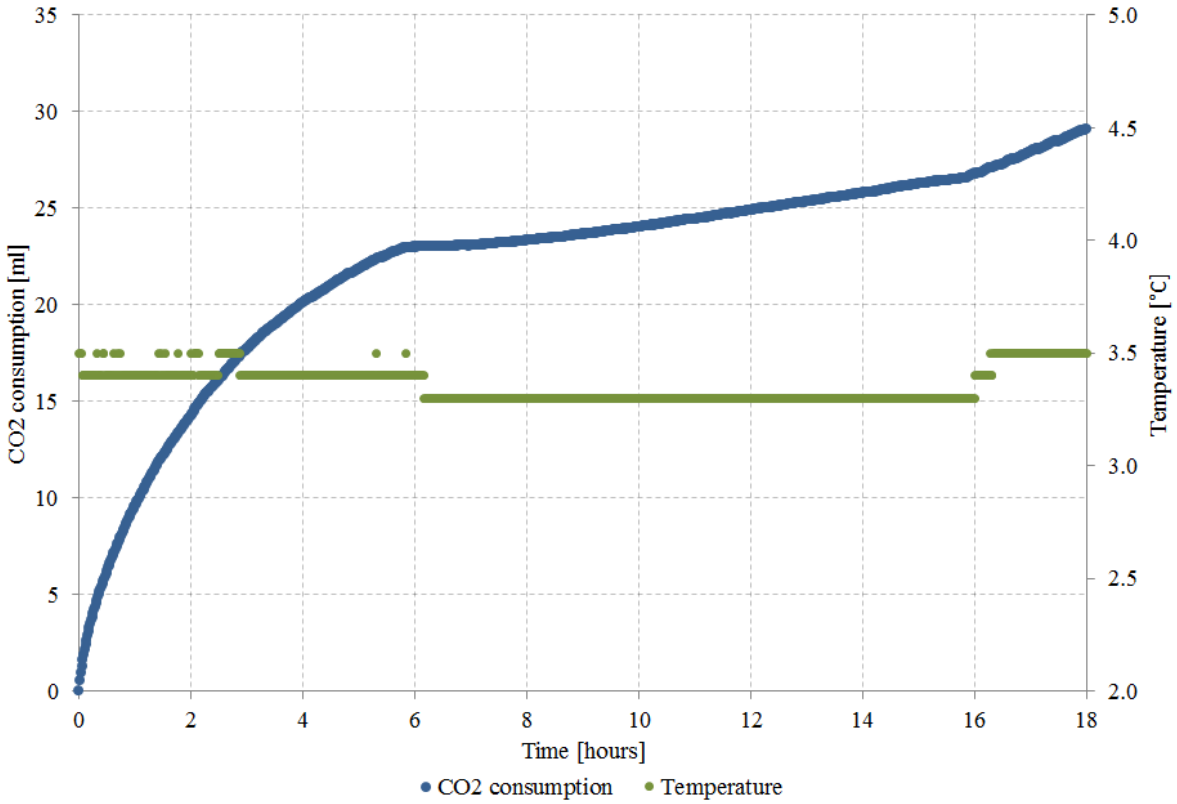

Figure 4.5.1 – CO_2 consumption as pump was set to constant pressure delivery at 8.55 MPa after the first CO_2 flush in HR52. This indicates that CO_2 forms hydrate with the excess water

The methods presented above do not provide quantitative information about the amount of CO_2 stored in each experiment. However, they all indicate that some amount of the injected CO_2 remains in the core either as hydrate or free CO_2. Unfortunately, multiple steps depressurization was not used in any of the experiments where the mass flow meter was implemented and it was therefore difficult to compare the methods to each other. Still, CO2-25 and HR48 was conducted at similar conditions, accept salinity. The method based on the produced amount of CH_4 estimates the fraction of CO_2 in hydrate to be around 0.191 for CO2-25. For comparison, the fraction was estimated between 0.399 and 0.680, based on the multiple steps depressurization method used in HR48.

4.6 Uncertainties

The experimental results presented in this thesis have been obtained by using equipment that all has a level of uncertainty. In addition, there are uncertainties related to human errors, assumptions made in the calculations and uncertainties as a result of experimental conditions, such as variation in temperature, leaks and equipment failure. For the experiments conducted in this thesis, the equipment uncertainties are relatively low compared to the others. This chapter will present and discuss all the relevant uncertainties.

4.6.1 Leaks

Leakage was a major cause of uncertainty affecting the experimental results. The experiments were conducted in systems containing gas under high pressures, making leaks inevitable. Several actions were made to minimize the impact of leaks on the experimental results. Extensive pressure testing and leakage detection was conducted prior to hydrate formation, giving estimates of the leakage rate that were taken into account in the calculations. The leakage rates varied between 0.001 ml/h and 0.139 ml/h for the different experiments and were measured before hydrate formation started and confirmed by consumption logs after the formation. Based on these measurements, it was assumed that the leakage rate remained constant for each experiment. However, mass balance calculations from CO2-25, presented in chapter 4.5, indicate that the leakage rate was significantly higher during CO_2 injection than during formation. This may be caused by CO_2 diffusion through the sleeve. In some of the experiments, the sleeve had to be replaced due to damage caused by the CO_2.

The leakage rate was only included in the hydrate formation calculations. During production, the number of components made it difficult to obtain estimates of the leakage rate and composition of the leaks. However, as discussed earlier, leaks result in an underestimation of the methane recovery and overestimation of CO_2 storage.

4.6.2 Temperature variations

Variations in room temperature affect several aspects of the experimental results, such as measured gas consumption, hydrate equilibrium pressure, confinement pressure, gas solubility and resistivity. Since the results and calculations are based on gas consumption logs and resistivity measurements, it is crucial that the temperature remain close to constant. However, daily temperature variations have proven to have a significant impact on both gas consumption and resistivity. Figure 4.6.1 shows how these temperature variations effected the gas consumption during hydrate formation in HR53.

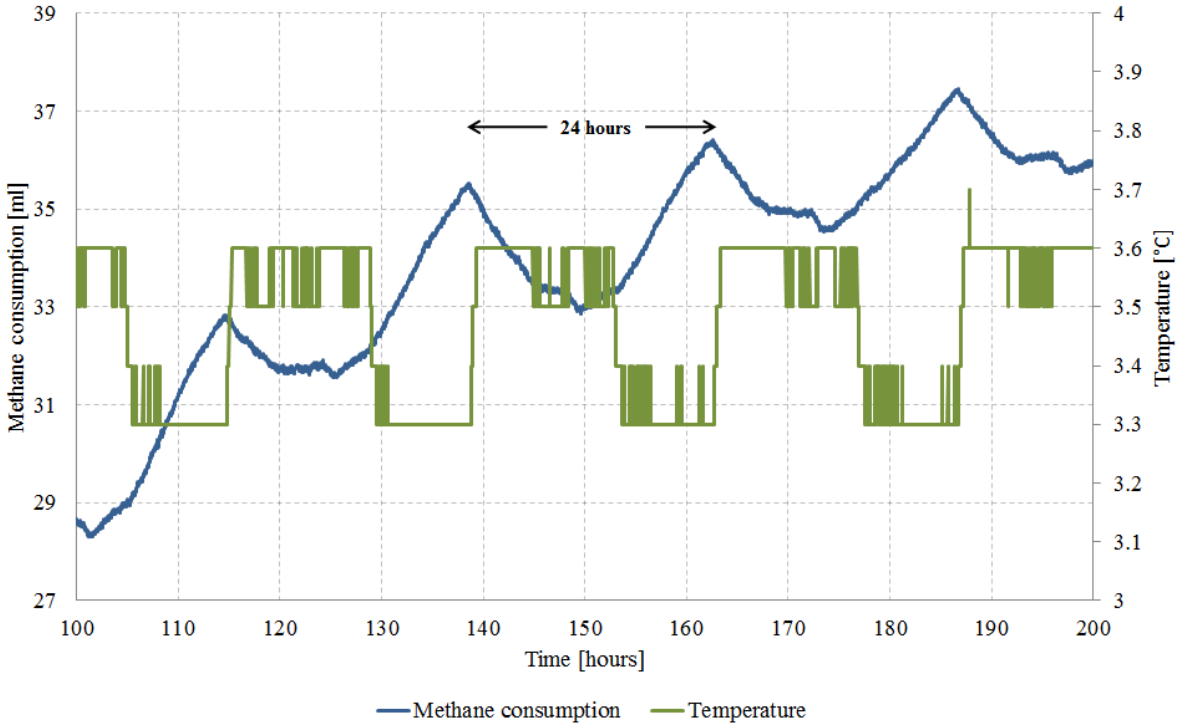

Figure 4.6.1 – Impact of daily temperature variations during hydrate formation in HR53

Resistivity measurements were used as an additional method for detecting hydrate in most of the experiments. The temperature affects the resistivity measurements in several ways. First of all, electrical conductivity is a direct function of temperature. In general, the resistivity of a material therefore decreases with increasing temperature. In addition, the resistivity is also a function of confinement pressure, due to the floating end piece system (chapter 4.1.2). When the confinement pressure increases, the floating end piece is pushed towards the core, reducing the resistivity. An increase in room temperature would therefore increase the confinement pressure, which would indirectly decrease the resistivity. The resistivity change with temperature is therefore a combined results of the two effects described above.

4.6.3 Assumptions made in the calculations

In order to perform mass balance calculations on hydrate formation and methane production in the different experiments, a series of assumptions were made. Some of these assumptions had to be made, or else the calculations would not be possible. Other assumptions were made in order to simplify the calculations without effecting the calculations significantly. Here is a list of assumptions that were made:

- The hydration number (N_H) was set to a constant value of 5.99
- The leakage rate was constant during the entire experiment

- The grain density for the Bentheim Sandstone was set to 2.65 g/ml
- 26 % volume expansion were used when water formed hydrate
- The room- and core temperature was set to constant values in the calculations
- The temperature gradient between the tubing and the core was not taken into account
- The density of water was set to 1.0 g/ml (before NaCl was added)
- The tubing volumes between core and inlet/outlet valves were set to 5 ml
- No leakage during production (discussed in chapter 4.6.1 above)
- Interpolation in the intervals where connection to the GC was lost
- No water production during CO_2 injection
- The tortuosity factor *b* in Archie's second law was set to 1.0
- The saturation index *n* in Archie's second law was assumed constant during formation
- The phase angle φ was set to zero when calculating resistivity from resistance

Some of these assumptions could have been taken into account in the calculations, e.g. calculate methane density as a function of temperature. However, this would make the calculations more complicated without having a significant effect on the result. For example, the largest temperature fluctuations in this thesis were observed in HR53 where the temperature varied between 3.3 and 3.6 °C. This corresponds to a methane density variation of ± 0.00007 g/ml at 8.3 MPa, i.e. ± 0.1 %. This uncertainty is neglectable compared to other factors, such as leaks.

Other uncertainties were not possible to include in the calculations with the equipment that was used. The assumption of no water production during CO_2 injection could lead to incorrect calculations of the effluent produced. Since water exists as a liquid at atmospheric conditions, it would have a major impact on the measured mass flow. The GC only measures the fractions of CH_4, N_2 and CO_2 and it is therefore crucial that no water is produced during injection. However, no water was observed in the effluent in any of the experiments.

4.6.4 Equipment uncertainties

The equipment uncertainties are given by the manufacturers and are relatively low compared to the uncertainties and assumptions described above. However, it is important to be aware that the measured values are not exact and may vary between certain intervals.

Table 4.4 present the specific uncertainties for the equipment used for logging or measurements in this thesis.

Table 4.4

Equipment uncertainties given by the manufacturer

Equipment	Measurement	Uncertainty	Unit
Slide caliper	Length	± 0.005	cm
GF-3000 Digital Balance	Weight	± 0.02	g
ST Stigma 500	Flow	± 0.1	%
	Pressure	± 0.1	%
HH506RA Thermometer	Temperature	± 0.1	°C
Druck PMP	Pressure	± 0.08	%

4.6.5 Calculating uncertainties

The uncertainties for the initial parameters obtained prior to hydrate formation were calculated based on equipment uncertainties by using equation (4.2). Uncontrollable uncertainties, such as water evaporation after the core had been weighed, were not taken into account. For the parameters that were obtained during the experiments, e.g. saturations, methane production and recovery, there was no point in calculating uncertainties based on equipment accuracy, because the accuracy of the equipment were neglectable compared to the uncontrollable uncertainties such as leaks, equipment failure and temperature variations. Equation (4.2) is an equation that is used to calculate the uncertainty propagation for independent variables, proposed by NIST (Taylor and Kuyatt, 1994). u_f is the standard deviation of the measured variable *f*, that varies with the parameters *x, y, z…* and their respective standard variations u_x, u_y, u_z.

$$u_f = \sqrt{\left(\frac{\partial f}{\partial x}\right)^2 \cdot u_x^2 + \left(\frac{\partial f}{\partial y}\right)^2 \cdot u_y^2 + \left(\frac{\partial f}{\partial z}\right)^2 \cdot u_z^2 + \ldots} \qquad (4.2)$$

Table 4.5 shows the calculated uncertainties for the initial conditions in the experiments conducted in this thesis. Note that only the equipment uncertainties are taken into account in those calculations and the real uncertainty may therefore be larger as a result of human errors and uncontrollable environmental factors. HR52 and HR53 were excluded because they contained fractured cores and the volumetric calculations on the core halves were therefore affected by the human accuracy when cutting the cores. In addition, the dry weight of the core samples was not measured before the cores were cut, which also makes

the calculations uncertain. The equipment accuracy would therefore be neglectable compared to the uncontrollable uncertainties.

Table 4.5

Calculated uncertainties (U_i) for the initial parameters: Bulk volume, pore volume, porosity and initial water saturation. Based on equipment uncertainties

Experiment name	V_b	U_{Vb}	V_p	U_{Vp}	Φ	U_Φ	S_{wi}	U_{Swi}
	[ml]	[ml]	[ml]	[ml]	[%]	[%]	[%]	[%]
CO2_20	280.0	± 1.1	64.2	± 1.4	22.9	± 0.5	41.6	± 1.0
CO2_25	292.6	± 1.2	73.8	± 1.4	25.2	± 0.5	40.5	± 0.9
HR_47	284.2	± 1.1	69.0	± 1.4	24.3	± 0.5	42.2	± 0.9
HR_48	273.8	± 1.1	62.1	± 1.3	22.7	± 0.5	40.5	± 1.0
HR_49	273.8	± 1.1	62.1	± 1.3	22.7	± 0.5	64.4	± 1.5
HR_50	283.8	± 1.1	63.9	± 1.4	22.5	± 0.5	64.7	± 1.5
HR_51	292.4	± 1.2	70.5	± 1.4	24.1	± 0.5	66.8	± 1.5
DEP_5	285.3	± 1.1	69.5	± 1.4	24.4	± 0.5	43.3	± 1.0

Chapter 5 - Conclusions and future work

5.1 Conclusions

Ten experiments have successfully been conducted in order to investigate hydrate formation and CO_2/CH_4 exchange in Bentheim sandstone cores. The main findings are:

Excess water saturations from 27 % to 50 % was achieved in gas-water-hydrate systems when high initial water saturations where established before hydrate formation.

It was confirmed that the injection of CO_2 into hydrate bearing sandstone with excess water could lead to additional hydrate formation and loss of injectivity. This problem was successfully met by injecting a binary mixture of N_2 and CO_2. It was discovered that nitrogen inhibited additional hydrate formation and also increased the total methane recovery and CO_2 storage potential by dissociating a fraction of the methane hydrate. It was also discovered that nitrogen could be used to re-establish flow in a plugged core.

The hydrate growth pattern was investigated by measuring gas consumption and resistivity during hydrate formation. The hydrate formation process seemed to be constrained by water availability and residual salinity at low initial water saturations. For high initial water saturations, the formation seemed to be limited by available reaction surface between water and gas. Resistivity measurement proved to be a useful tool in detecting gas hydrates, especially at low residual water saturations

"The memory effect" was observed in experiments featuring multiple hydrate formations and dissociations. The rate of hydrate formation was higher in the formations conducted after thermal dissociations because the high pressure was maintained, leaving a larger amount of methane in solution.

The implementation of a mass flow meter improved mass balance calculations and indicated that previous assumptions used in the calculations resulted in underestimation of methane recovery.

CO_2 sequestration was observed by several different methods. It was found that the injection of CO_2 into hydrate bearing sediments could result in CO_2 sequestration either by the formation of additional hydrate with the excess water or by replacing CH_4 as a guest molecule.

5.2 Future work

The experiments presented in this thesis have been conducted at gradually increasing initial water saturations in order to obtain water in excess. However, the experiments were still conducted as excess gas systems, because methane was used to pressurize the systems. Experiments conducted with CO_2 injection in pure excess water systems should be conducted in order to further investigate the loss of injectivity as a result of additional hydrate formation.

Co-injecting nitrogen together with CO_2 proved to be an effective solution to avoid further hydrate formation with the excess water. Further research on the injected mixed composition could be beneficial in order to improve the CO_2 utilization and optimize the exchange process. The successful usage of nitrogen for preventing injectivity loss has also introduced the possibility of co-injecting other hydrate inhibitors with CO_2 in hydrate bearing sediments with excess water.

The experiments in this thesis were conducted at a core scale. In order to improve the understanding of macroscopic effects such as CO_2 sweep efficiency and the effect of hydrate distribution, experiments should be conducted at a larger scale. In addition, the experimental work should be implemented and compared to numerical simulations at both core and reservoir scale.

All the continuous CO_2 injections were performed at a constant rate of 1.2 ml/h. This induces considerable uncertainties related to leakage rates and the measured mass flow. In addition, these experiments are rather time-consuming. By investigating CO_2 injection at higher rates, the uncertainties could be reduced, and the experiments might be conducted more efficiently and over a smaller period of time.

References

Archie (1942) *The Electrical Resistivity Log as an Aid in Determining Some Reservoir Characteristics*.

Atkins & De Paula (2006) *Atkins' Physical chemistry,* Oxford ; New York, Oxford University Press.

Birkedal (2009) Hydrate formation and CH4 production from natural gas hydrates : emphasis on boudary conditions and production methods.

Birkedal, et al. (2011) Electrical Resistivity Measurements of CH_4 Hydrate Bearing Sandstone During Formation.

Birkedal, et al. (2013a) Numerical Reproduction of Empirical Methane Hydrate Dissociation and Reformation in Sandstone, *In Prep*.

Birkedal, et al. (2013b) Electrical Resistivity Measurements in Sandstone during CH4 Hydrate Formation and CH4-CO2 Exchange, *In Prep*.

Boswell & Collett (2006) The Gas Hydrate Resource Pyramid. *Fire in the Ice,* Vol. 6,

Bringedal (2011) Impacts of Temperature on Methane Production from Hydrates by CO_2 injection.

Buchanan, et al. (2005) Search for memory effects in methane hydrate: Structure of water before hydrate formation and after hydrate decomposition. *Journal of Chemical Physics,* Vol. 123,

Churaev, Bardasov & Sobolev (1993) On the Non-Freezing Water Interlayers between Ice and a Silica Surface. *Colloids and Surfaces a-Physicochemical and Engineering Aspects,* Vol. 79, 11-24

Chuvilin, Istomin & Safonov (2011) Residual nonclathrated water in sediments in equilibrium with gas hydrate: Comparison with unfrozen water. *Cold Regions Science and Technology,* Vol. 68, 68-73

Clennell, et al. (1999) Formation of Natural Gas Hydrates in Marine Sediments: 1. Conceptual Model of Gas Hydrate Growth Conditioned by Host Sediment Properties.

Davidson, et al. (1986) Crystallographic Studies of Clathrate Hydrates .1. *Molecular Crystals and Liquid Crystals,*

Deusner, et al. (2012) Methane Production from Gas Hydrate Deposits through Injection of Supercritical CO2. *Energies,* Vol. 5, 2112-2140

Edmonds, et al. (1996) A Practical Model for the Effect of Salinity on Gas Hydrate Formation.

Ersland (2008) *Studies of flow mechanisms and hydrate phase transitions in fractured rocks,* Norway, University of Bergen.

Ersland (2013) Personal Communication,

Ersland, et al. (2010) Measuring gas hydrate formation and exchange with CO2 in Bentheim sandstone using MRI tomography. *Chemical Engineering Journal,* Vol. 158, 25-31

Ersland, et al. (2008) Measurements of Gas Permeability and Non-Darcy Flow in Gas-Water-Hydrate Systems.

Etheridge, et al. (1998) Atmospheric methane between 1000 A.D. and present: Evidence of anthropogenic emissions and climatic variability. *Journal of Geophysical Research: Atmospheres,* Vol. 103, 15979-15993

ExxonMobil (2013) The Outlook for Energy: A View to 2040.

Gabitto & Tsouris (2010) Physical Properties of Gas Hydrates: A Review. *Journal of Thermodynamics,*

Gerami & Pooladi-Darvish (2006) Material Balance and Boundary-Dominated Flow Models for Hydrate-Capped Gas Reservoirs.

Graue, et al. (2006a) CO2 storage in natural-gas-hydrate reservoirs benefits from associated methane production. Vol. 58, 3
Graue, et al. (2006b) Environmentally Friendly CO2 Storage in Hydrate Reservoirs Benefits From Associated Spontaneous Methane Production. *Offshore Technology Conference.* Houston, Texas.
Graue, et al. (2006c) Magnetic Resonance Imaging of Methane - Carbon Dioxide Reactions in Sandstone Pores. 12
Gupta (2007) *Methane Hydrate Dissociation Measurements and Modeling: The Role of Heat Transfer and Reaction Kinetics*, Colorado School of Mines.
Handa (1990) Effect of hydrostatic pressure and salinity on the stability of gas hydrates. *The Journal of Physical Chemistry,* Vol. 94, 2652-2657
Hauge (2011) Resistivity Measurements during Gas Hydrate Formation and Subsequent CO2 Exchange in Porous Sandstone.
Hauge (2013) In-house database - University of Bergen. 1.6 ed.
Hauge, et al. (2012) Effects of Initial Saturation and Salinity on Methane Hydrate Growth in Bentheim Sandstone.
Helgerud (2001) Wave speeds in gas hydrate and sediments containing gas hydrate: A laboratory and modeling study.
Hester & Brewer (2009) Clathrate Hydrates in Nature. 27
Hirohama, et al. (1996) Conversion of CH4-hydrate to CO2-hydrate in liquid CO2. *Journal of Chemical Engineering of Japan,* Vol. 29, 1014-1020
Hossainpour (2013) Catalysts for Enhanced CO2 – CH4 Exchange in Natural Gas Hydrates: An experimental feasibility study of exchange enhancement by use of chemical additives.
Husebø (2008) Monitoring depressurization and CO_2-CH_4 exchange production scenarios for natural gas hydrates. 146
Husebø, et al. (2009) Effects of salinity on hydrate stability and implications for storage of CO2 in natural gas hydrate reservoirs. *Energy Procedia,* 3731-3738
International Energy Agency (2012) Key World Energy Statistics. International Energy Agency.
Jeffrey (1984) Hydrate Inclusion Compounds. 12
Jung & Santamarina (2010) CH4-CO2 replacement in hydrate-bearing sediments: A pore-scale study. *Geochemistry, Geophysics, Geosystems,* Vol. 11, n/a-n/a
Jung & Santamarina (2012) Hydrate formation and growth in pores. *Journal of Crystal Growth,* Vol. 345, 61-68
Kang, et al. (2005) Numerical modeling of pore-scale phenomena during CO2 sequestration in oceanic sediments. *Fuel Processing Technology,* Vol. 86, 1647-1665
Kingston, Clayton & Priest (2008) Gas Hydrate Growth Morphologies and Their Effect on the Stiffness and Damping of a Hydrate Bearing Sand.
Kleinberg, et al. (2003) Deep sea NMR: Methane hydrate growth habit in porous media and its relationship to hydraulic permeability, deposit accumulation, and submarine slope stability. *Journal of Geophysical Research-Solid Earth,* Vol. 108,
Kneafsey, Nakagawa & Borglin (2013) Properties of Hydrate-Bearing Sediments Subjected to Changing Gas Compositions. Lawrence Berkeley National Laboratory.
Kneafsey, et al. (2007) Methane hydrate formation and dissociation in a partially saturated core-scale sand sample. *Journal of Petroleum Science and Engineering,* Vol. 56, 108-126
Kvamme (2012) Lecture notes PTEK232: Fundamentals of Natural Gas Hydrates and Practical Implications.

Kvamme, et al. (2011) Thermodynamics and Kinetic Modelling of CH_4/CO_2 Exchange in Hydrates.
Kvenvolden (1988) Methane Hydrate - a Major Reservoir of Carbon in the Shallow Geosphere. *Chemical Geology,* Vol. 71, 41-51
Kvenvolden (1993) Gas Hydrates - Geological Perspective and Global Change. *Reviews of Geophysics,* Vol. 31, 173-187
Lee, et al. (2003) Recovering Methane from Solid Methane Hydrate with Carbon Dioxide. 4
Li, et al. (2010) Resistivity in Formation and Decomposition of Natural Gas Hydrate in Porous Medium. *Chinese Journal of Chemical Engineering,* Vol. 18, 39-42
Lien (2004) PTEK211 - Grunnleggende reservoarfysikk.
Liu, et al. (2008) Raman Spectroscopic Observations on the Structural Characteristics and Dissociation Behavior of Methane Hydrate Synthesized in Silica Sands with Various Sizes. *Energy & Fuels,* Vol. 22, 3986-3988
MacDonald (1990) Role of methane clathrates in past and future climates. *Climatic Change,* Vol. 16, 247-281
Makogon (1981) *Hydrates of natural gas,* Tulsa, Okla., PennWell Books.
Makogon (1997) *Hydrates of hydrocarbons,* Tulsa, Okla., PennWell Books.
Makogon (2009) Natural Gas Hydrates - A promising source of energy.
Makogon & Omelchenko (2013) Commercial gas production from Messoyakha deposit in hydrate conditions. *Journal of Natural Gas Science and Engineering,* Vol. 11, 1-6
Masuda, et al. (2008) Prediction of methane hydrate dissociation behavior by nitrogen injection. *Proceedings of the 6th International Conference on Gas Hydrates,*
McCabe, Smith & Harriot (2004) Unit Operations of Chemical Engineering.
McGrail, et al. (2007) Using Carbon Dioxide to Enhance Recovery of Methane from Gas Hydrate Reservoirs: Final Summary Report.
Moridis, et al. (2009) Toward Production From Gas Hydrates: Current Status, Assessment of Resources, and Simulation-Based Evaluation of Technology and Potential. *Spe Reservoir Evaluation & Engineering,* Vol. 12, 745-771
Moridis & Sloan (2007) Gas production potential of disperse low-saturation hydrate accumulations in oceanic sediments. *Energy Conversion and Management,* Vol. 48, 1834-1849
Mullin (2001) Crystallization 4th Edition.
Nago & Nieto (2011) Natural Gas Production from Methane Hydrate Deposits Using CO2 Clathrate Sequestration: State-of-the-Art Review and New Technical Approaches. *Journal of Geological Research,*
Ohgaki, Takano & Moritoki (1994) Exploitation of CH_4 Hydrates under the Nankai Trough in Combination with CO_2 Storage. *Kagaku Kogaku Ronbunshu,* Vol. 20, 121-123
Ohgaki, et al. (1996) Methane exploitation by carbon dioxide from gas hydrates - Phase equilibria for CO2-CH4 mixed hydrate system. *Journal of Chemical Engineering of Japan,* Vol. 29, 478-483
Ota, et al. (2005) Replacement of CH4 in the hydrate by use of liquid CO2. *Energy Conversion and Management,* Vol. 46, 1680-1691
Panter, et al. (2011) Hydrate Plug Dissociation via Nitrogen Purge: Experiments and Modeling. *Energy & Fuels,* Vol. 25, 2572-2578
Park, et al. (2008) Swapping Carbon Dioxide for Complex Gas Hydrate Structures.
Pooladi-Darvish (2004) Gas production from hydrate reservoirs and its modeling. *Journal of Petroleum Technology,* Vol. 56, 65-71

Rees, Kneafsey & Yongkoo (2011) Methane Hydrate Distribution from Prolonged and Repeated Formation in Natural and Compacted Sand Samples: X-Ray CT Observations.
Rodger (2000) Methane Hydrate: Melting and Memory. *Annals of the New York Academy of Sciences,* Vol. 912, 474-482
Ruppel (2011) Methane Hydrates and Contemporary Climate Change. *Nature Education Knowledge,*
Schmuck & Paull (1993) Evidence for Gas Accumulation Associated with Diapirism and Gas Hydrates at the Head of the Cape Fear Slide. *Geo-Marine Letters,* Vol. 13, 145-152
Schoderbek & Boswell (2011) Iġnik Sikumi #1, Gas Hydrate Test Well ,Successfully Installed on the Alaska North Slope. *Fire in the Ice,* Vol. 11,
Schoderbek, et al. (2012) North Slope Hydrate Fieldtrial: CO2/CH4 Exchange. *OTC Arctic Technology Conference.* Houston, Texas, USA.
Sloan & Koh (2008) *Clathrate hydrates of natural gases,* Boca Raton, Fla., CRC Press.
Soloviev (2002) Global Estimation of Gas. *Russian Geology and Geophysics.*
Stillinger (1980) Water Revisited. Vol. 209, 8
Taylor & Kuyatt (1994) Guidelines for Evaluating and Expressing the Uncertainty of NIST Measurement Results. *NIST Technical Note 1297,*
The National Institute of Standards and Technology (2013) NIST Chemistry WebBook
Tohidi, et al. (2001) Visual observation of gas-hydrate formation and dissociation in synthetic porous media by means of glass micromodels. *Geology,* Vol. 29, 867-870
Trofimuk, Cherskii & Tsarev (1973) Specificities of Natural-Gas Accumulation in Hydrate-Formation Zones of World Ocean. *Doklady Akademii Nauk Sssr,* Vol. 212, 931-934
U.S. Energy Information Administration (2013a) Annual Energy Outlook 2013. U.S. Energy Information Administration.
U.S. Energy Information Administration (2013b) Carbon Dioxide Emissions Coefficients http://www.eia.gov/environment/emissions/co2_vol_mass.cfm
Voitkovskii (1960) The Mechanical Properties of Ice.
Yakushev & Collett (1992) Gas hydrates in Arctic regions - Risks to drilling and production.
Yoon, et al. (2004) Transformation of Methane Hydrate to Carbon Dioxide Hydrate: In Situ Raman Spectroscopic Observations. *The Journal of Physical Chemistry A,* Vol. 108, 5057-5059
Zhenhao & Shide (2006) A thermodynamic model for calculating methane solubility, density and gas phase composition of methane-bearing aqueous fluids from 273 to 523 K and from 1 to 2000 bar.
Zolotukhin & Ursin (2000) *Introduction to Petroleum Reservoir Engineering*.

APPENDIX

Nomenclature

ΔG	Gibbs Free Energy
N_H	Hydration number
φ	Porosity/Phase angle
S_i	Saturation of fluid *i*
S_{wi}	Initial water saturation
S_{wf}	Final water saturation
K	Permeability
u	Darcy velocity
ρ	Density
μ	Viscosity
ψ	Flow potential
P	Pressure
g	Gravity component
R_e	Reynolds number
D_H	Hydraulic diameter
P_c	Capillary Pressure
σ	Interfacial tension
Θ	Wetting Angle
R	Electrical resistance
F	Formation factor
I	Resistivity index
A	Cross sectional area
L	Inductance
R_{CH4}	Methane recovery factor

Appendix A – Experimental Designs

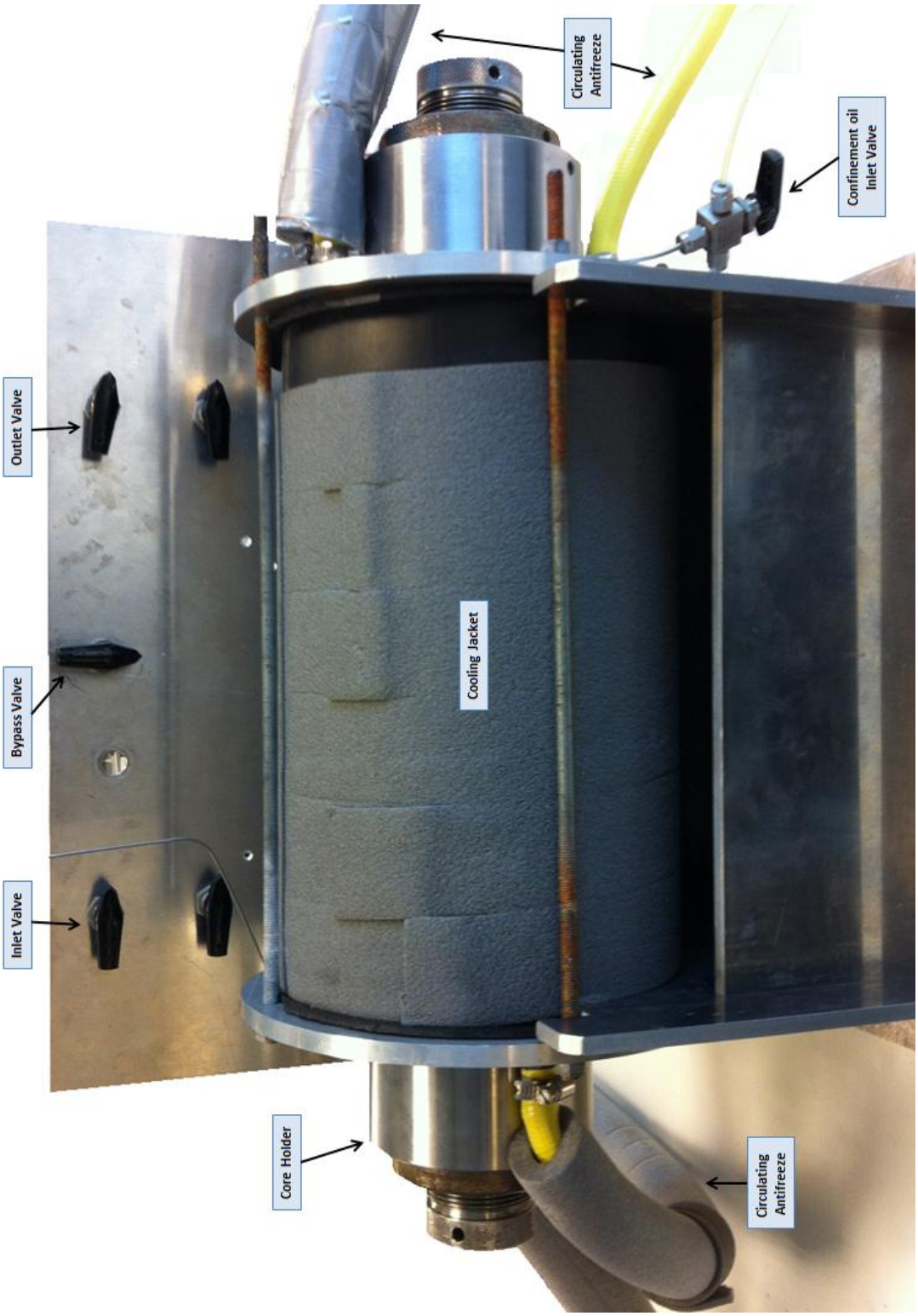

Appendix Figure I – Experimental set-up B: Hassler core holder coated by cooling jacket and mounted in a rack. The same configuration was used in set-up C

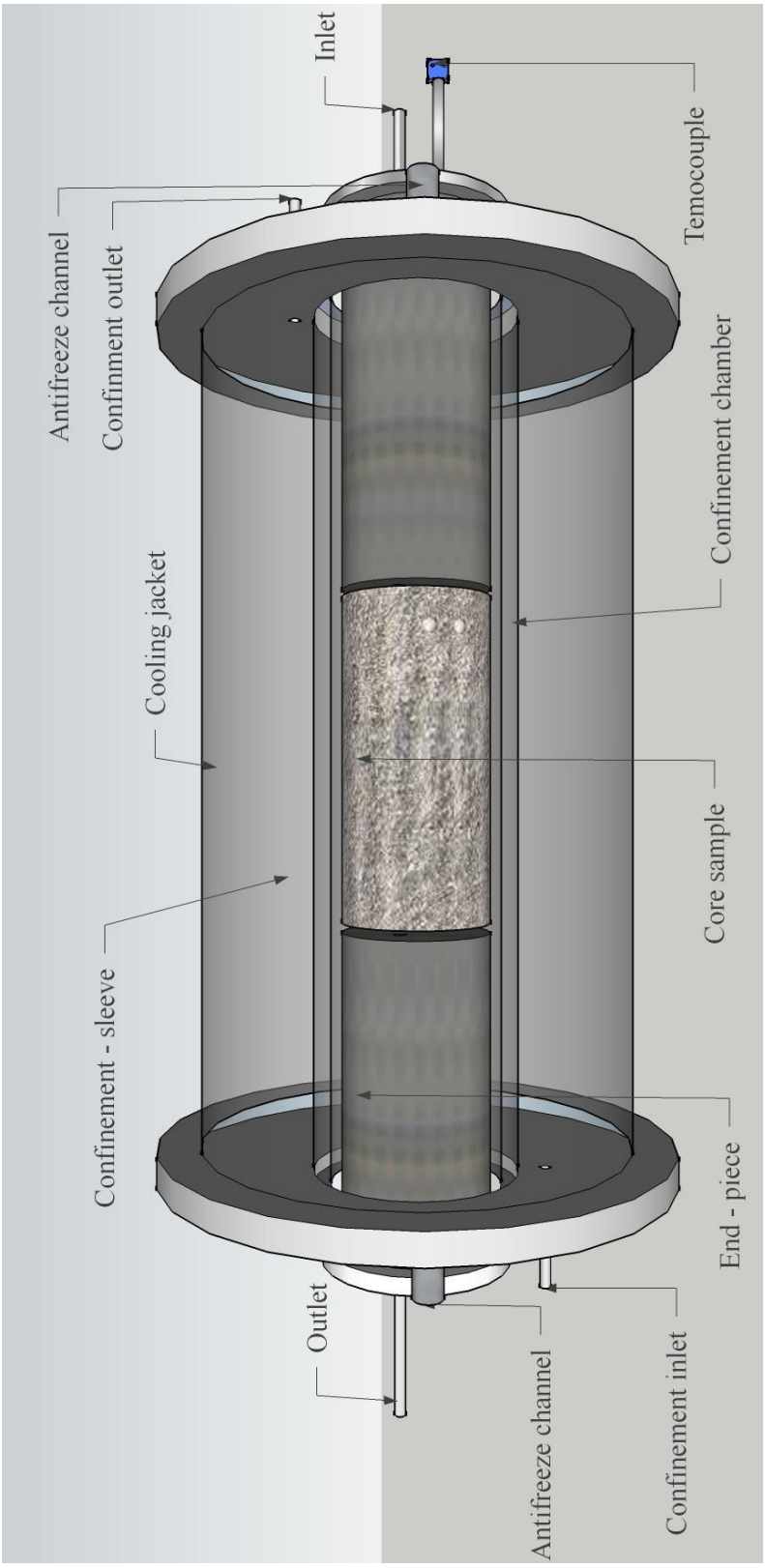

Appendix Figure II – 3D model of the core holder used in setup B and C (Hossainpour, 2013)

Appendix B – In-house Database

Appendix Table 1

Experiments from UiB in-house database (Hauge, 2013), including the experiments conducted in this thesis. Showing initial brine salinity, initial and final phase saturations and methane recovery

Name	Salinity	S_{wi}	S_h	S_{wf}	R_{CH4}
CO2_13	3.5	0.40	0.52	0.00	-
CO2_15	0.1	0.41	0.47	0.04	4.0*
CO2_17	0.1	0.41	0.45	0.05	-
CO2_18	0.1	0.41	0.60	0.00	-
CO2_19	0.1	0.62	0.71	0.05	-
CO2_20	0.1	0.42	0.53	0.04	-
CO2_21	0.1	0.41	0.48	0.03	37.0
CO2_22	0.1	0.38	0.48	0.00	-
CO2_23	0.1	0.41	0.48	0.03	51.0
CO2_24	0.1	0.41	0.48	0.03	37.0
CO2_25	0.1	0.41	0.51	0.05	45.0
CO2_26	0.1	0.43	0.48	0.06	59.0
CO2_28	0.1	0.40	0.40	0.08	-
DEP5_1	0.1	0.43	0.46	0.06	-
DEP5_2	0.1	0.43	0.45	0.07	-
DEP5_3	0.1	0.43	0.44	0.08	-
HR07	0.1	0.75	0.53	0.33	-
HR10	3.5	0.65	0.41	0.33	-
HR19	1.0	0.55	0.55	0.11	-
HR21	1.0	0.53	0.64	0.03	-
HR29	1.0	0.70	0.64	0.20	-
HR33	0.1	0.74	0.65	0.23	-
HR38	3.5	0.50	0.53	0.09	-
HR39	3.5	0.47	0.42	0.14	-
HR40	0.1	0.41	0.50	0.01	-
HR41	0.1	0.41	0.52	0.00	-
HR44	0.1	0.41	0.42	0.07	22.0
HR45	0.1	0.40	0.50	0.00	-
HR46	3.5	0.40	0.47	0.03	-
HR47	3.5	0.42	0.38	0.12	-
HR48	3.5	0.40	0.42	0.08	23.0*
HR49	3.5	0.64	0.46	0.29	26.0*
HR50	3.5	0.65	0.47	0.28	-
HR51	3.5	0.67	0.51	0.27	61.0
HR52	3.5	0.74	0.35	0.47	29.0
HR53	3.5	0.81	0.41	0.50	-

* Recovery calculated without mass flow meter